Supplementary Information

O-I-O Halogen Bond of Halonium Ions

Sofia Lindblad, Flóra Boróka Németh, Tamás Földes, Alan Vanderkooy, Imre Pápai, and Máté Erdélyi

Table of Contents

1. Supplementary figures S2
2. SYNTHESIS S3
  1.1. General information S3
  1.2. Synthesis S3
2. NMR SPECTRA OF SYNTHESIZED COMPOUNDS S8
  2.1. 4-Methoxypyridine *N*-oxide and complexes S8
  2.2. 4-Methylpyridine *N*-oxide and complexes S22
  2.3. Dibenzofuran complexes S41
3. COMPUTATIONS S46
  3.1. Computational approach S46
  3.2. Structure of $[RO\text{-}X\text{-}OR]^+$ complexes S46
  3.3. Relative stability of $[RO\text{-}X\text{-}OR]^+$ complexes S49
  3.4. Formation of halogen bonded $RO\cdots I_2$ complexes S50
  3.5. Coordination of acetonitrile to $[RO\text{-}X\text{-}OR]^+$ complexes S50
  3.6. Computed ^{15}N NMR chemical shifts S52
  3.7. Total energy data S53
  3.8. Cartesian coordinates S54
4. REFERENCES S73

1. Supplementary figures

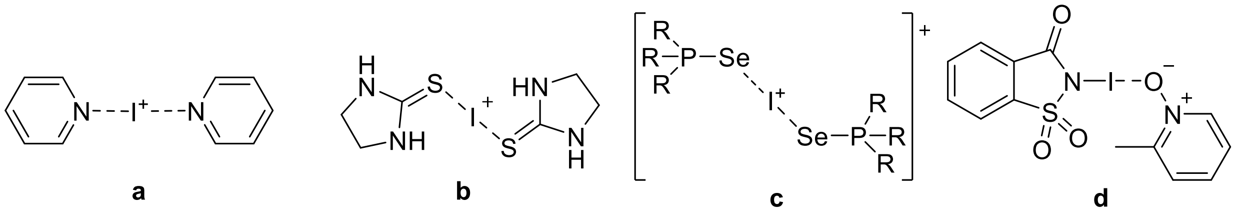

Figure S1. Some examples of literature known 3c4e halogen bond complexes with nitrogen, sulfur, selenium and mixed nitrogen-oxygen Lewis bases as halogen bond accceptors.[1-6]

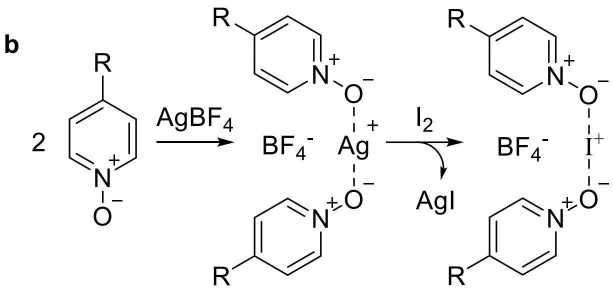

Figure S2. Synthetic scheme for the formation of [bis(4-methoxypyridine *N*-oxide)iodine(I)]$^+$ tetrafluoroborate (**(1-*OMe*)$_2$-I,** R = OMe) and [bis(4-methylpyridine *N*-oxide)iodonine(I)]$^+$ tetrafluoroborate (**(1-*Me*)$_2$-I,** R = Me), via the corresponding intermediate silver(I) complexes **(1-*OMe*)$_2$-Ag** and **(1-*Me*)$_2$-Ag**.

2. SYNTHESIS

1.1. General information

Chemicals were purchased from commercial suppliers and used without further purification, unless stated otherwise. Dry deuterated solvents were obtained by opening a fresh bottle in a glovebox, adding molecular sieves (3 Å), and allowing it to stand at least overnight. All synthesis was performed in a glovebox with glassware that had been dried in an oven (150 °C) or *in vacuo* at least overnight. For LC-MS analyses an Agilent 1100 Series HPLC system with a C8 column (GRACE Genesis Lighting) connected to a Waters Micromass ZQ mass spectrometer was used. Acetonitrile and 1% formic acid in MQ-water was used as mobile phase, with gradient elution using 5-95 % acetonitrile over 10 min. For recording NMR spectra either an Agilent MR-400 equipped with a OneNMR probe, a Varian Mercury Plus 400 equipped with a two channel ATB probe, or a Bruker Avance Neo 500 equipped with a TXO cryogenic probe was used. Chemical shifts are reported on the δ scale (ppm), using the residual solvent signal as internal standard; CD_3CN (δ_H 1.94, δ_C 118.26, 1.32). The ^{15}N NMR chemical shifts were referenced relative to the proton spectra using the Absolute Reference function in MestReNova ($MeNO_2$ reference scale δ_N 0.0). ^1H NMR resonances were assigned based on chemical shift (δ), observed multiplicities, observed coupling constants (*J* Hz), and number of hydrogens. Recorded TOCSY, NOESY, COSY, $^1H,^{13}C$ HSQC, $^1H,^{13}C$ HMBC, and $^1H,^{15}N$ HMBC were also used as aids to make the correct assignments. Multiplicities are denoted as s (singlet), d (doublet), t (triplet), q (quartet), h (heptet), and m (multiplet). NMR spectra were processed using MestReNova 11.0.

1.2. Synthesis

[Bis(4-methoxypyridine *N*-oxide)silver(I)]$^+$ tetrafluroborate (**(1-*OMe*)$_2$-Ag**)

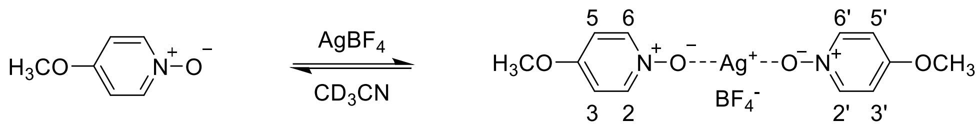

In a glovebox, 4-methoxypyridine *N*-oxide hydrate (0.244 g, 1.71 mmol) was dissolved in dry CH_2Cl_2 (16 mL), and the solution was left standing over molecular sieves (3 Å) over night. A portion of the solution (8 mL, 0.85 mmol) was added to a vial with $AgBF_4$ (0.089 g, 0.46 mmol, 0.5 equiv). The solution was stirred, causing formation of a white precipitate. To ensure full precipitation, dry *n*-hexane (16 mL) was added. Upon standing, the precipitate sedimented, and the supernatant was removed with a syringe. The precipitate was dried *in vacuo* overnight to yield **(1-*OMe*)$_2$-Ag** as a white solid (0.156 g, 0.35 mmol, 82 %). ^1H NMR (500 MHz, 25 °C, CD_3CN) δ 7.99 (m, 4H, H2/2'/6/6'), 6.90 (m, 4H, H3/3'/5/5'), 3.38 (s, 6H, 2x-OCH_3); ^{13}C NMR (126 MHz, 25 °C, CD_3CN) δ 158.4 (C4/4'), 140.6 (C2/2'/6/6'), 113.0 (C3/3'/5/5'), 57.0 (2x-OCH_3); ^{15}N NMR (51 MHz, detected via HMBC at 500 MHz for ^1H, 25 °C, CD_3CN) δ −105.1.

[Bis(4-methoxypyridine *N*-oxide)iodine(I)]$^{+}$ tetrafluroborate (**(1-*OMe*)$_2$-I**)

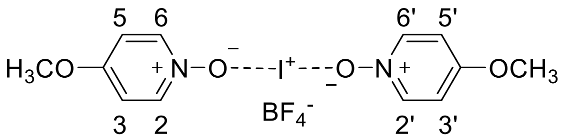

In a glovebox, I_2 (0.024 g, 0.09 mmol) was dissolved in CD_3CN (2.37 mL). To an NMR tube with (**1-*OMe*)$_2$-Ag** (2 mg, 0.004 mmol) in CD_3CN (0.4 mL), a portion of the I_2 solution was added (0.22 mL, 0.008 mmol, 2 equiv), causing formation of a yellow precipitate, leaving **(1-*OMe*)$_2$-I** in solution.* ^{1}H NMR (500 MHz, 25 °C, CD_3CN) δ 8.34 (m, 4H, H2/2'/6/6'), 7.21 (m, 4H, H3/3'/5/5'), 3.99 (s, 6H, 2x-OCH_3); ^{13}C NMR (126 MHz, 25 °C, CD_3CN) δ 167.8 (C4/4'), 142.9 (C2/2'/6/6'), 114.4 (C3/3'/5/5'), 58.62 (2x-OCH_3); ^{15}N NMR (51 MHz, detected via HMBC at 500 MHz for ^{1}H, 25 °C, CD_3CN) δ −134.2.

[4-Methoxypyridine *N*-oxide]I_2 Complex (**(1-*OMe*)-I$_2$**)

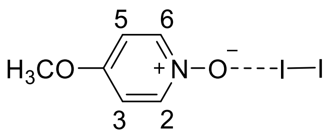

In a glovebox, 4-methoxypyridine *N*-oxide hydrate (0.011 g, 0.08 mmol) was dissolved in dry CD_3CN (3.5 mL), and the solutions was left standing over molecular sieves (3 Å) over night. I_2 (0.024 g, 0.09 mmol) was dissolved in CD_3CN (2.37 mL). A portion of the 4-methoxypyridine *N*-oxide solution (0.4 mL, 0.009 mmol) was added to an NMR tube, along with I_2 solution (0.22 mL, 0.009 mmol, 1 equiv.). ^{1}H NMR (500 MHz, 25 °C, CD_3CN) δ 8.17 (m, 2H, H2/6), 7.07 (m, 2H, H3/5), 3.91 (s, 3H, -OCH_3); ^{13}C NMR (126 MHz, 25 °C, CD_3CN) δ 163.3 (C4), 142.0 (C2/6), 113.6 (C3/5), 57.7 (-OCH_3); ^{15}N NMR (51 MHz, detected via HMBC at 500 MHz for ^{1}H, 25 °C, CD_3CN) δ −122.8.

[1-Hydroxy-4-methoxypyridin-1-ium]$^{+}$ 2,2,2-trifluoroacetate (**(1-*OMe*)-H**)

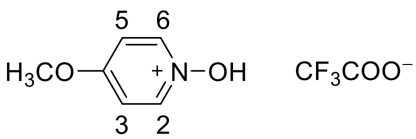

In a glovebox, 4-methoxypyridine *N*-oxide hydrate (0.011 g, 0.08 mmol) was dissolved in dry CD_3CN (3.5 mL), and the solutions was left standing over molecular sieves (3 Å) over night. A portion of the solution (0.4 mL, 0.009 mmol) was added to an NMR tube, along with a small amount of TFA (approx. 5-10 µL, 0.065-0.130 mmol). ^{1}H NMR (500 MHz, 25 °C, CD_3CN) δ 8.52 (m, 2H, H2/6), 7.30 (m, 2H, H3/5), 4.03 (s, 3H, -OCH_3); ^{13}C NMR (126 MHz, 25 °C, CD_3CN) δ 169.0 (C4), 142.9 (C2/6), 114.1 (C3/5), 58.7 (-OCH_3); ^{15}N NMR (51 MHz, detected via HMBC at 500 MHz for ^{1}H, 25 °C, CD_3CN) δ −154.4.

* The complex used for the reaction with 4-penten-1-ol was prepared in the same way, but with a 1:1 stoichiometry of the silver complex and iodine, i.e. without excess iodine.

[Bis(4-methylpyridine *N*-oxide)silver(+I)]$^+$ tetrafluroborate (**(1-*Me*)$_2$-Ag**)

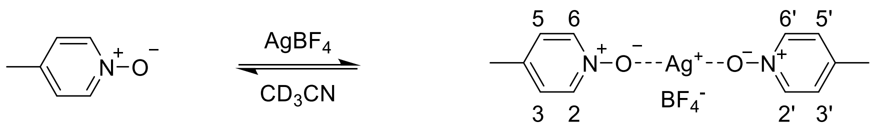

In a glovebox, $AgBF_4$ (0.019 g, 0.10 mmol) and 4-methylpyridine *N*-oxide (0.024 g, 0.22 mmol, 2.2 equiv) were dissolved in dry CH_2Cl_2 (8 mL) and stirred to generate a cloudy, white solution. Dry *n*-hexane (16 mL) was added, causing better precipitation of **(1-*Me*)$_2$-Ag** . The vial was centrifuged for 10 min at 2500 rpm, after which the supernatant was removed. The precipitate was dried *in vacuo* overnight to yield **(1-*Me*)$_2$-Ag** as a white solid (0.042 g, 0.10 mmol, 99 %). ^{1}H NMR (500 MHz, 25 °C, CD_3CN) δ 7.97 (m, 4H, H2/2'/6/6'), 7.13 (m, 4H, H3/3'/5/5'), 2.29 (s, 6H, 2x-CH_3); ^{13}C NMR (126 MHz, 25 °C, CD_3CN) δ 139.1 (C2/2'/6/6'), 137.4 (C4/4'), 127.9 (C3/3'/5/5'), 20.0 (2x-CH_3); ^{15}N NMR (51 MHz, detected via HMBC at 500 MHz for ^{1}H, 25 °C, CD_3CN) δ −92.0.

[Bis(4-methylpyridine *N*-oxide)iodine(I)]$^+$ tetrafluroborate (**(1-*Me*)$_2$-I**) in CD_2Cl_2

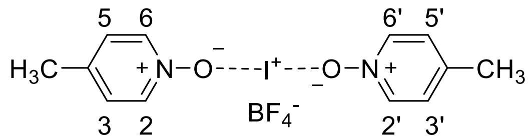

In the glovebox, **(1-*Me*)$_2$-Ag** (0.003 g, 0.007 mmol) was attempted to be dissolved in CD_2Cl_2 (0.8 mL), generating a cloudy, white solution. I_2 (0.002 g, 0.008 mmol, 1.1 equiv.) was added, and the vial was shaken until AgI had precipitated. The clear, pale red solution with **(1-*Me*)$_2$-I** was transferred to an NMR tube. ^{1}H NMR (500 MHz, 25 °C, CD_2Cl_2) δ 8.37 (H2/2'/6/6'), 7.56 (H3/3'/5/5'), 2.51 (2x-CH_3); ^{13}C NMR (126 MHz, 25 °C, CD_2Cl_2) δ 152.9 (C4/4'), 140.3 (C2/2'/6/6'), 129.2 (C3/3'/5/5'), 21.8 (2x-CH_3); ^{15}N NMR (51 MHz, detected via HMBC at 500 MHz for ^{1}H, 25 °C, CD_2Cl_2) δ −119.4.

[Bis(4-methylpyridine *N*-oxide)iodine(I)]$^+$ tetrafluroborate (**(1-*Me*)$_2$-I**) in CD_3CN

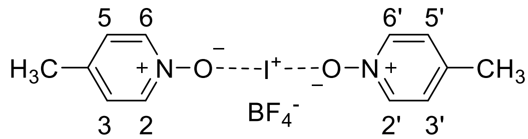

In the glovebox, 4-methylpyridine *N*-oxide (0.018 g, 0.16 mmol) was dissolved in dry CD_3CN (1 mL) and the resulting solution was dried over molecular sieves (3 Å) for three days. A portion of the solution (0.16 mL, 0.026 mmol) was added to a vial with $AgBF_4$ (0.0034 g, 0.017 mmol, 0.7 equiv). I_2 (0.0048 g, 0.019 mmol, 0.7 equiv) was dissolved in CD_3CN (0.48 mL), and the solution was added to the same vial. AgI precipitated, leaving a yellow, clear solution with **(1-*Me*)$_2$-I**, which was transferred to an NMR tube. ^{1}H NMR (500 MHz, 25 °C, CD_3CN) δ 8.37 (H2/2'/6/6', **(1-*Me*)$_2$-I**), 8.10 (H2/2'/6/6', protonated **1-*Me***), 7.59 (H3/3'/5/5', **(1-*Me*)$_2$-I**) 7.28 (H3/3'/5/5', protonated **1-*Me***), 2.46 (2x-CH_3, **(1-*Me*)$_2$-I**), 2.37 (2x-CH_3; protonated **1-*Me***); ^{13}C NMR (126 MHz, 25 °C, CD_2Cl_2) δ 154.0 (C4/4', **(1-*Me*)$_2$-I**), 140.8 (C2/2'/6/6', **(1-*Me*)$_2$-I**), 139.4 (C2/2'/6/6', protonated **1-*Me***), 129.8

(C3/3'/5/5', **(1-*Me*)$_2$-I**), 128.4 (C3/3'/5/5', protonated **1-*Me***) 21.5 (2x-CH_3, **(1-*Me*)$_2$-I**), 20.4 (2x-CH_3, protonated **1-*Me***); ^{15}N NMR (500 and 51 MHz, 25 °C, CD_3CN) δ −121.2 (**(1-*Me*)$_2$-I**), −105.0 (protonated **1-*Me***).

[4-methylpyridine *N*-oxide]I_2 Complex in CD_3CN

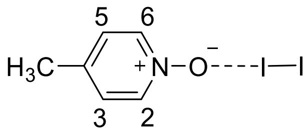

In a glovebox, 4-methylpyridine *N*-oxide (0.0066 g, 0.052 mmol) was dissolved in dry CD_3CN (1 mL) and the resulting solution was dried over molecular sieves (3 Å) over night. A portion of the solution (0.4 mL, 0.026 mmol) was added to a vial with I_2 (0.0048 g, 0.019 mmol). More dry CD_3CN (0.24 mL) was added. When the I_2 had dissolved, the solution was transferred to an NMR tube and the sample was analyzed by NMR. ^1H NMR (500 MHz, 25 °C, CD_3CN) δ 8.08 (2H, H2/6), 7.28 (2H, H3/5), 2.36 (3H, -CH_3); ^{13}C NMR (126 MHz, 25 °C, CD_3CN) δ 142.5 (C4), 139.7 (C2/6), 128.4 (C3/5), 20.5 (-CH_3); ^{15}N NMR (51 MHz, 25 °C, CD_3CN) δ −102.2.

[4-methylpyridine *N*-oxide]I_2 Complex in CD_2Cl_2

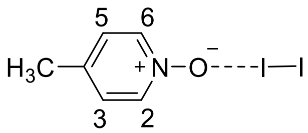

In a glovebox, 4-methylpyridine *N*-oxide (0.0036 g, 0.028 mmol) was dissolved in dry CD_2Cl_2 (1 mL) and the resulting solution was dried over molecular sieves (3 Å) over night. A portion of the solution (0.33 mL, 0.014 mmol) was added to a vial with I_2 (0.0022 g, 0.008 mmol). More dry CD_2Cl_2 (0.47 mL) was added. When the I_2 had dissolved, the solution was transferred to an NMR tube and the sample was analyzed by NMR. ^1H NMR (500 MHz, 25 °C, CD_2Cl_2) δ 8.07 (2H, H2/6), 7.16 (2H, H3/5), 2.37 (3H, -CH_3); ^{13}C NMR (126 MHz, 25 °C, CD_2Cl_2) δ 139.1 (C2/6), 127.4 (C3/5), 20.6 (-CH_3); ^{15}N NMR (51 MHz, 25 °C, CD_2Cl_2) δ −98.9.

Dibenzofuran complexes (attempts)

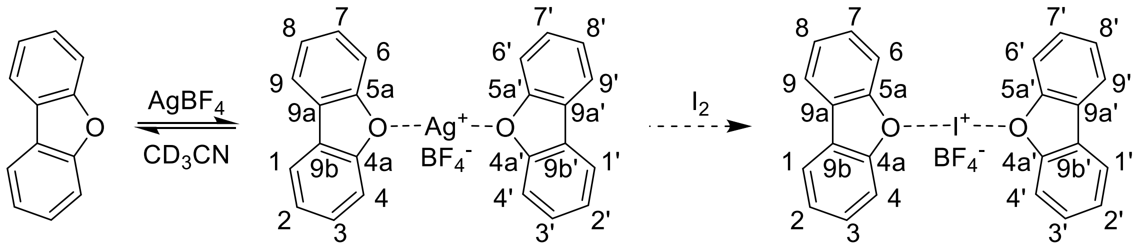

The attempt to form [bis(dibenzofuran)silver(I)]$^+$ tetrafluroborate was carried out as follows. In a glovebox, dibenzofuran (0.004 g, 0.024 mmol) was dissolved in CD_3CN (0.4 mL) and transferred to a vial containing $AgBF_4$ (0.003 g, 0.015 mmol, 0.6 equiv). The resulting solution was transferred to an NMR tube. ^{1}H NMR (500 MHz, 25 °C, CD_3CN) δ 8.07 (ddd, *J* = 7.7, 1.3, 0.7 Hz, 4H, H4/4'/6/6'), 7.62 (ddd, *J* = 8.4, 1.0, 0.7 Hz, 4H, H1/1'/9/9'), 7.51 (ddd, *J* = 8.4, 7.3, 1.3 Hz, 4H, H2/2'/8/8'), 7.40 (ddd, *J* = 7.7, 7.3, 1.0 Hz, 4H, H3/3'/7/7'); ^{13}C NMR (126 MHz, detected via HMCB and HSQC at 500 MHz for ^{1}H, 25 °C, CD_3CN) δ 156.5 (C4a/4a'/5a/5a'), 125.9 (9a/9a'/9b/9b'), 122.5 (C2/2'/8/8'), 118.0 (C3/3'/7/7'), 116.0 (C4/4'/6/6'), 106.5 (C1/1'/9/9').

The attempt to form [bis(dibenzofuran)iodine(I)]$^+$ tetrafluroborate was performed as follows. In a glovebox, I_2 (0.031 g, 0.12 mmol) was dissolved in CD_3CN (3.08 mL). A portion of the solution (0.2 mL, 0.008 mmol) was added to an NMR sample containing the product of the procedure described above (0.012 mmol "silver complex", 1.5 equiv). ^{1}H NMR (500 MHz, 25 °C, CD_3CN) δ 8.07 (ddd, *J* = 7.7, 1.3, 0.7 Hz, 4H, H4/4'/6/6'), 7.62 (ddd, *J* = 8.4, 1.0, 0.7 Hz, 4H, H1/1'/9/9'), 7.51 (ddd, *J* = 8.4, 7.3, 1.3 Hz, 4H, H2/2'/8/8'), 7.40 (ddd, *J* = 7.7, 7.3, 1.0 Hz, 4H, H3/3'/7/7'); ^{13}C NMR (126 MHz, detected via HMCB and HSQC at 500 MHz for ^{1}H, 25 °C, CD_3CN) δ 157.5 (C4a/4a'/5a/5a'), 127.8 (9a/9a'/9b/9b'), 122.0 (C2/2'/8/8'), 118.6 (C3/3'/7/7'), 116.3 (C4/4'/6/6'), 106.9 (C1/1'/9/9').

Halenium transfer reaction (iodocyclization):

The halocylclization of 4-penten-1-ol to form the 2-(iodomethyl)tetrahydrofuran was performed by adding of a solution of 4-penten-1-ol in CD_2Cl_2 (0.1 mL, 14 mg/mL, 16 µmol), to an NMR sample of complex (**1**-*OMe*)$_2$-I in CD_2Cl_2 which had been derived by starting from 8 mg of the silver complex **1**-*OMe* (6 µmol). Observation of 2-(iodomethyl)tetrahydrofuran by NMR and MS (EI) confirmed that iodonium transfer took place.

2. NMR SPECTRA OF SYNTHESIZED COMPOUNDS

2.1. 4-Methoxypyridine *N*-oxide and complexes

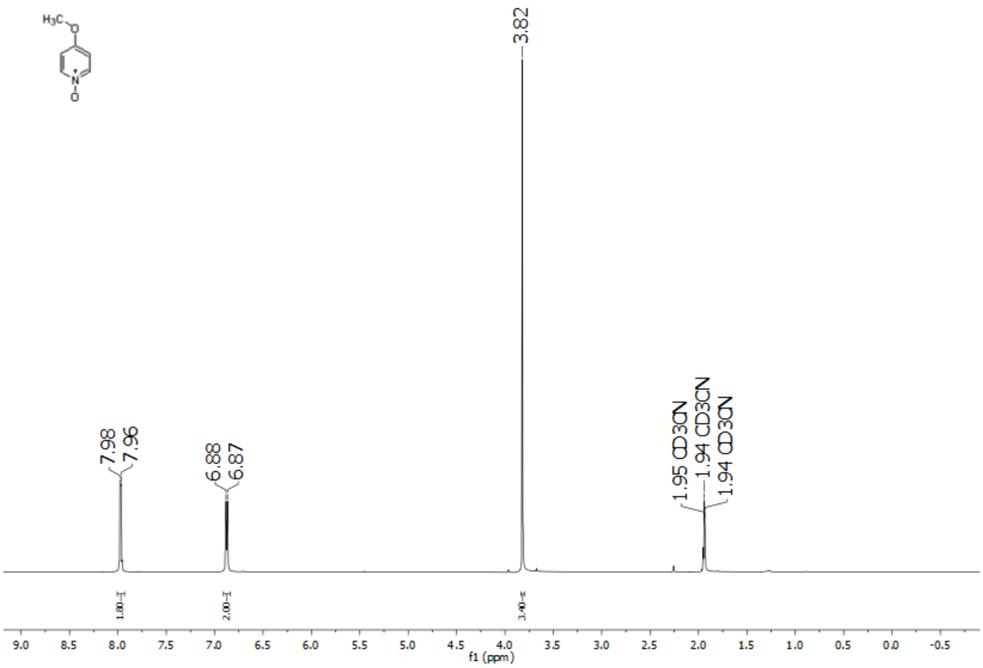

Figure S3. ^1H NMR spectrum of **1-*OMe*** (500 MHz, CD_3CN, 25 °C).

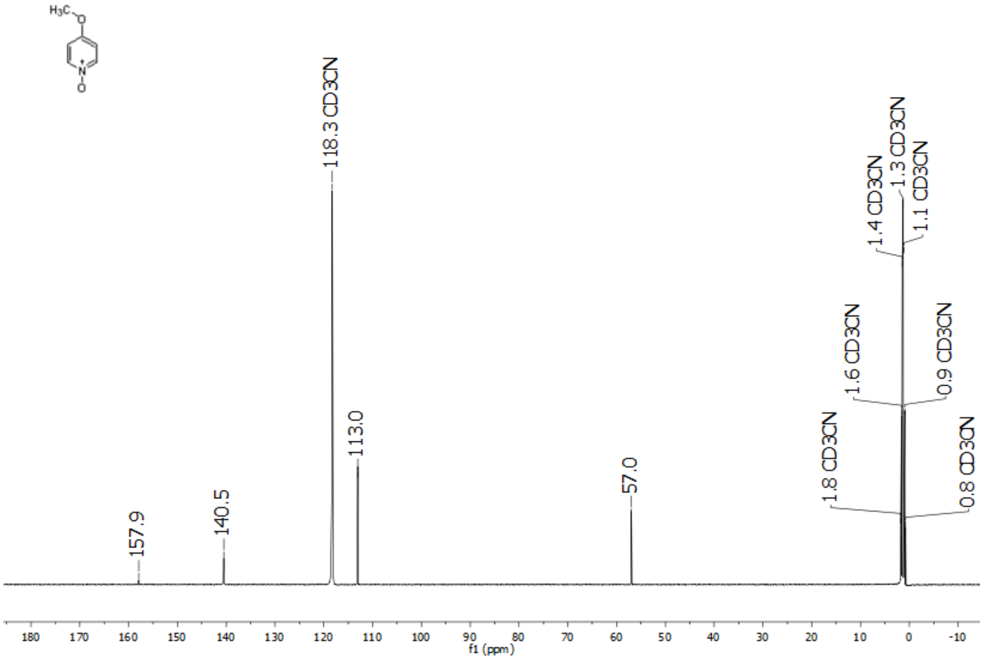

Figure S4. ^{13}C NMR spectrum of ***1-OMe*** (126 MHz, CD_3CN, 25 °C).

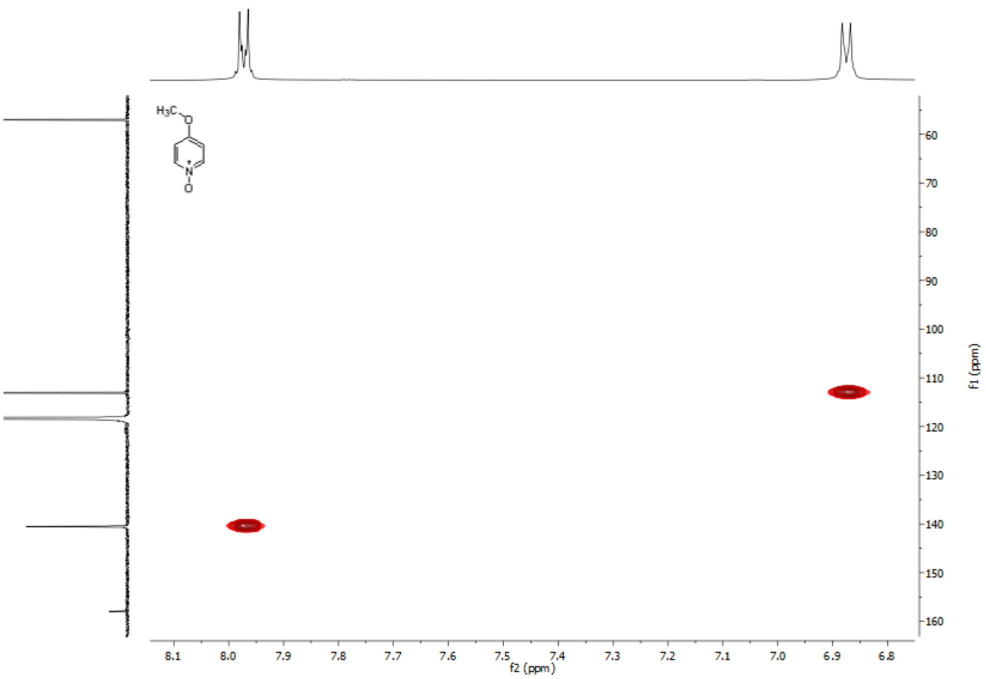

Figure S5. $^{1}H,^{13}C$ HSQC NMR spectrum of **1-*OMe*** (500 and 126 MHz, CD_3CN, 25 °C).

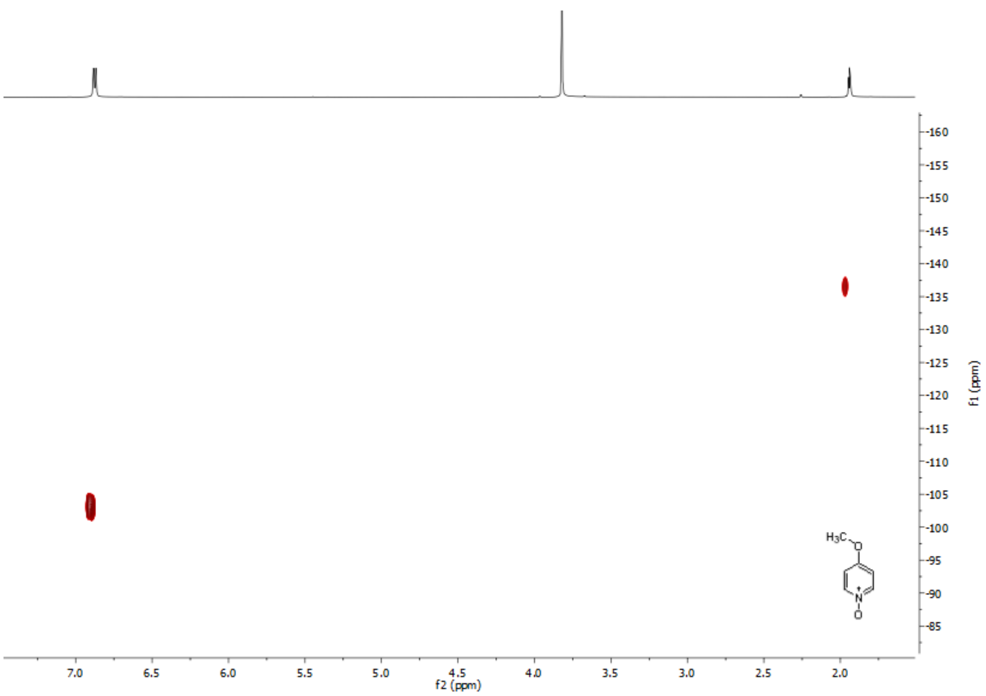

Figure S6. $^{1}H,^{15}N$ HMBC NMR spectrum of **1-*OMe*** (500 and 51 MHz, CD_3CN, 25 °C).

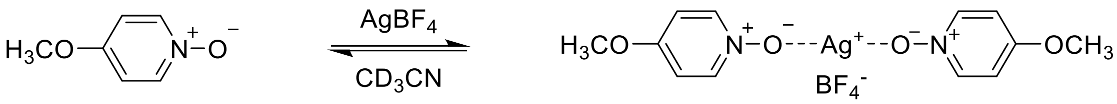

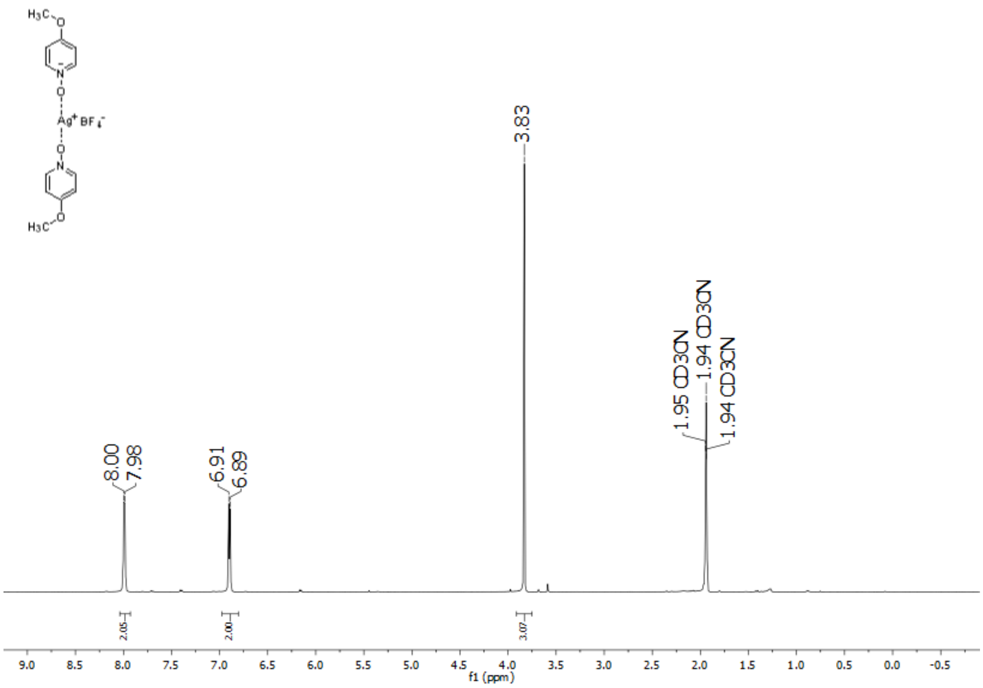

Figure S7. [1]H NMR spectrum of **(1-*OMe*)$_2$-Ag** (500 MHz, CD_3CN, 25 °C).

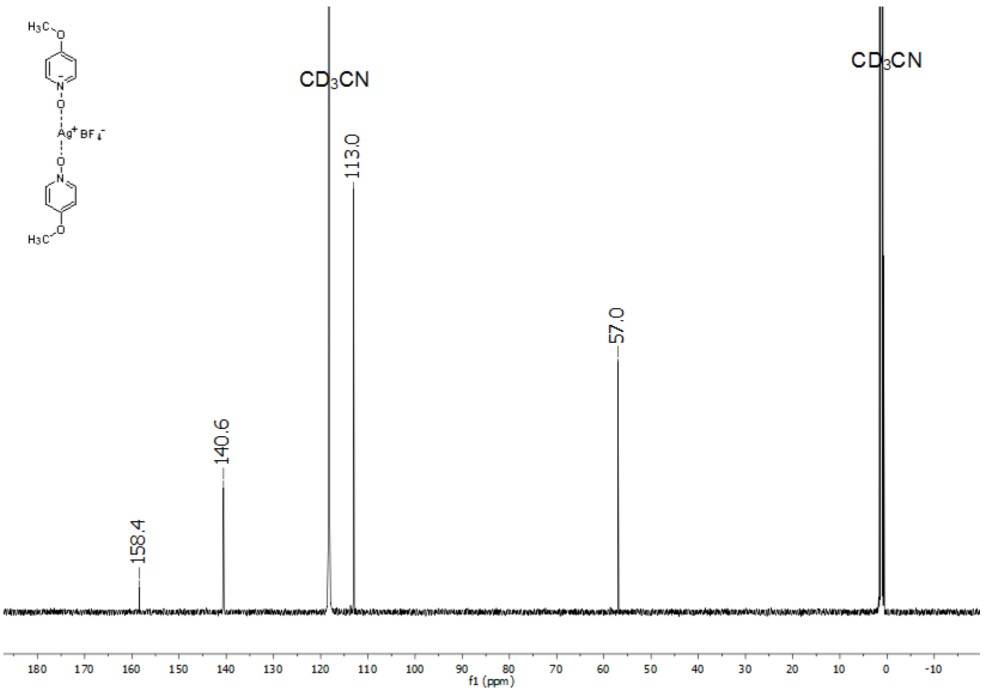

Figure S8. [13]C NMR spectrum of **(1-*OMe*)$_2$-Ag** (126 MHz, CD_3CN, 25 °C).

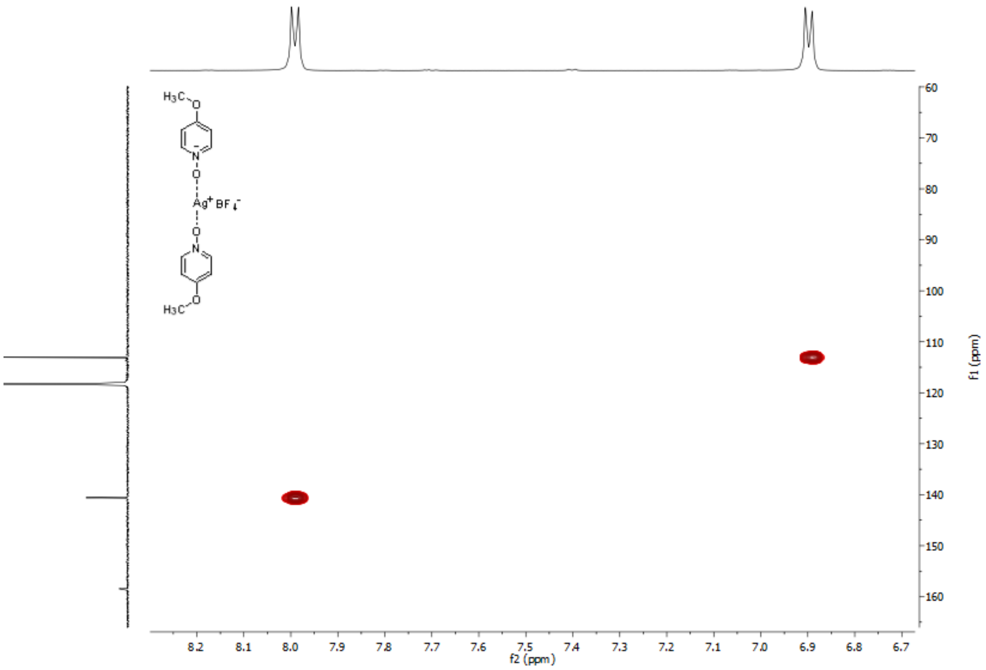

Figure S9. $^{1}H,^{13}C$ HSQC NMR spectrum of **(1-*OMe*)$_2$-Ag** (500 and 126 MHz, CD_3CN, 25 °C).

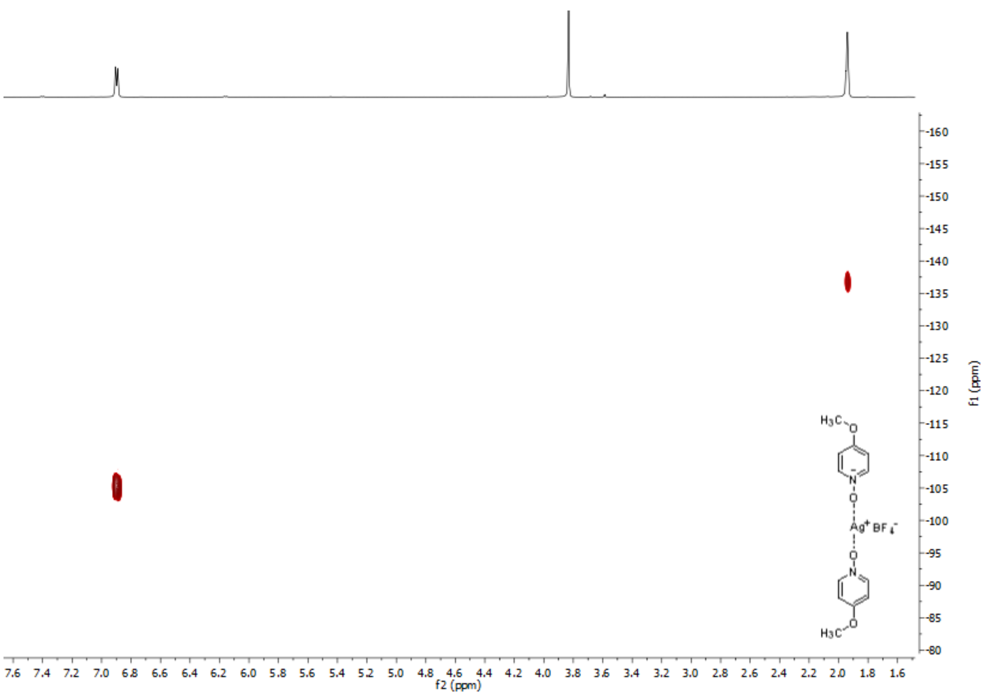

Figure S10. $^{1}H,^{15}N$ HMBC NMR spectrum of **(1-*OMe*)$_2$-Ag** (500 and 51 MHz, CD_3CN, 25 °C).

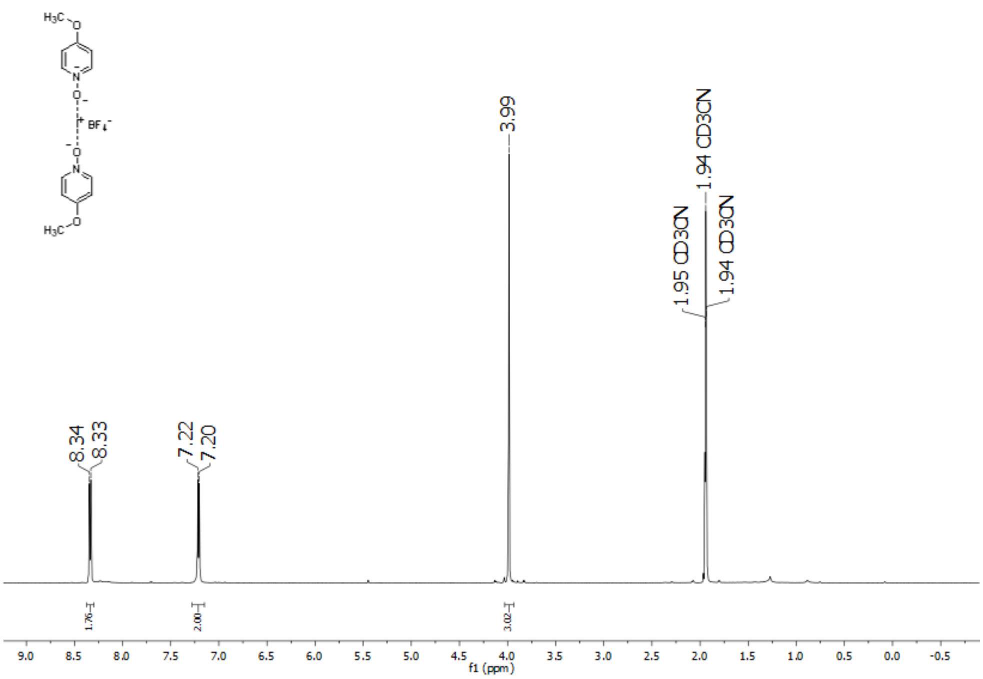

Figure S11. ^{1}H NMR spectrum of **(1-*OMe*)$_2$-I** (500 MHz, CD_3CN, 25 °C).

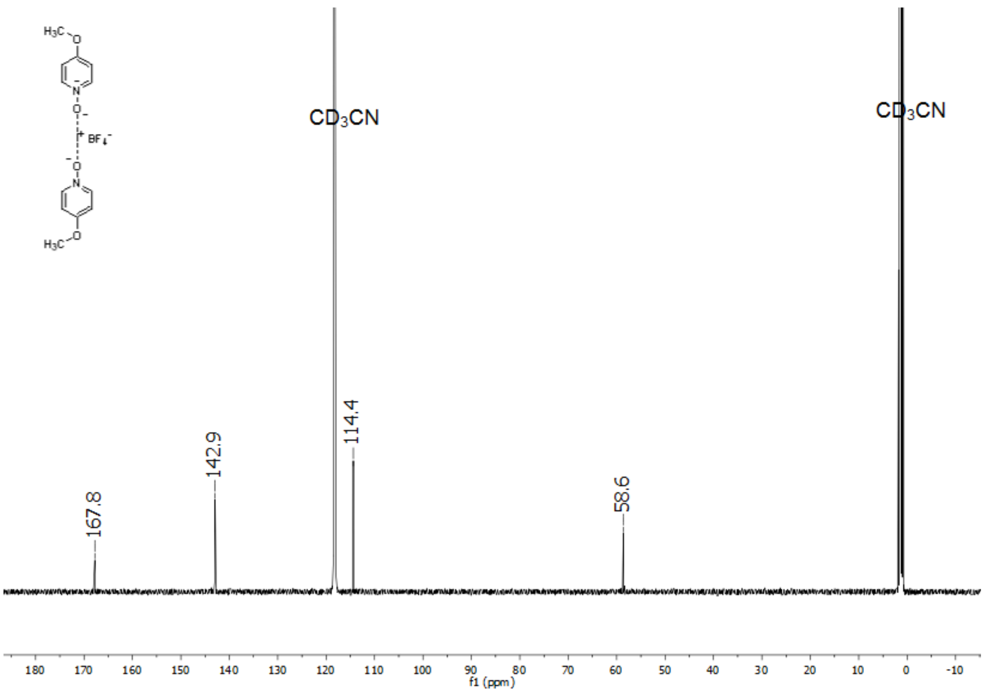

Figure S12. ^{13}C NMR spectrum of **(1-*OMe*)$_2$-I** (126 MHz, CD_3CN, 25 °C).

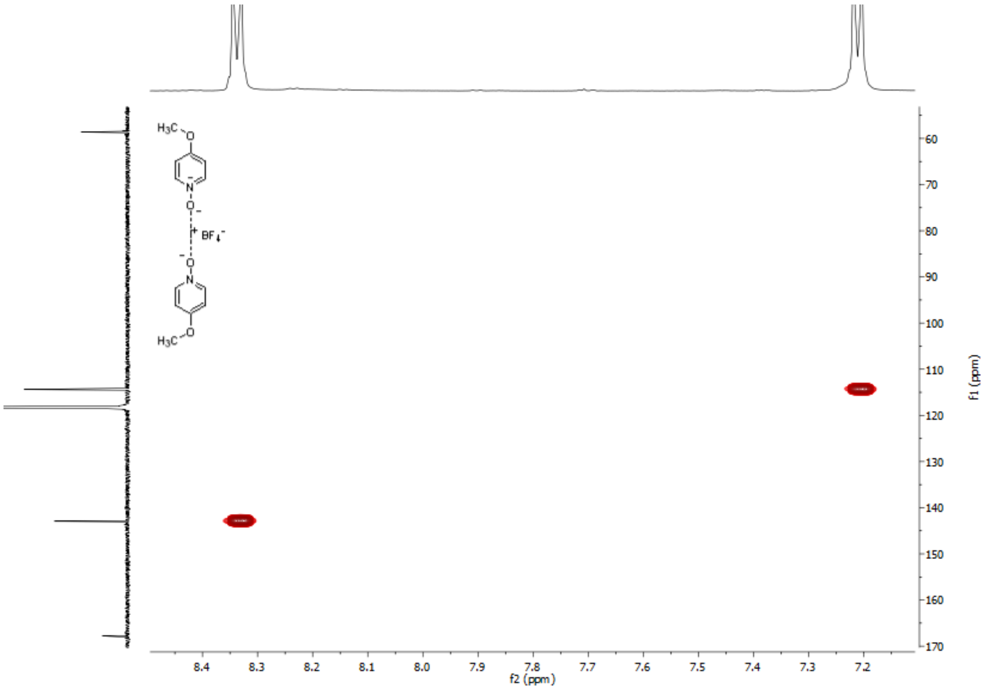

Figure S13. ¹H,¹³C HSQC NMR spectrum of **(1-*OMe*)₂-I** (500 and 126 MHz, CD_3CN, 25 °C).

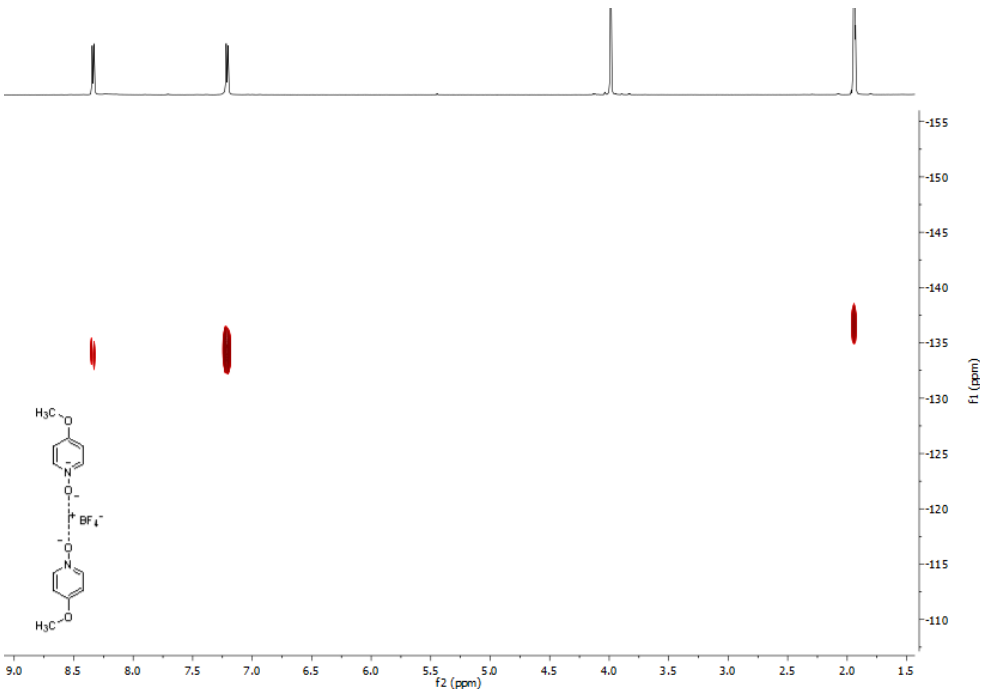

Figure S14. ¹H,¹⁵N HMBC NMR spectrum of **(1-*OMe*)₂-I** (500 and 51 MHz, CD_3CN, 25 °C).

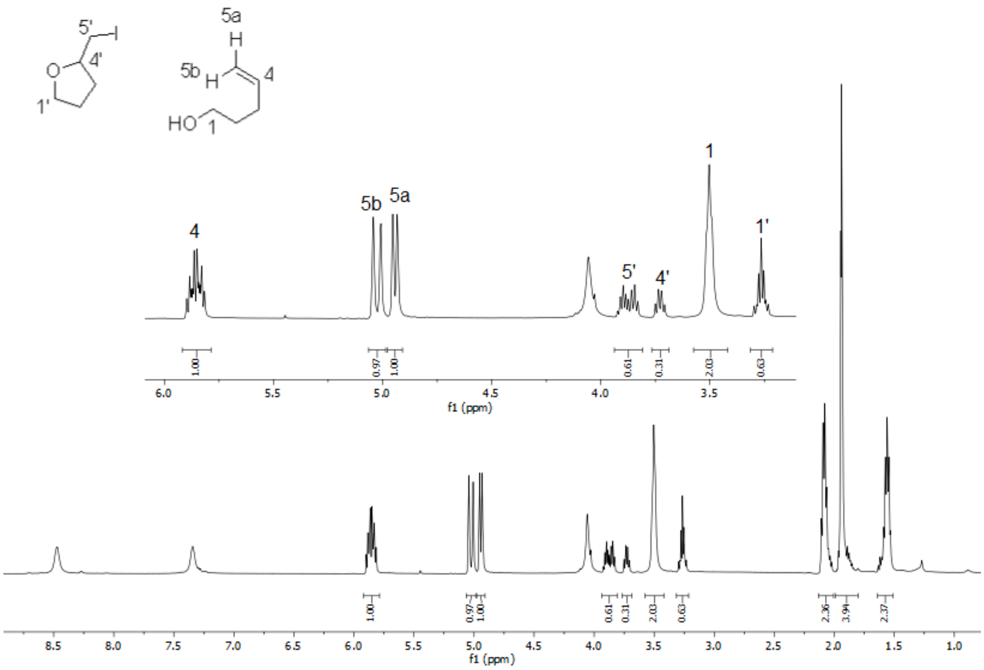

Figure S15. After addition of 4-penten-1-ol (20 µmol) to **(1-*OMe*)$_2$-I** (8.7 µmol), both the alkene itself and the iodocyclized product are visible in the resulting ^{1}H NMR spectrum.

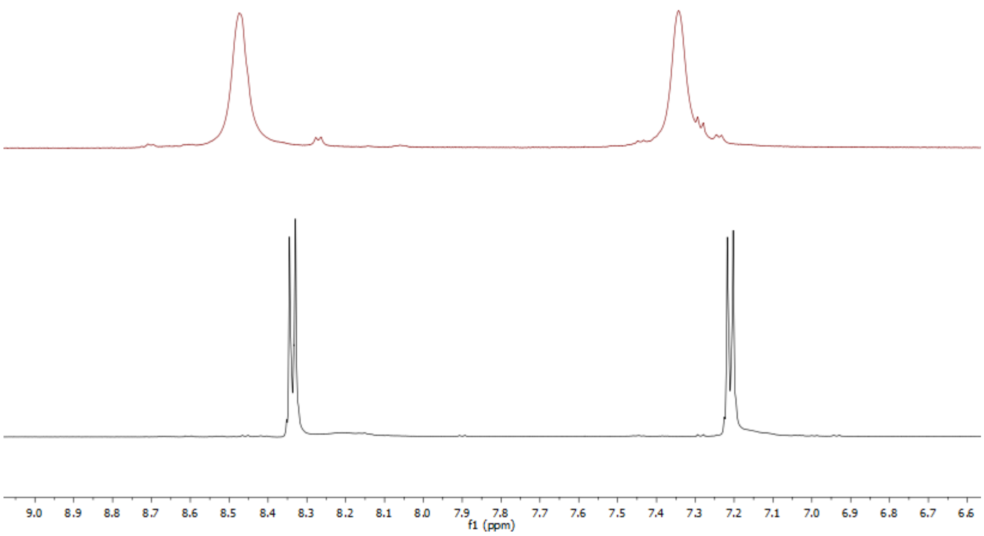

Figure S16. The ^{1}H spectra in CD_3CN of the I^+ complex **(1-*OMe*)$_2$-I** (8.7 µmol) (bottom), and after addition of 4-penten-1-ol (2 µL, 20 µmol, 2.3 equiv.) (top). The pyridyl signals changed upon addition of the alkene, in accordance with an I^+ transfer, suggesting formation of **(1-*OMe*)$_2$-I** was successful.

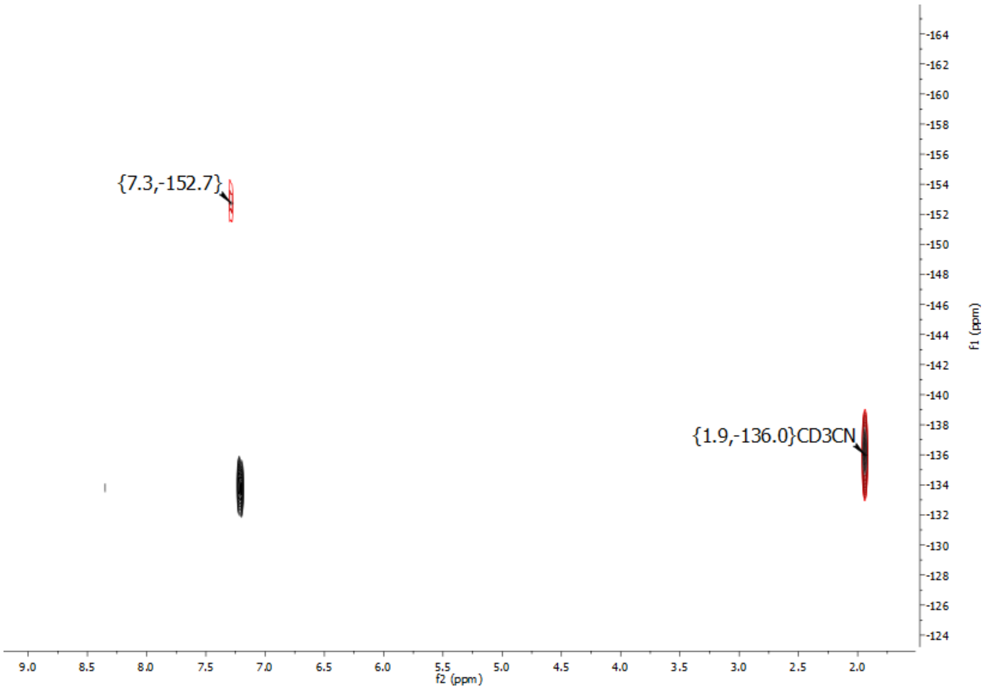

Figure S17. The stacked ^{1}H,^{15}N HMBC spectra in CD_3CN of **(1-*OMe*)$_2$-I** (8.7 µmol) (black), and after addition of 4-penten-1-ol (2 µL, 20 µmol, 2.3 equiv.) (red) with the new chemical shift indicated (−152.7). The substantial change further indicates an I^+ transfer from **(1-*OMe*)$_2$-I** when the alkene is added, which is further evidence for successful formation of the iodine(I) complex **(1-*OMe*)$_2$-I**.

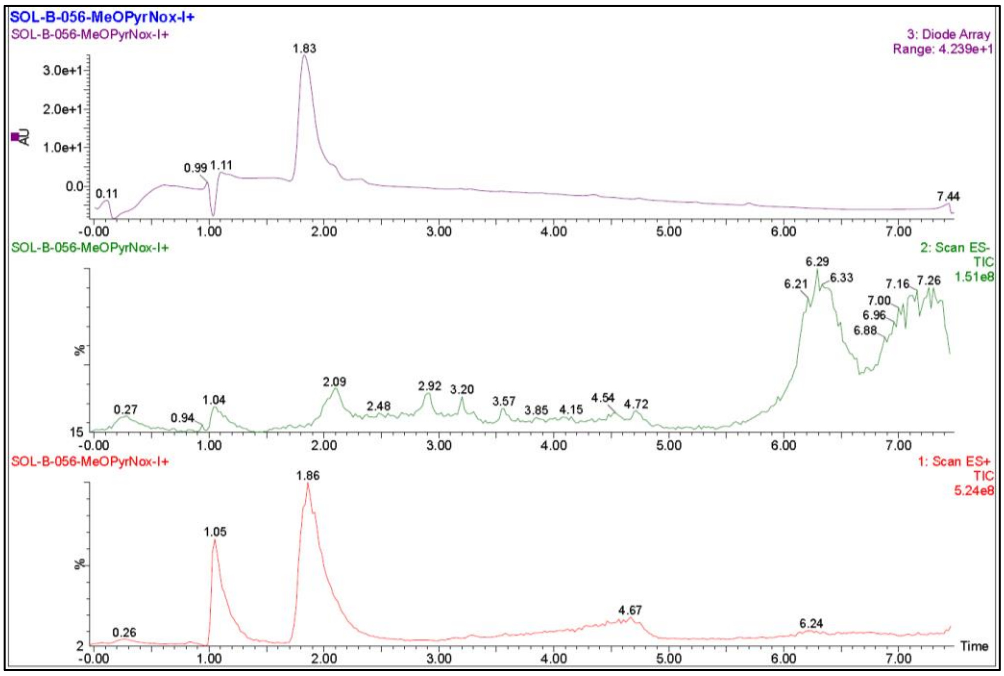

Figure S18. LC-MS chromatograms of **(1-*OMe*)$_2$-I**.

Figure S19. LC-MS mass spectrum (positive mode) of the peak at 1.9 minutes of **(1-*OMe*)$_2$-I**, which shows a peak consistent with the mass to charge of the protonated ligand.

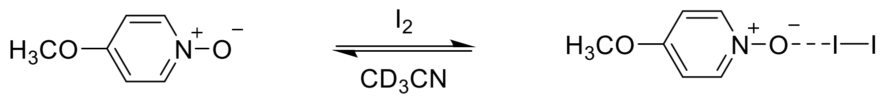

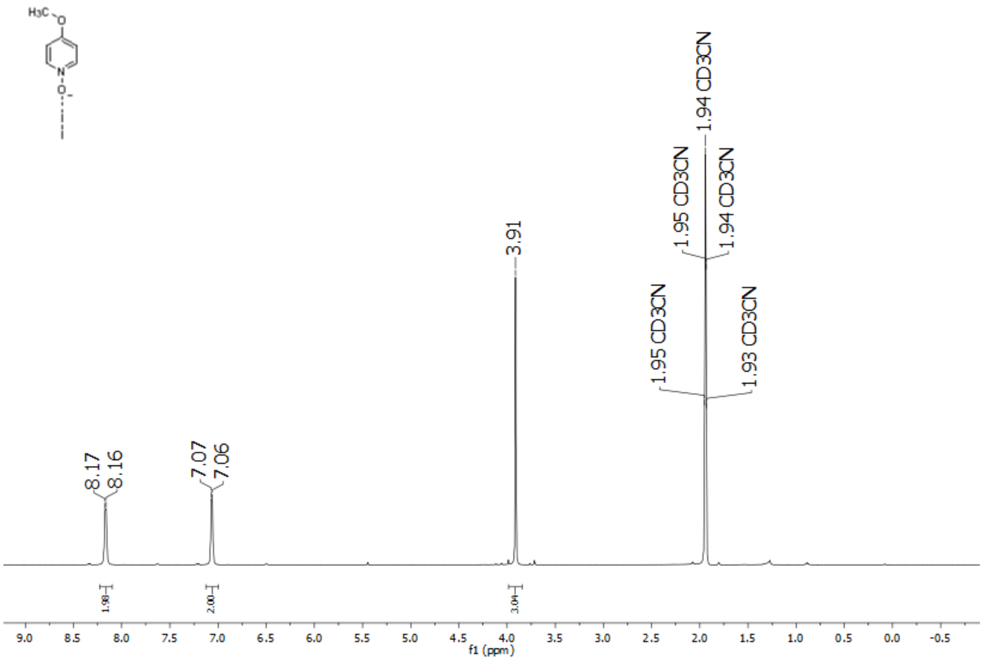

Figure S20. [1]H NMR spectrum of the control solution of **(1-*OMe*)-I₂** (500 MHz, CD_3CN, 25 °C).

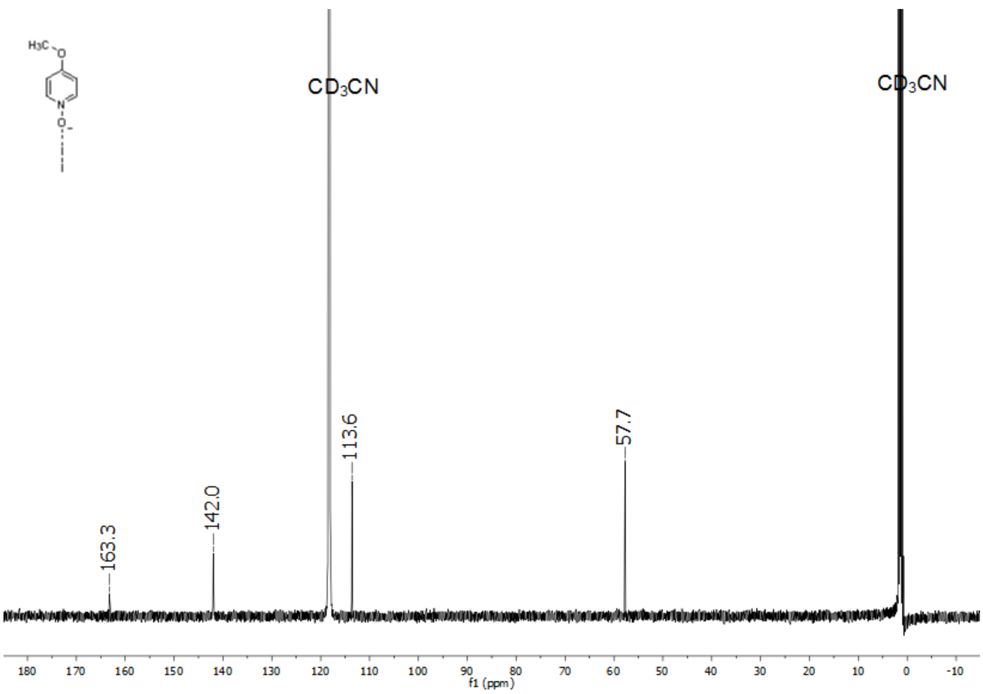

Figure S21. [13]C NMR spectrum of the control solution of **(1-*OMe*)-I_2** (126 MHz, CD_3CN, 25 °C).

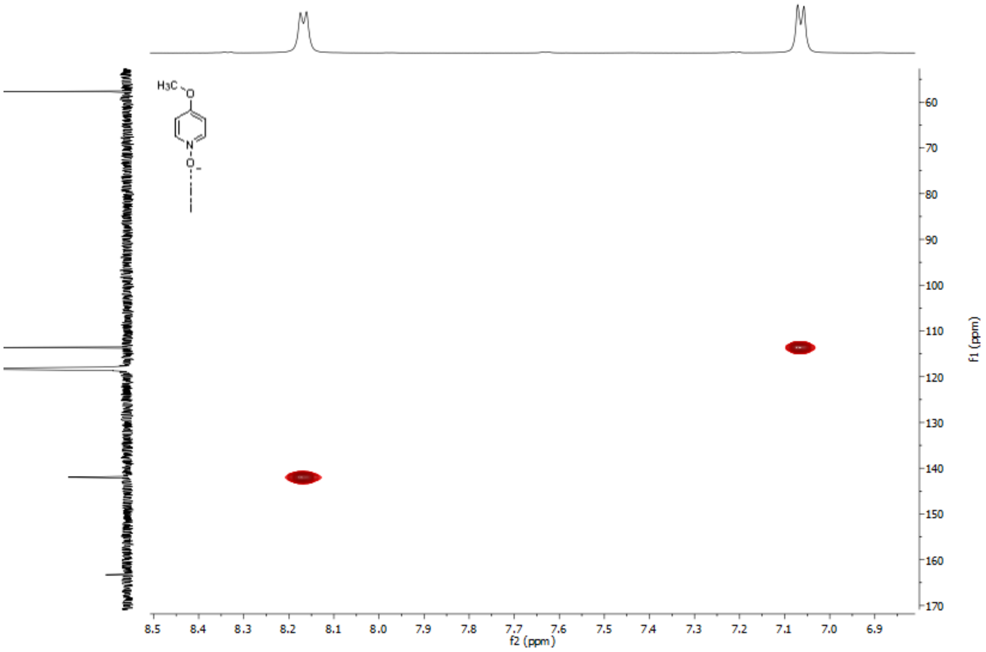

Figure S22. $^{1}H,^{13}C$ HSQC NMR spectrum of the control solution of **(1-*OMe*)-I_2** (500 and 126 MHz, CD_3CN, 25 °C).

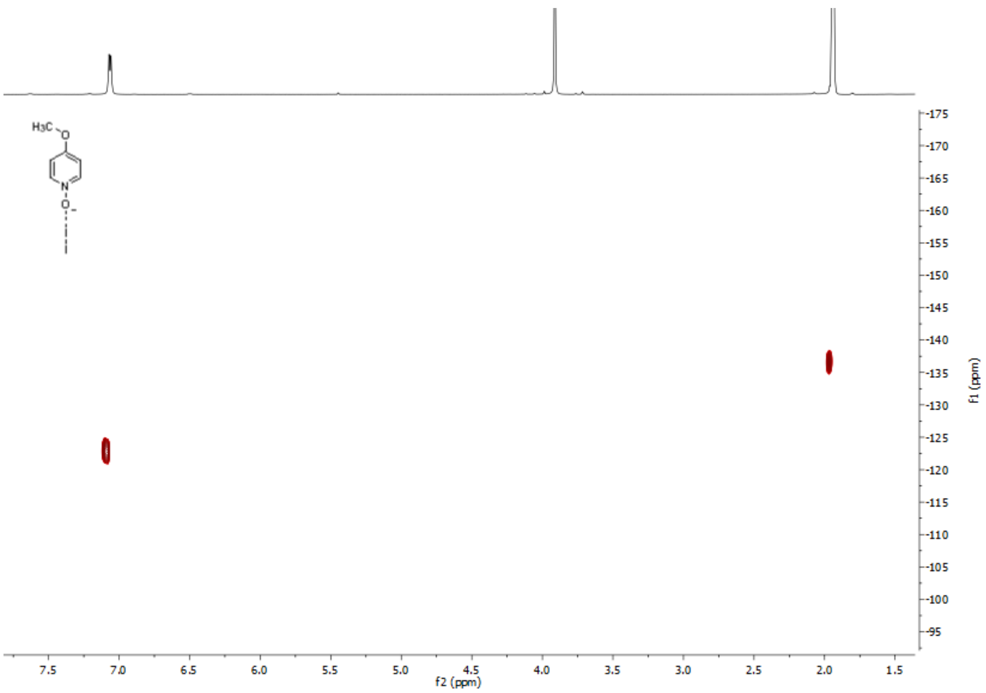

Figure S23. $^{1}H,^{15}N$ HMBC NMR spectrum of the control solution of **(1-*OMe*)-I_2** (500 and 51 MHz, CD_3CN, 25 °C).

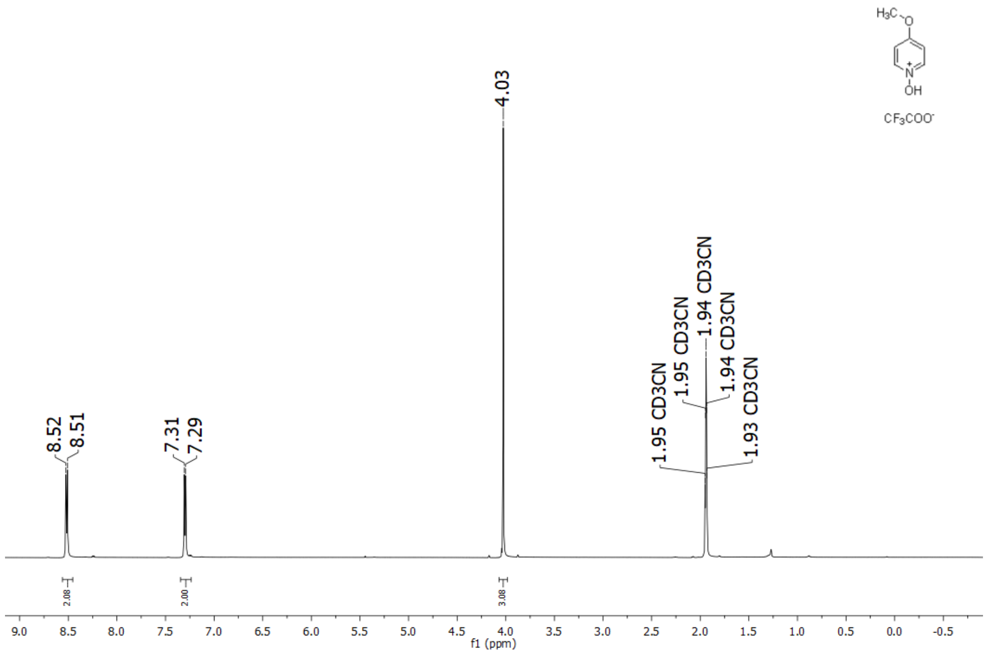

Figure 24. ^{1}H NMR spectrum of **(1-*OMe*)-H** (500 MHz, CD_3CN, 25 °C).

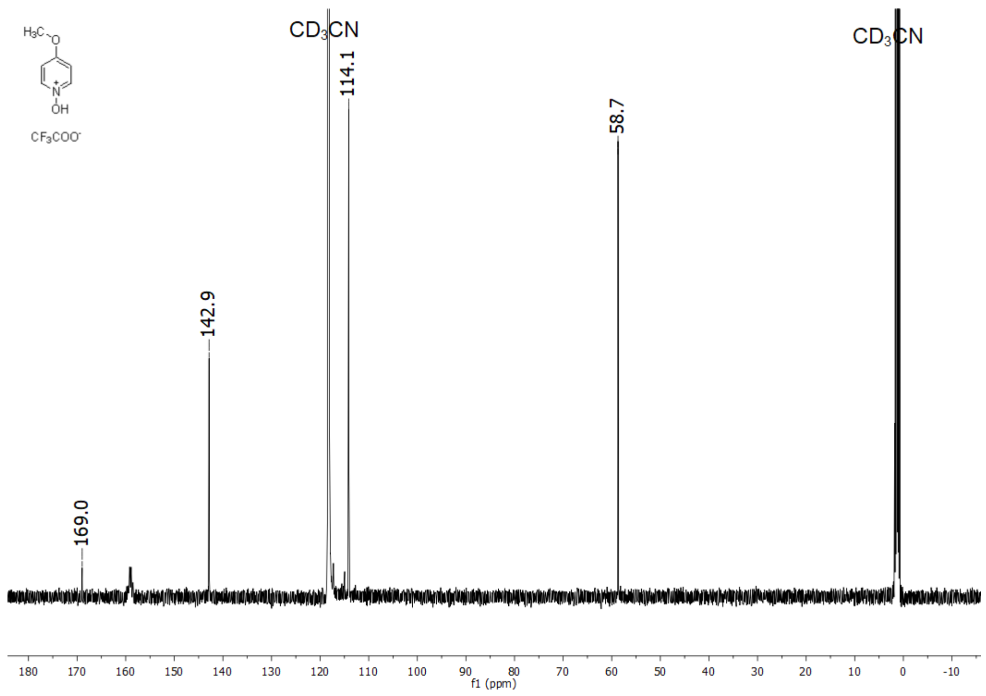

Figure 25. ^{13}C NMR spectrum of **(1-*OMe*)-H** (126 MHz, CD_3CN, 25 °C).

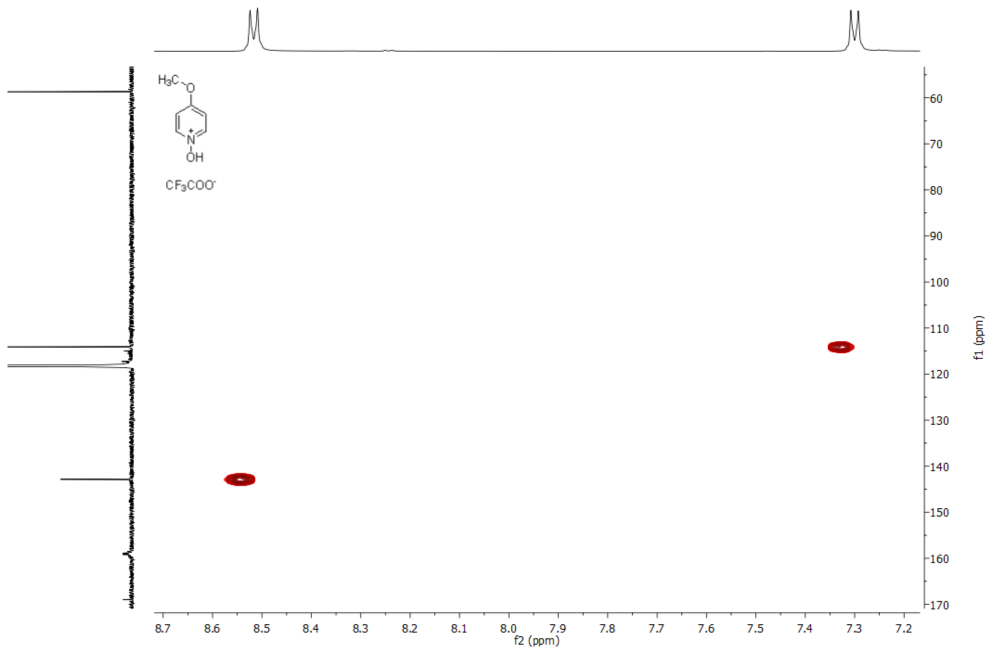

Figure 26. $^{1}H,^{13}C$ HSQC NMR spectrum of **(1-*OMe*)-H** (500 and 126 MHz, CD_3CN, 25 °C).

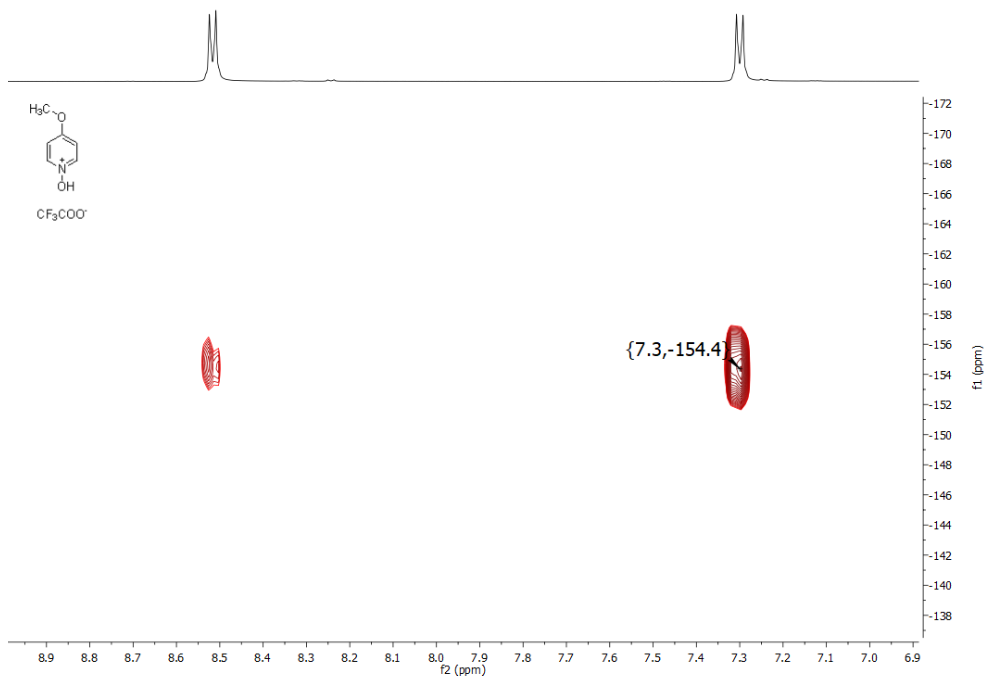

Figure 27. $^{1}H,^{15}N$ HMBC NMR spectrum of **(1-*OMe*)-H** (500 and 51 MHz, CD_3CN, 25 °C).

2.2. 4-Methylpyridine *N*-oxide and complexes

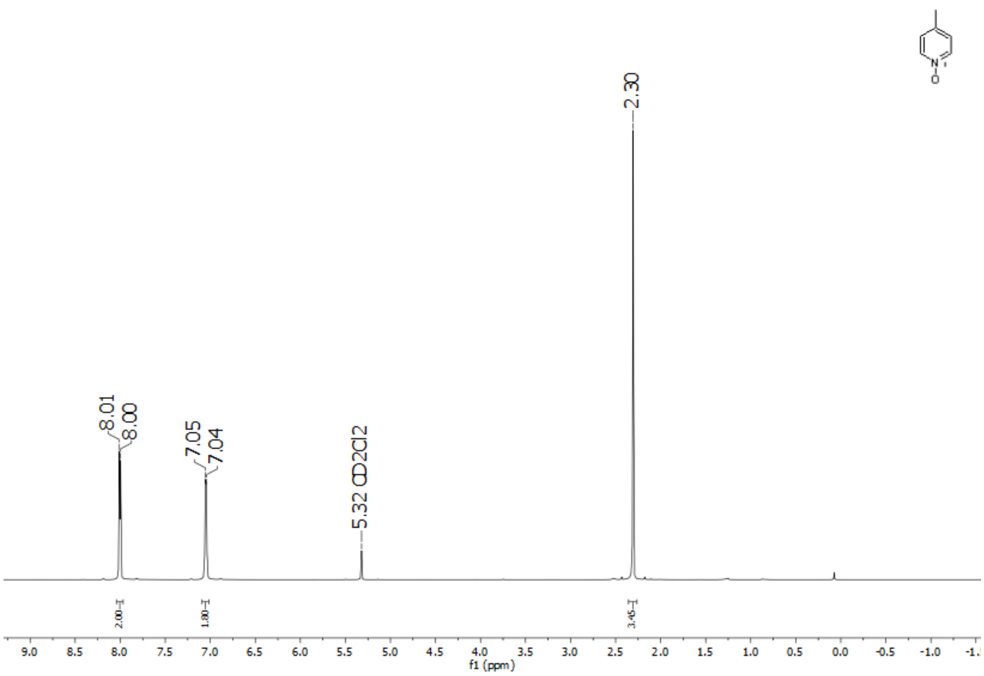

Figure S28. ^{1}H NMR spectrum of **1-*Me*** (500 MHz, CD_2Cl_2, 25 °C).

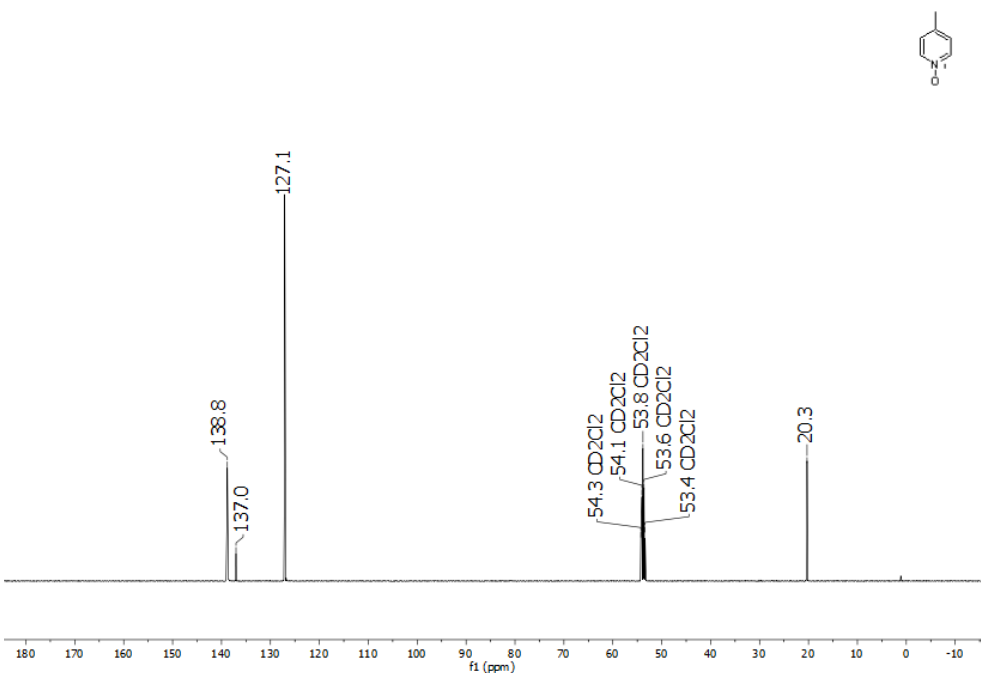

Figure S29. ^{13}C NMR spectrum of **1-*Me*** (126 MHz, CD_2Cl_2, 25 °C).

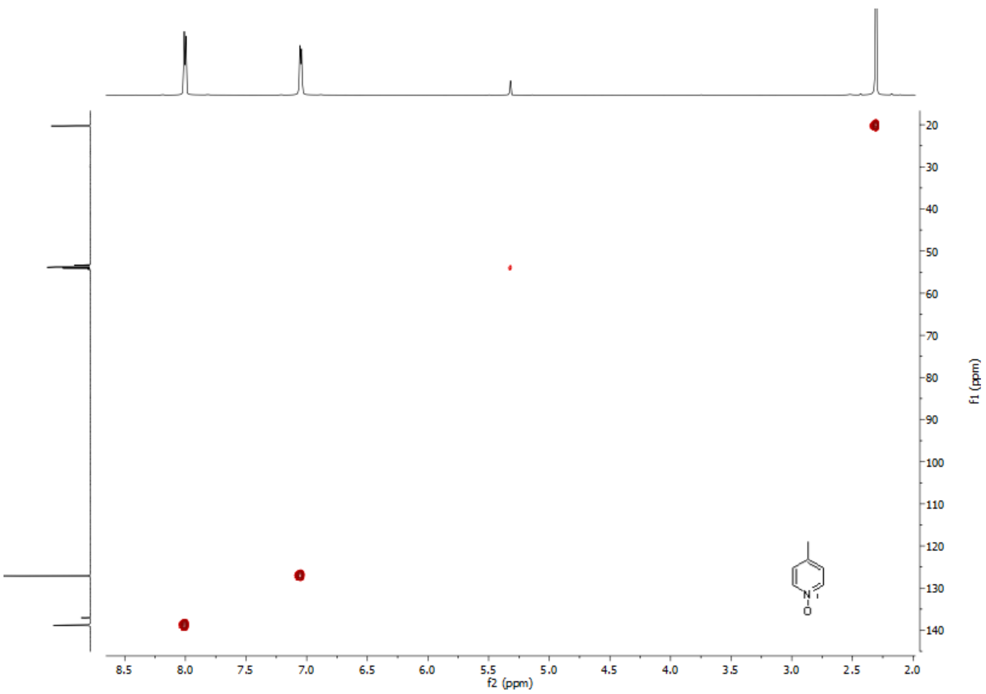

Figure S30. $^{1}H,^{13}C$ HSQC NMR spectrum of **1-*Me*** (500 and 126 MHz, CD_2Cl_2, 25 °C).

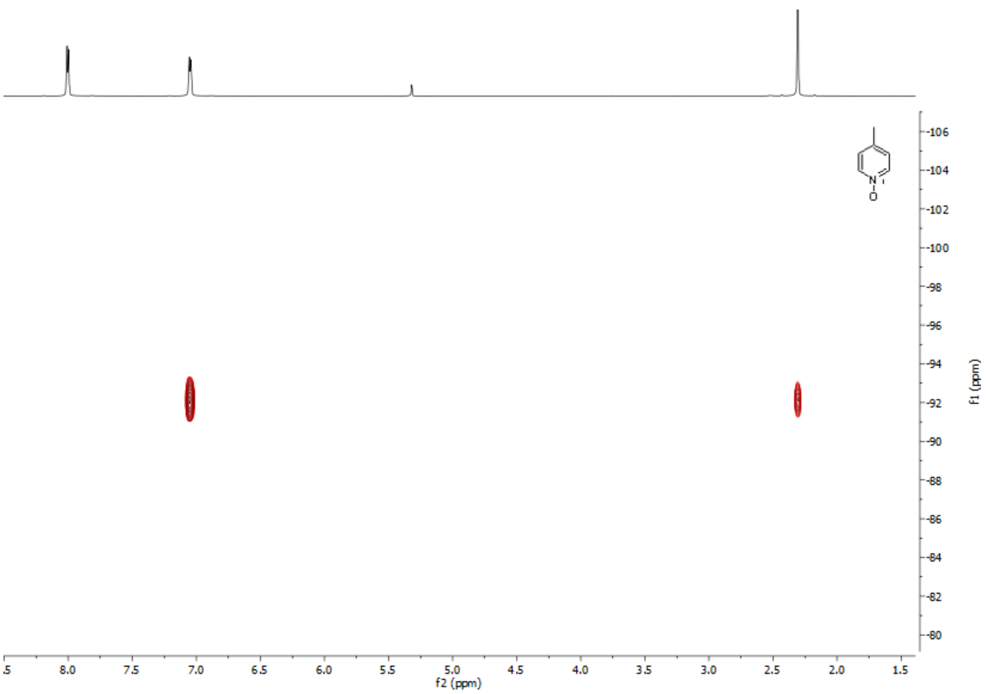

Figure S31. $^{1}H,^{15}N$ HMBC NMR spectrum of **1-*Me*** (500 and 51 MHz, CD_2Cl_2, 25 °C).

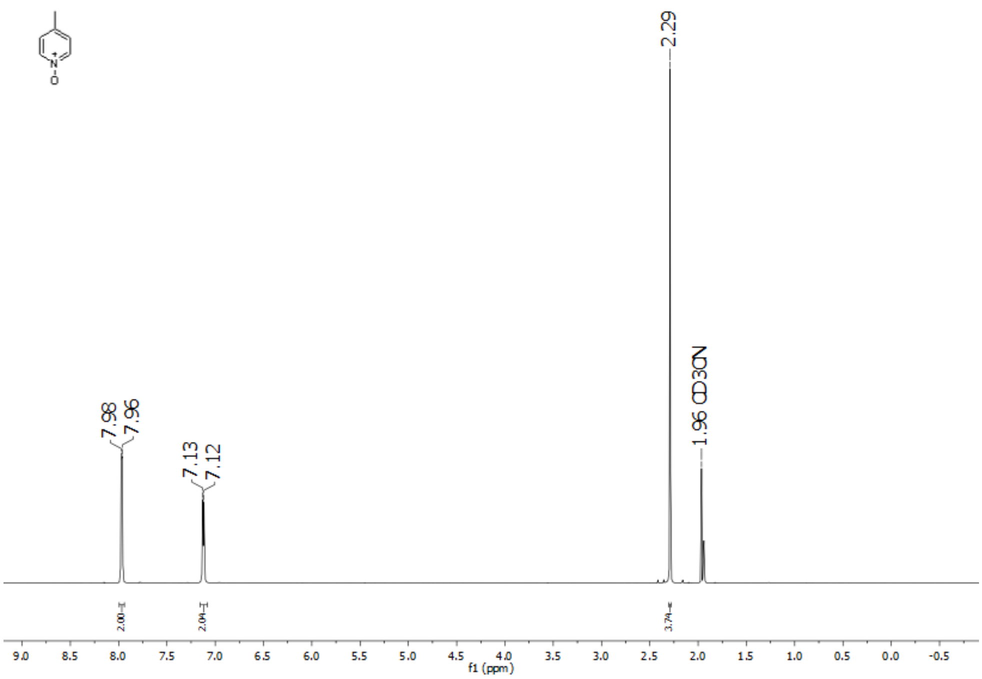

Figure S32. ^{1}H NMR spectrum of **1-*Me*** (500 MHz, CD_3CN, 25 °C).

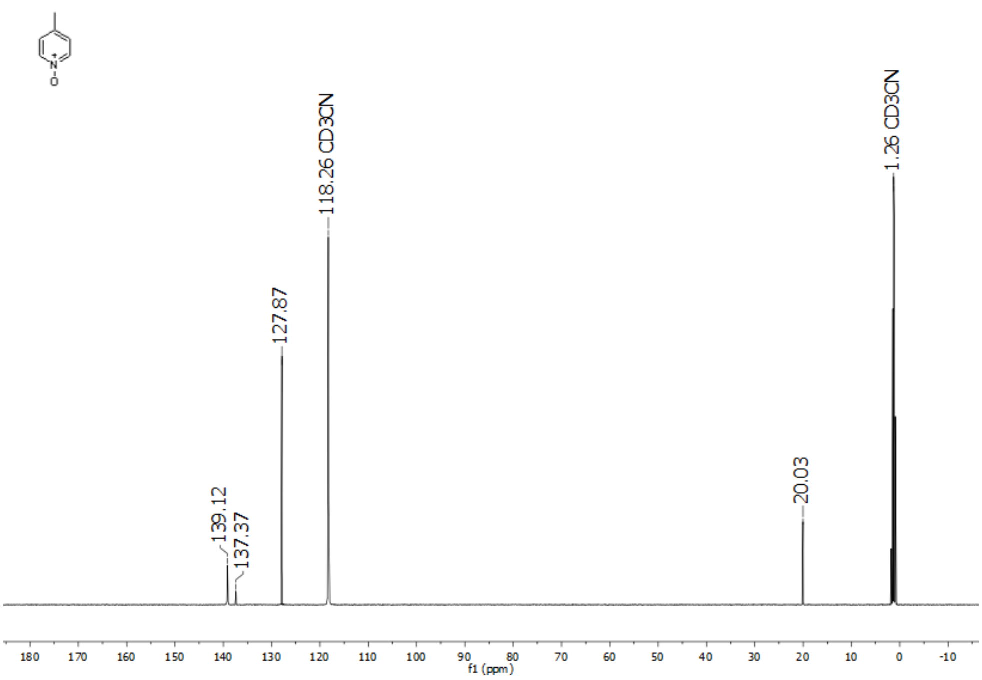

Figure S33. ^{13}C NMR spectrum of **1-*Me*** (126 MHz, CD_3CN, 25 °C).

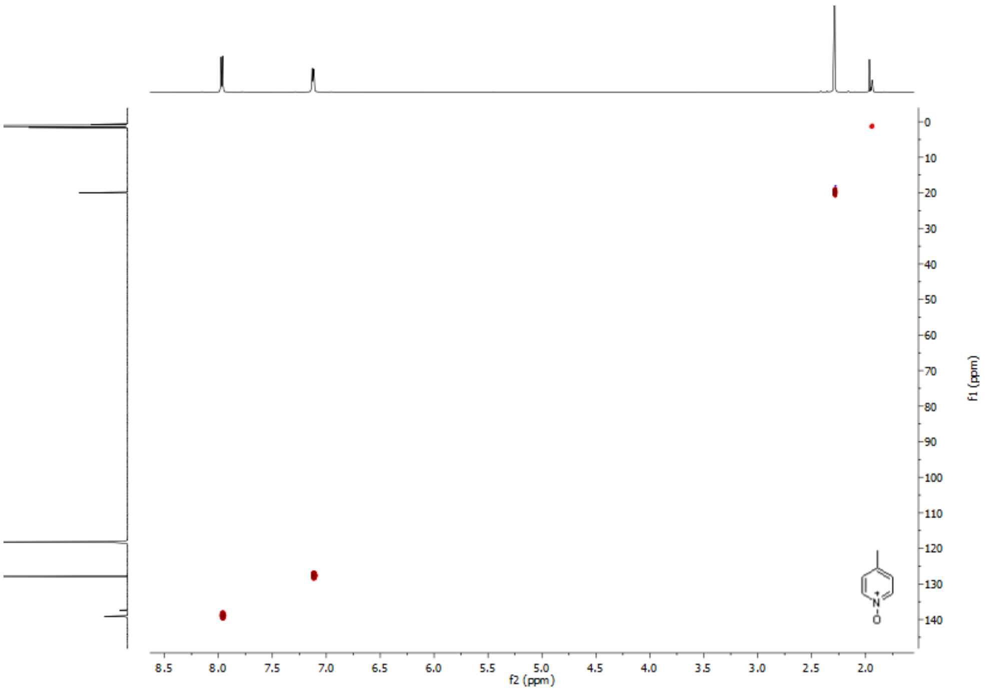

Figure S34. $^{1}H,^{13}C$ HSQC NMR spectrum of **1-*Me*** (500 and 126 MHz, CD_3CN, 25 °C).

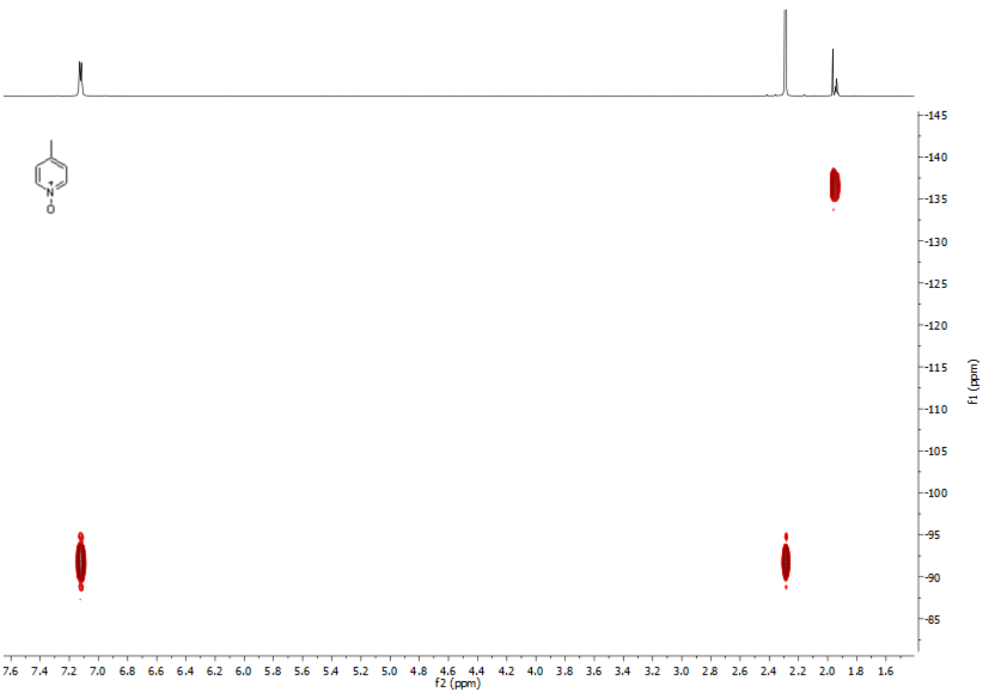

Figure S35. $^{1}H,^{15}N$ HMBC NMR spectrum of **1-*Me*** (500 and 51 MHz, CD_3CN, 25 °C).

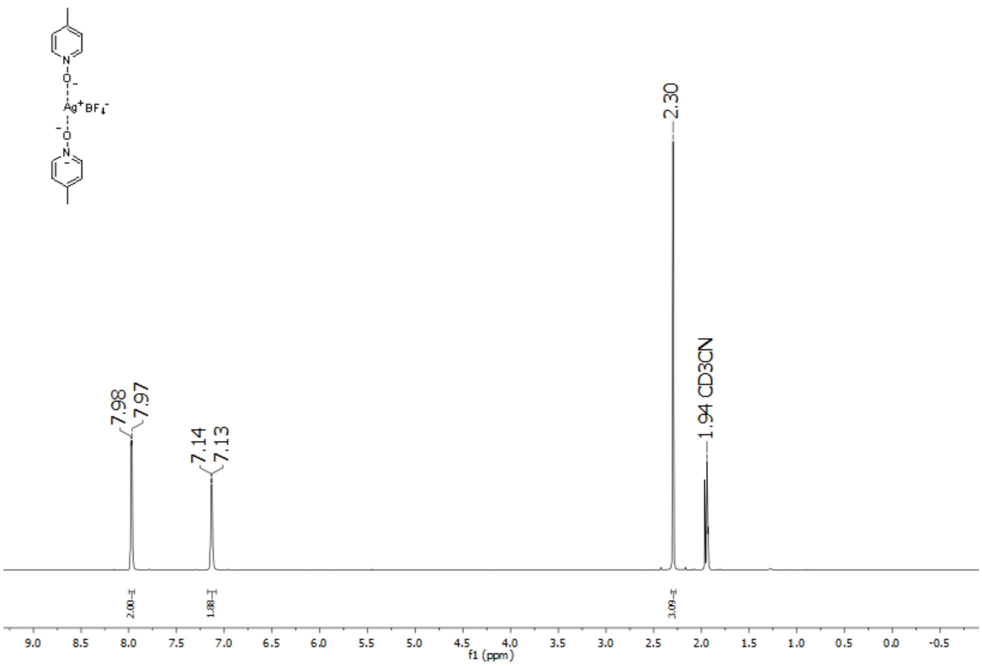

Figure S36. [1]H NMR spectrum of **(1-*Me*)$_2$-Ag** (500 MHz, CD_3CN, 25 °C).

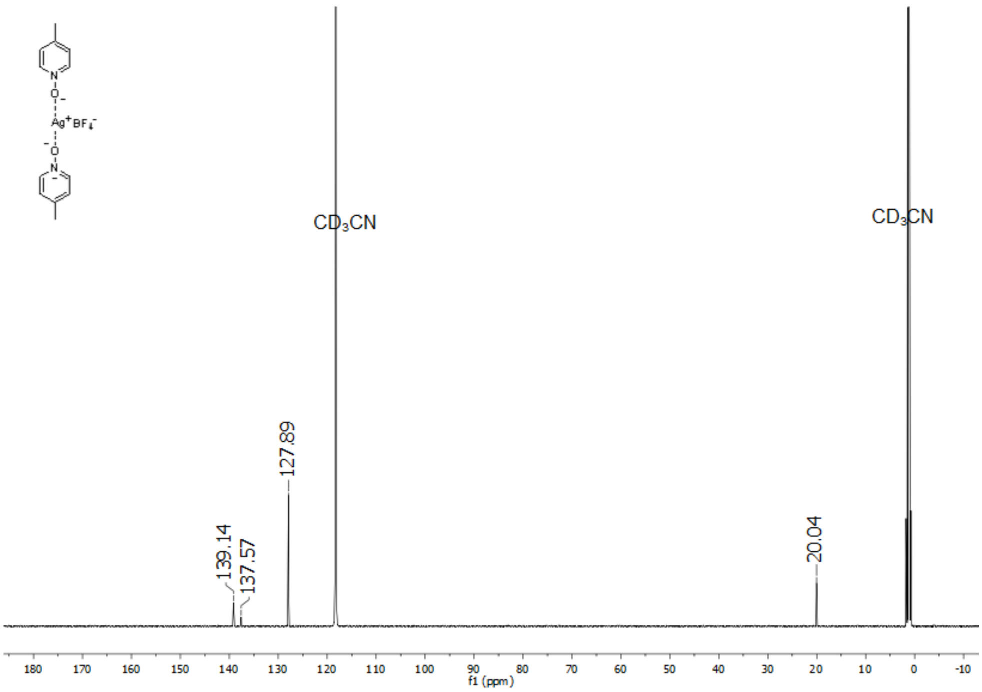

Figure S37. [13]C NMR spectrum of **(1-*Me*)$_2$-Ag** (126 MHz, CD_3CN, 25 °C).

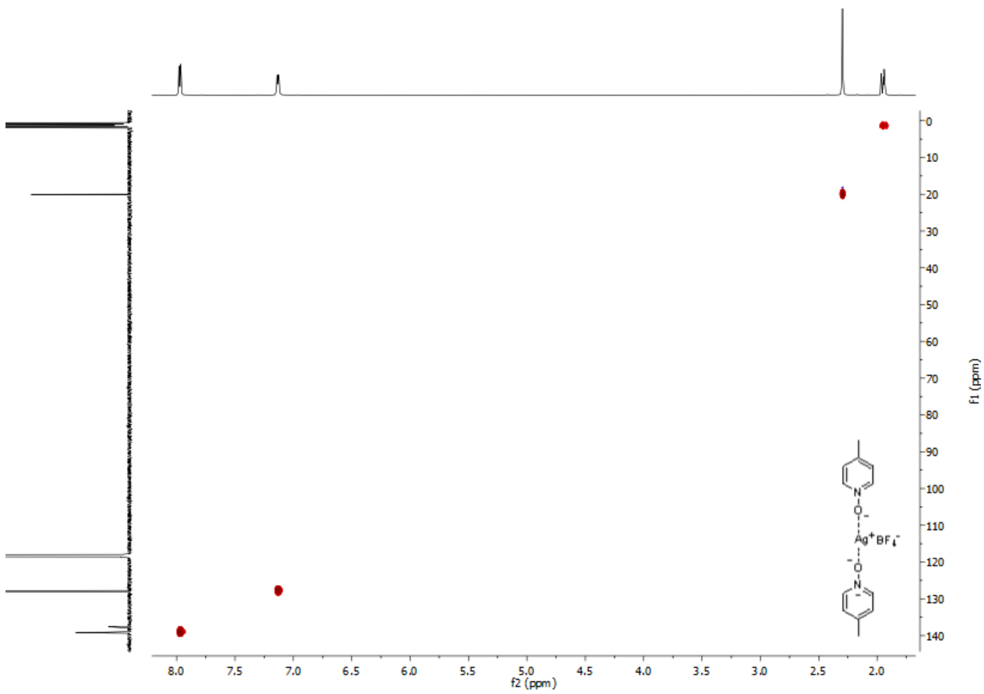

Figure S38. $^{1}H,^{13}C$ HSQC NMR spectrum of **(1-*Me*)$_2$-Ag** (500 and 126 MHz, CD_3CN, 25 °C).

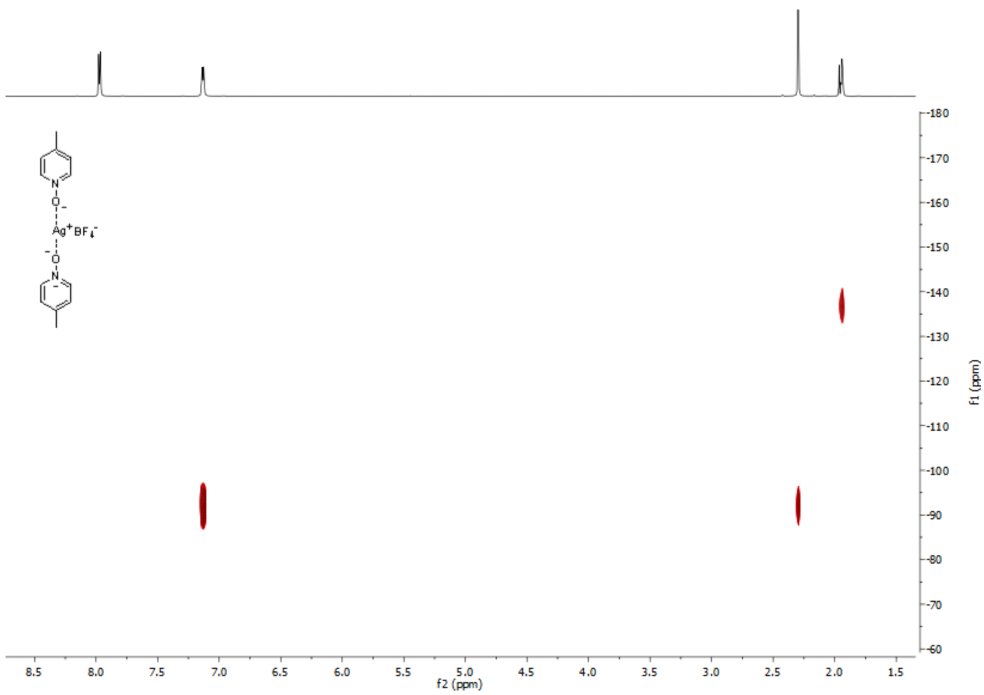

Figure S39. $^{1}H,^{15}N$ HMBC NMR spectrum of **(1-*Me*)$_2$-Ag** (500 and 51 MHz, CD_3CN, 25 °C).

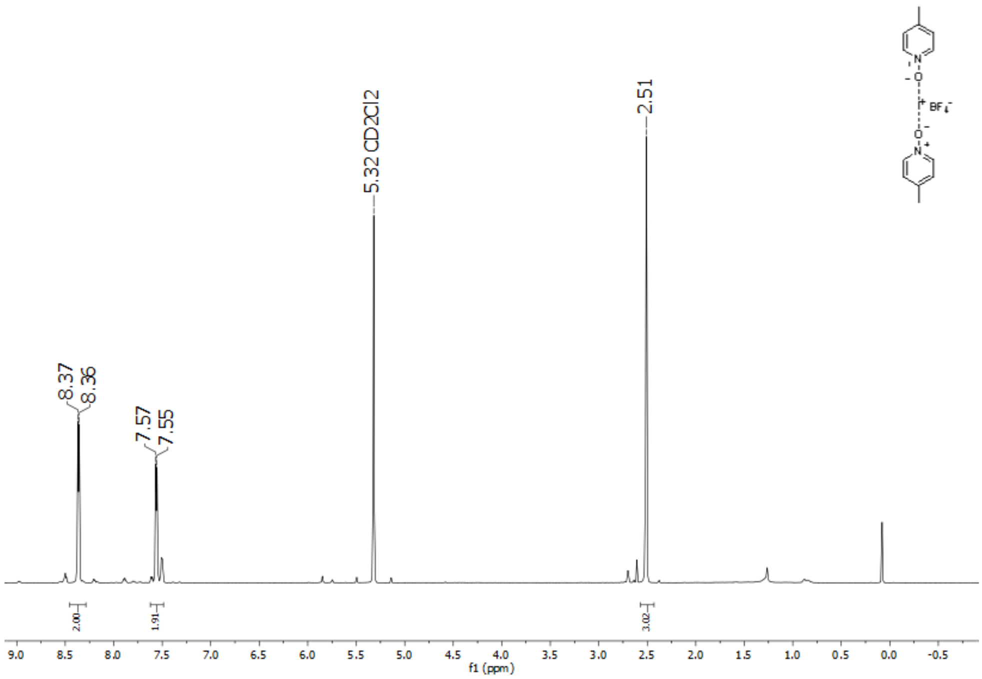

Figure S40. ^{1}H NMR spectrum of **(1-*Me*)$_2$-I** (500 MHz, CD_2Cl_2, 25 °C).

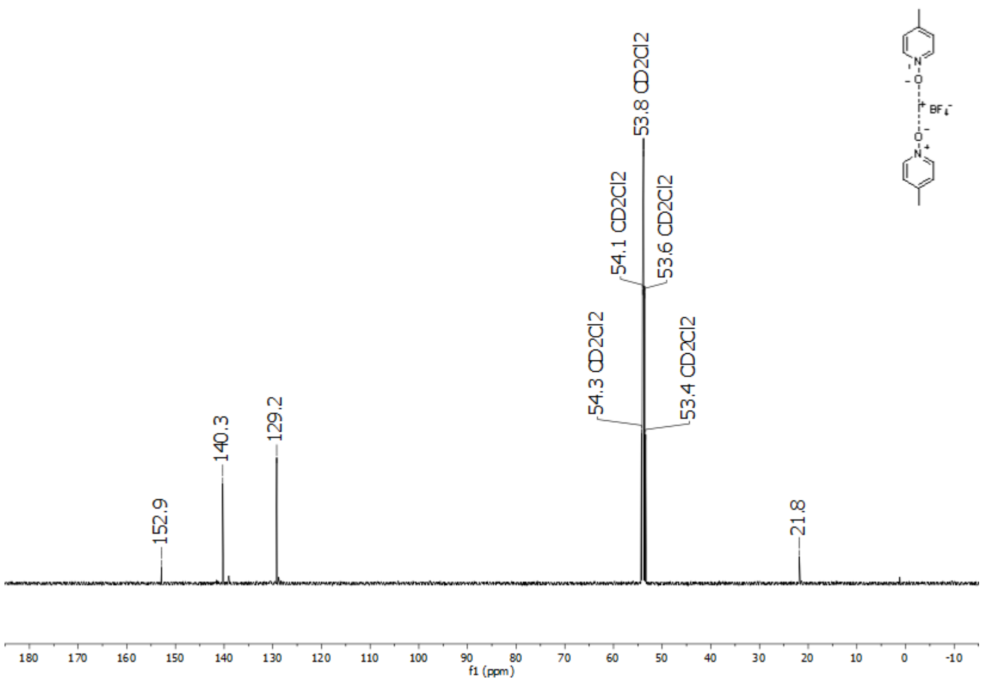

Figure S41. ^{13}C NMR spectrum of **(1-*Me*)$_2$-I** (126 MHz, CD_2Cl_2, 25 °C).

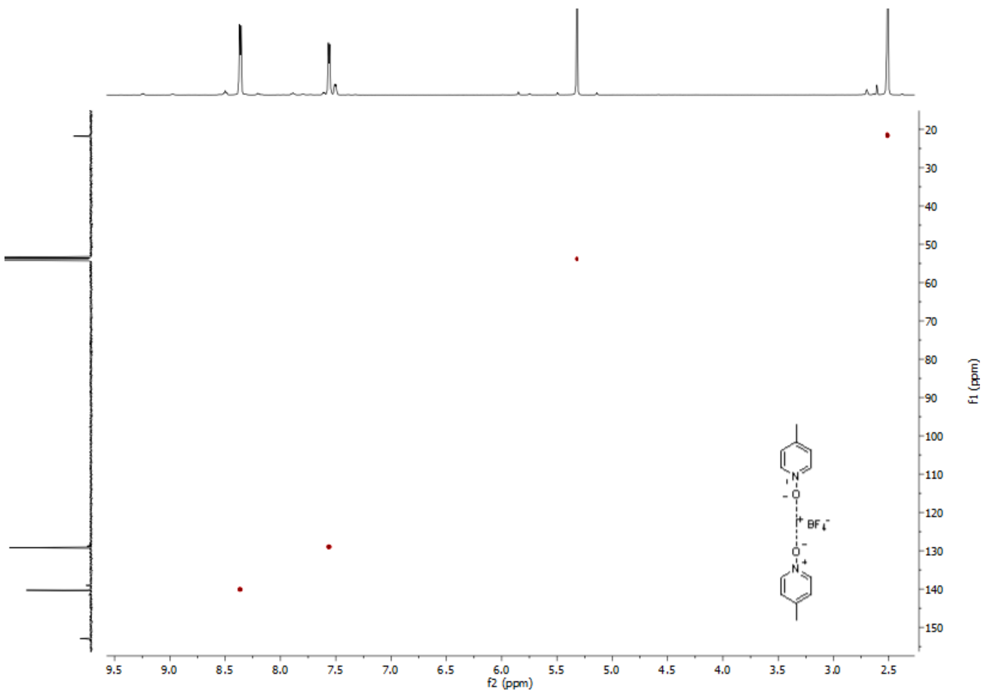

Figure S42. $^{1}H,^{13}C$ HSQC NMR spectrum of **(1-*Me*)$_2$-I** (500 and 126 MHz, CD_2Cl_2, 25 °C).

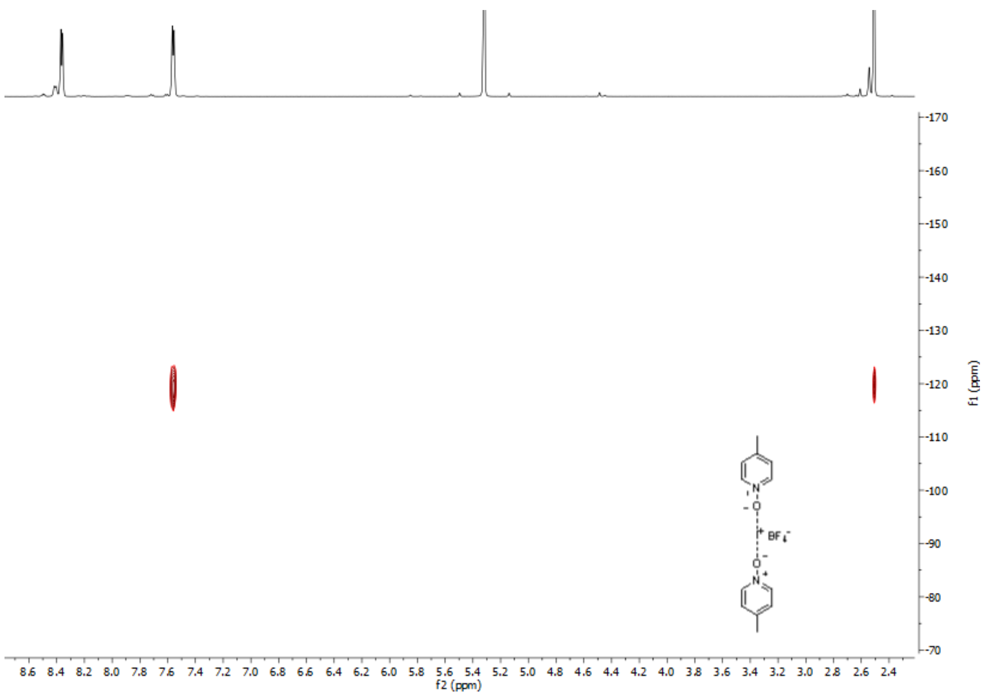

Figure S43. $^{1}H,^{15}N$ HMBC NMR spectrum of **(1-*Me*)$_2$-I** (500 and 51 MHz, CD_2Cl_2, 25 °C).

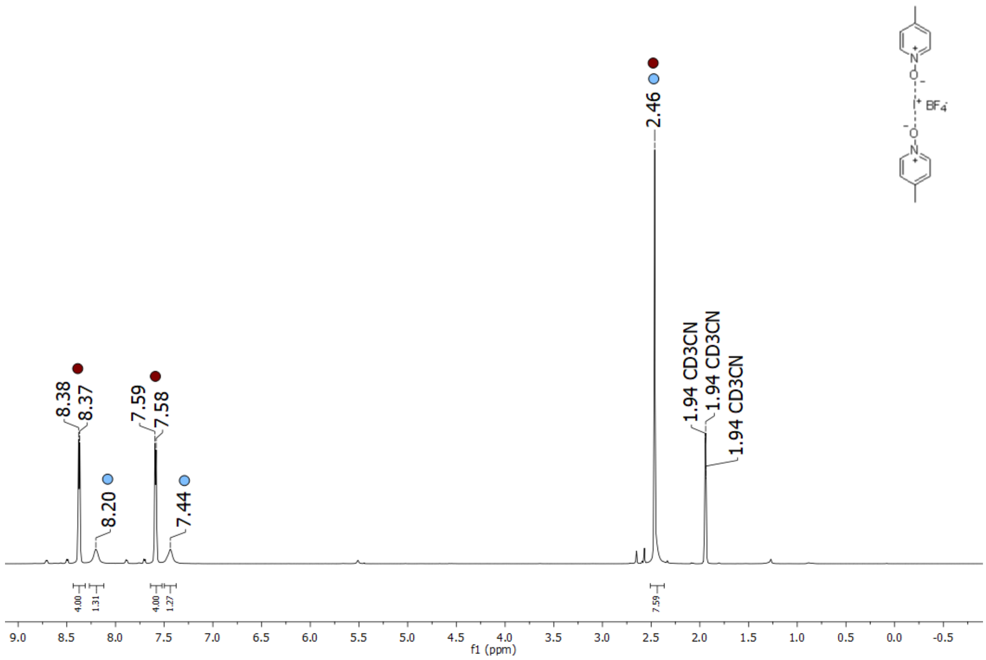

Figure S44. [1]H NMR spectrum of **(1-*Me*)$_2$-I** in CD_3CN (500 MHz, 25 °C). Broad signals (marked with blue) corresponding to the protonated 4-methylpyridine *N*-oxide can be seen along with the signals (marked with maroon) of the iodine(I) complex.

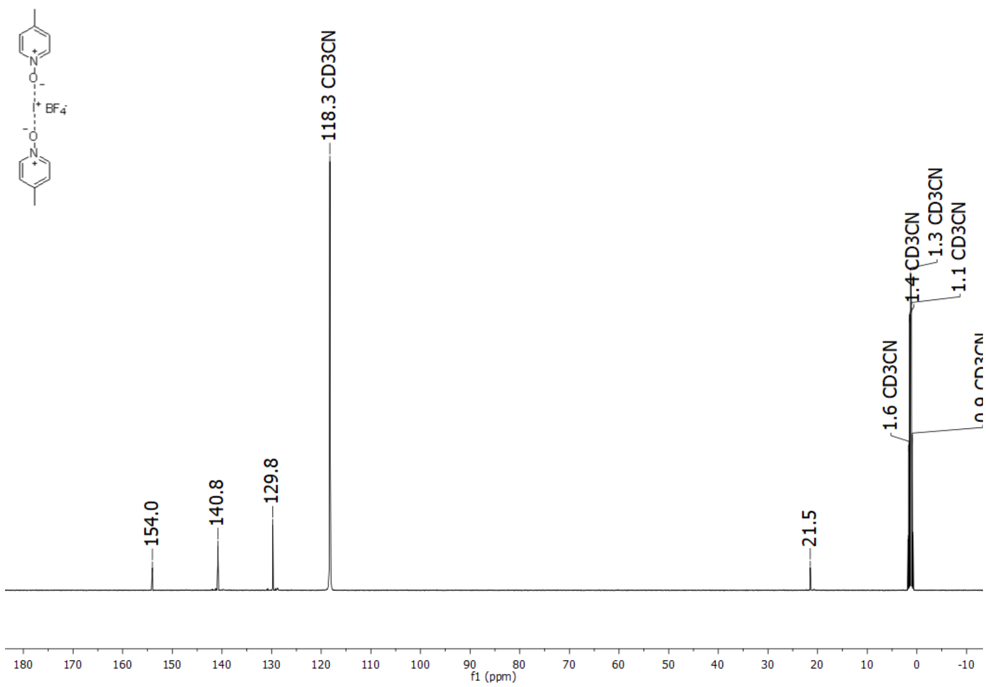

Figure S45. [13]C NMR spectrum of **(1-*Me*)$_2$-I** in CD_3CN (500 MHz, 25 °C).

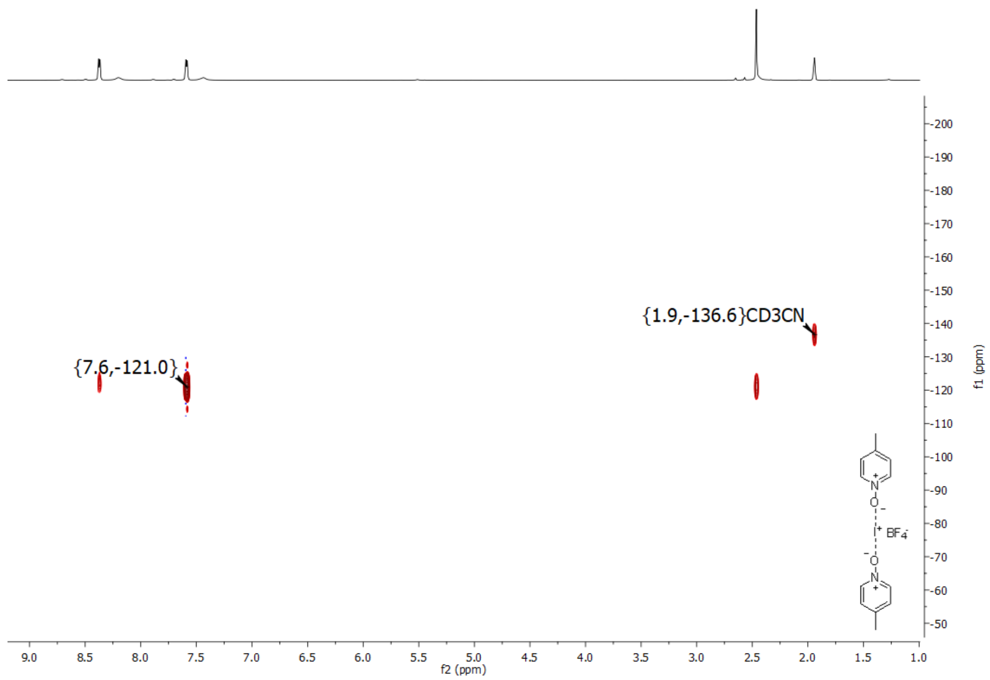

Figure S46. $^{1}H,^{15}N$ HMBC NMR spectrum of **(1-Me)$_2$-I** in CD_3CN (500 and 51 MHz, 25 °C).

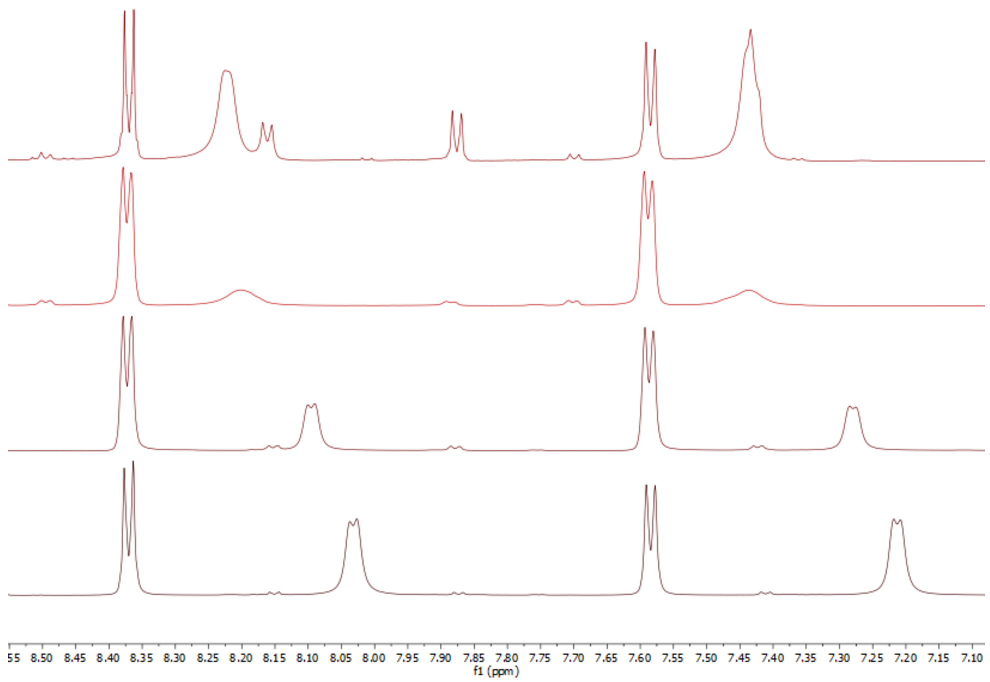

Figure S47. ^{1}H NMR spectra of repeated formations of **(1-*Me*)$_2$-I** in CD_3CN (500 MHz, 25 °C). Mixtures of the protonated 4-methylpyridine *N*-oxide and **(1-*Me*)$_2$-I** are consistently obtained. The broad signals of protonated 4-methylpyridine *N*-oxide appear at varying chemical shifts, which is indicative of different pH of the samples.

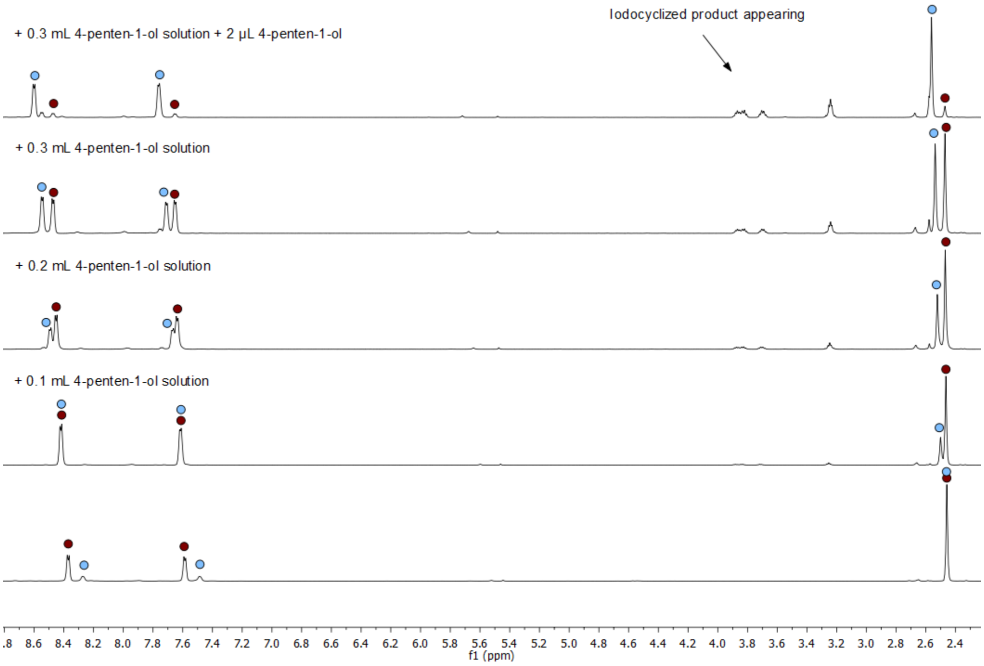

Figure 48. ^{1}H NMR spectra of **(1-*Me*)$_2$-I** (32 µmol) in CD_3CN (500 MHz, 25 °C) before (bottom) and after successively adding portions of a solution of 4-penten-1-ol (2 µL, 20 µmol) in CD_3CN (0.6 mL). The sharp signals belonging to **(1-*Me*)$_2$-I** (marked with maroon) decrease upon addition, while the partially protonated **1-*Me*** signals (marked with blue) shifts due to the changed pH.

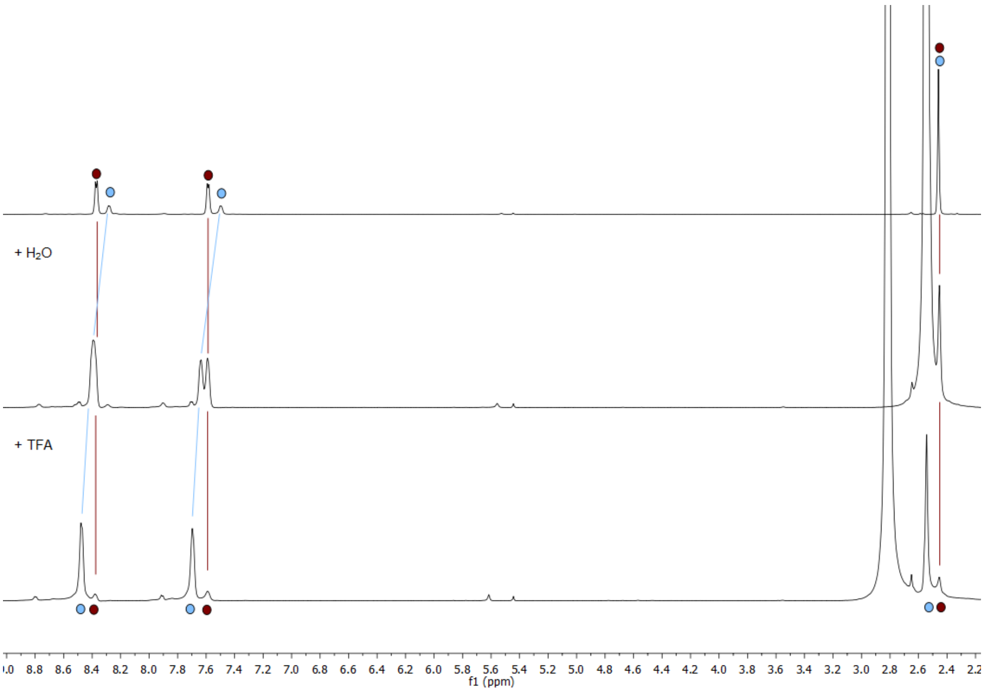

Figure 49. ^{1}H NMR spectra of **(1-*Me*)$_2$-I** (32 µmol) in CD_3CN (500 MHz, 25 °C) before (top) and after successively adding a drop of H_2O (middle) and a drop of TFA (bottom). The sharp signals belonging to **(1-*Me*)$_2$-I** (marked with maroon) decrease upon addition, while the partially protonated **1-*Me*** signals (marked with blue) increase and shifts due to the changed pH.

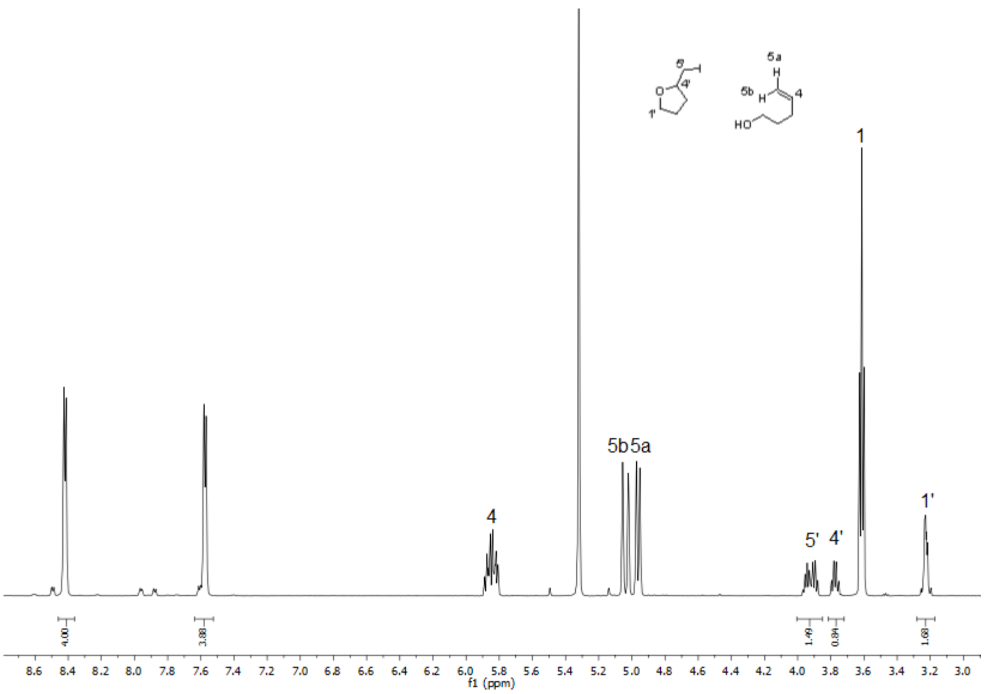

Figure S50. The ^{1}H spectrum in CD_2Cl_2 resulting from addition of 4-penten-1-ol (2 µL, 20 µmol, 0.8 equiv.) to the I^{+} complex **(1-*Me*)$_2$-I** shows formation of 1 equivalent of the iodocyclized product.

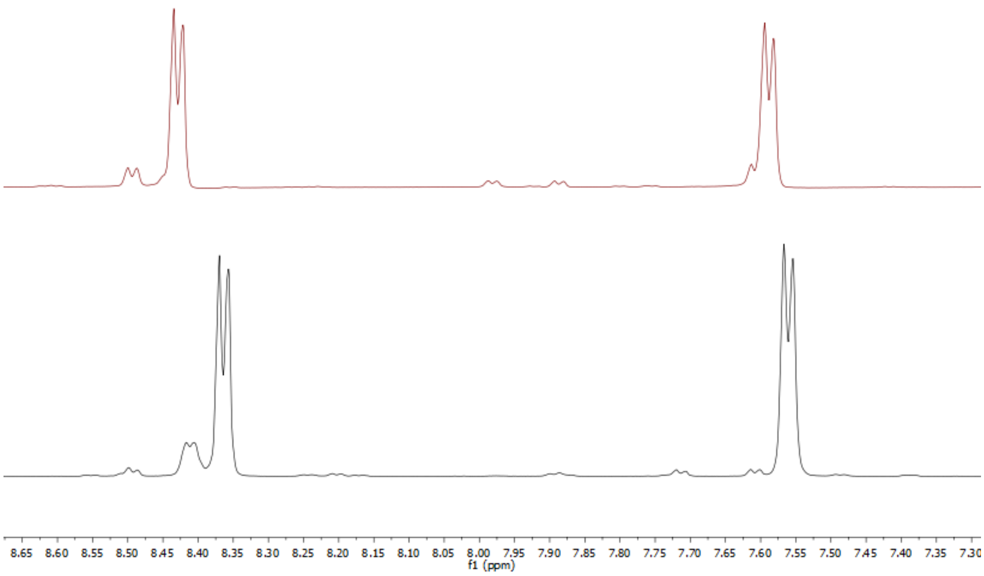

Figure S51. The ^{1}H spectra in CD_2Cl_2 of the I^{+} complex **(1-*Me*)$_2$-I** (8 µmol) (bottom), and after addition of 4-penten-1-ol (2 µL, 20 µmol, 2.5 equiv.) (top). The pyridine signals changed upon addition of the alkene, in accordance with an I^{+} transfer, suggesting formation of **(1-*Me*)$_2$-I** was successful.

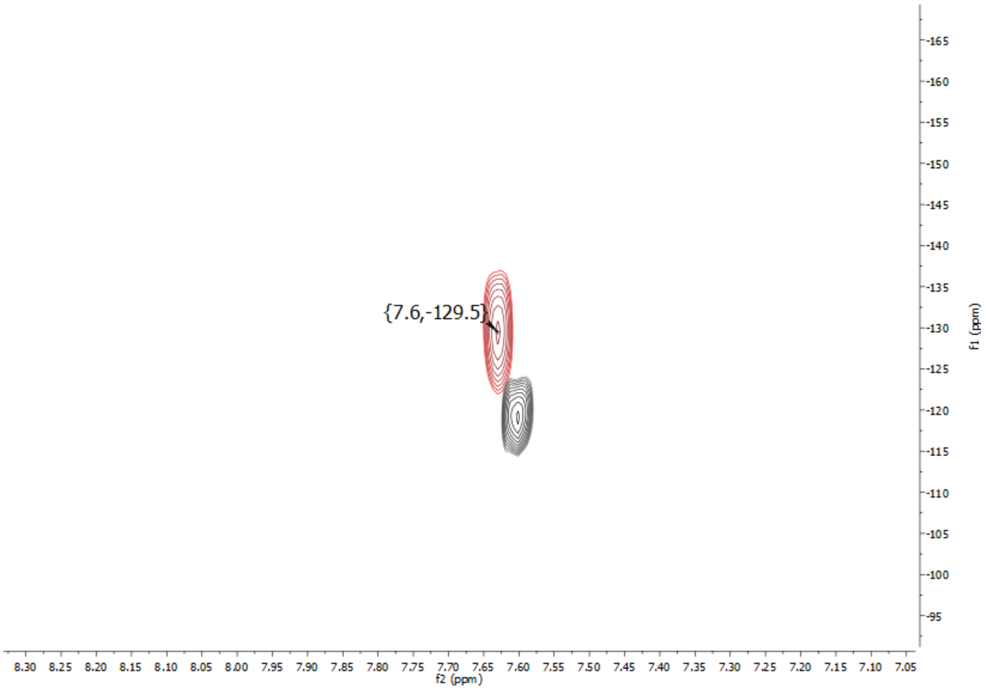

Figure S52. The stacked ^{1}H,^{15}N HMBC spectra in CD_2Cl_2 of **(1-*Me*)$_2$-I** (8 µmol) (black), and after addition of 4-penten-1-ol (2 µL, 20 µmol, 2.5 equiv.) (red) with the new chemical shift indicated (−129.5). The ~10 ppm change in chemical shift is consistent with an I^+ transfer from **(1-*Me*)$_2$-I** to the alkene, which provides further evidence for the successful formation of the iodine(I) complex **(1-*Me*)$_2$-I**.

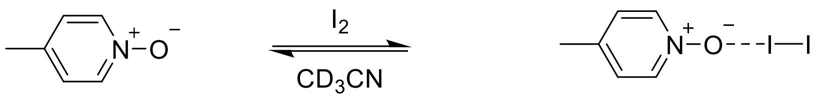

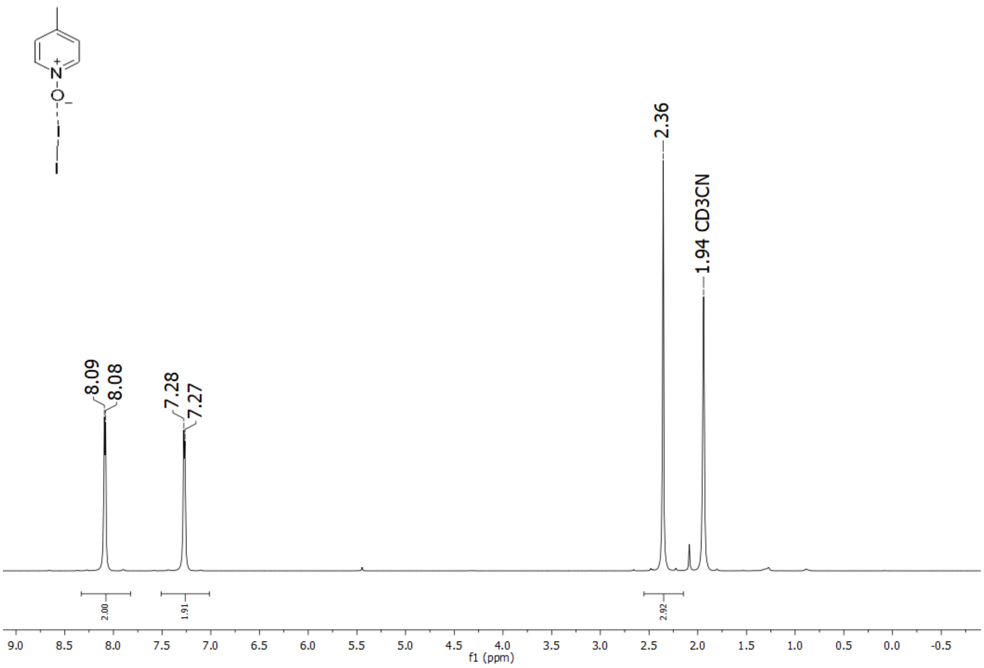

Figure S53. [1]H NMR spectrum of the control solution of **(1-*Me*)-I$_2$** (500 MHz, CD_3CN, 25 °C).

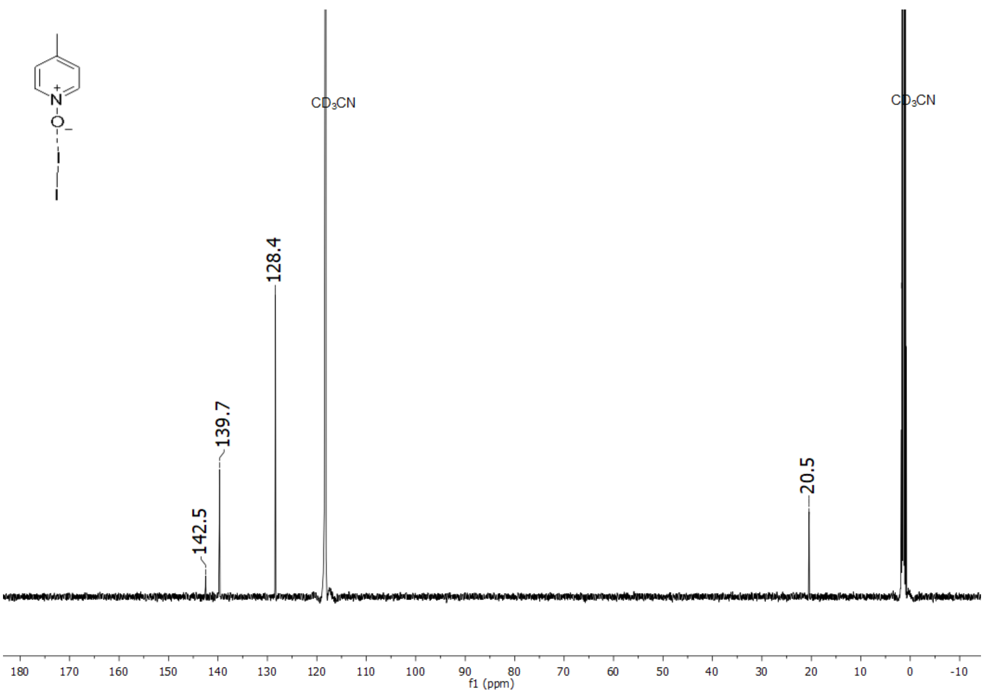

Figure S54. [13]C NMR spectrum of the control solution of **(1-*Me*)-I$_2$** (126 MHz, CD_3CN, 25 °C).

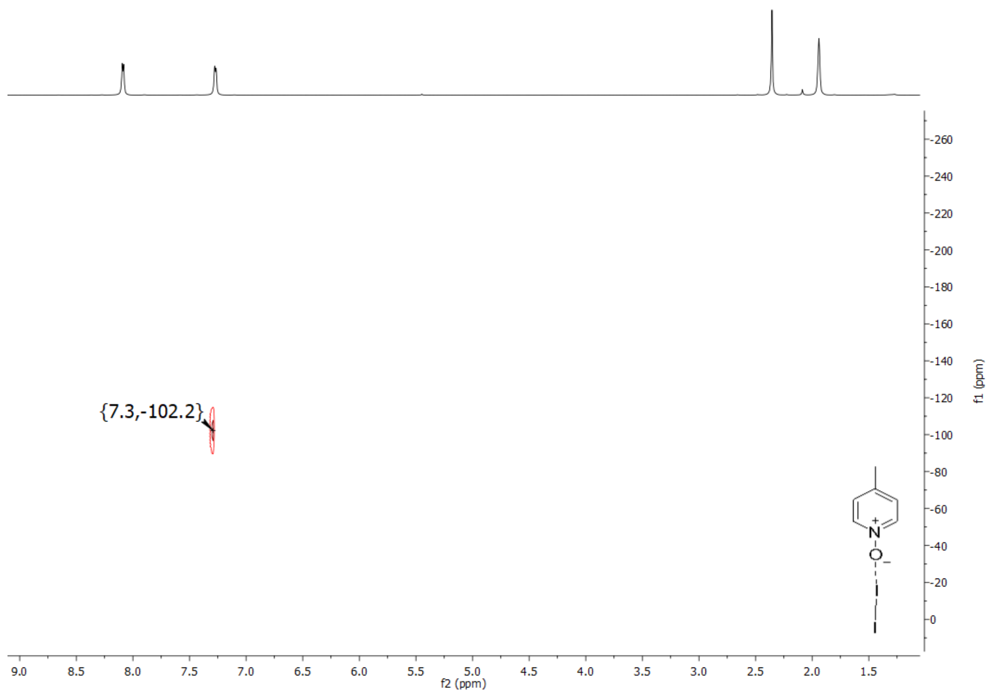

Figure S55. ^{1}H,^{15}N NMR spectrum of the control solution of **(1-*Me*)-I$_2$** (500 and 51 MHz, CD_3CN, 25 °C).

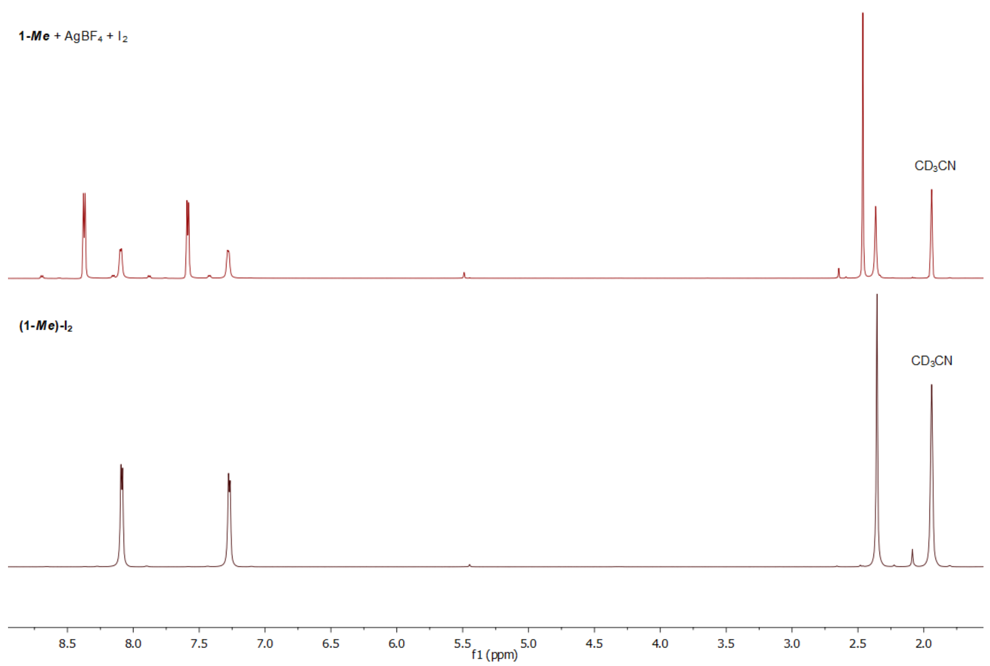

Figure S56. Comparison of the ^{1}H NMR spectra of the control solution of **(1-*Me*)-I$_2$** (bottom) and of the **(1-*Me*)$_2$-I** in CD_3CN described in the synthetic information (top) (500 MHz, 25 °C). The small signals of the top spectrum matches the ones of **(1-*Me*)-I$_2$** very well, but are actually originating from protonated 4-methylpyridine *N*-oxide (see Figures S47-S52 and S59).

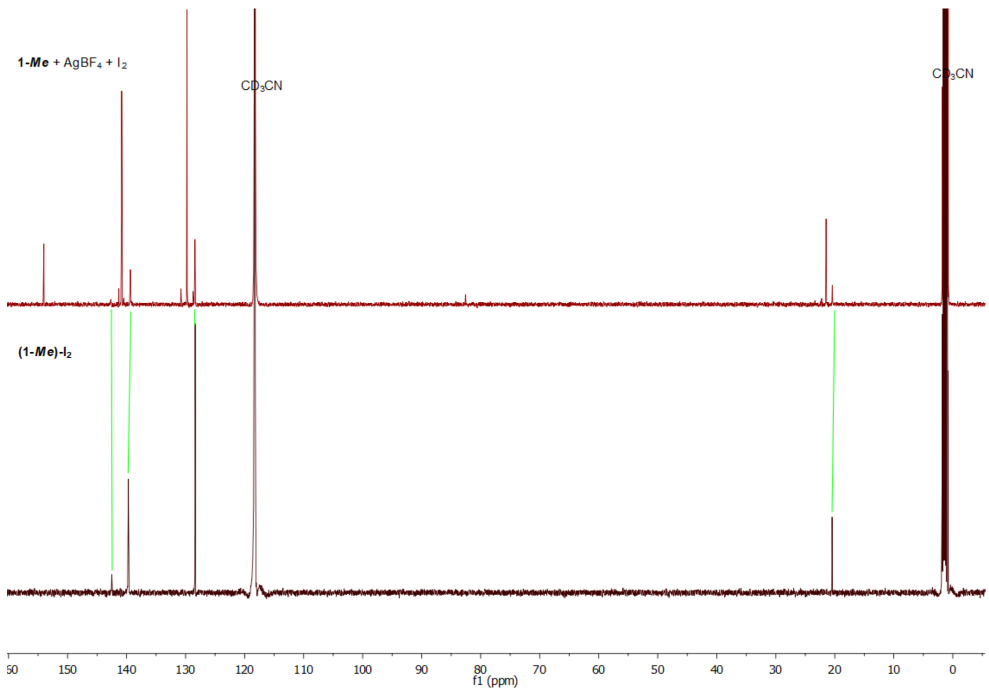

Figure S57. Comparison of the ^{13}C NMR spectra of the control solution of **(1-*Me*)-I$_2$** (bottom) and of the **(1-*Me*)$_2$-I** in CD_3CN described in the synthetic information (top) (126 MHz, 25 °C). The small signals of the top spectrum matches the ones of **(1-*Me*)-I$_2$** very well, but are actually protonated 4-methylpyridine *N*-oxide (see Figures S47-52, and S59).

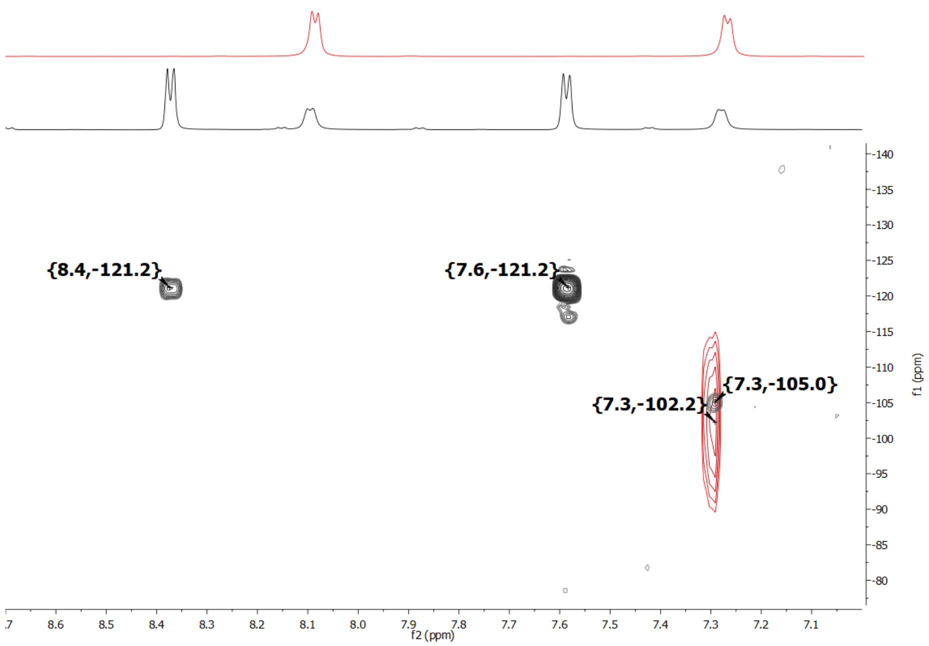

Figure 58. Comparison of the ^{1}H,^{15}N HMBC NMR spectra of the control solution of **(1-*Me*)-I$_2$** (red) and of the **(1-*Me*)$_2$-I** in CD_3CN described in the synthetic information (black) (126 MHz, 25 °C). The signal at −105.0 of the black spectrum matches the ones of **(1-*Me*)-I$_2$** very well, but are actually originating from protonated 4-methylpyridine *N*-oxide (see Figures S47-S52, and S59).

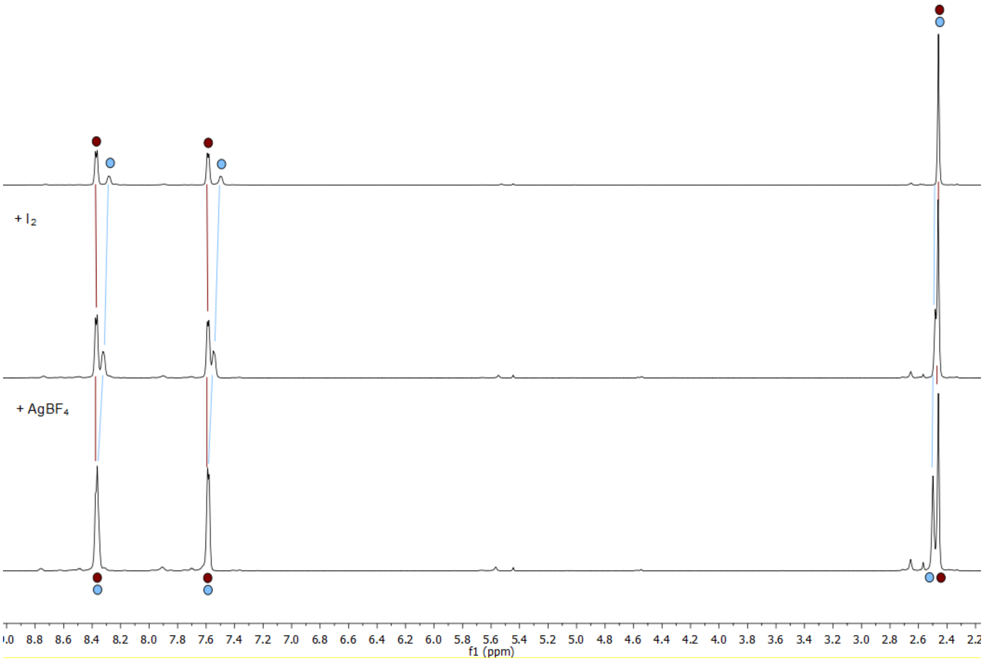

Figure S59. [1]H NMR spectra of **(1-*Me*)$_2$-I** (32 µmol) in CD_3CN (500 MHz, 25 °C) before (top) and after successively adding I_2 (13 µmol) (middle) and $AgBF_4$ (9 µmol) (bottom). Adding I_2 caused the signals marked in blue to grow, which could be in agreement with them being **(1-*Me*)-I$_2$**. However, addition of $AgBF_4$ does not cause the blue signals to be converted into iodine(I) complex (signals marked with maroon), which would have been expected if they originated from **(1-*Me*)-I$_2$**. This is instead in agreement with the blue signals being protonated 4-methylpyridine *N*-oxide. Each addition result in increasing amounts of moisture in the sample, which reacts with part of the iodine(I) complex to form more protonated 4-methylpyridine *N*-oxide, responsible also for the change in pH making the blue signals shift slightly.

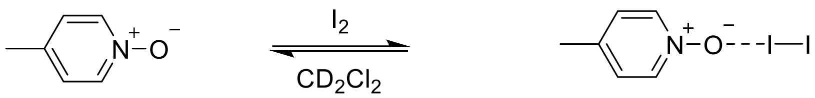

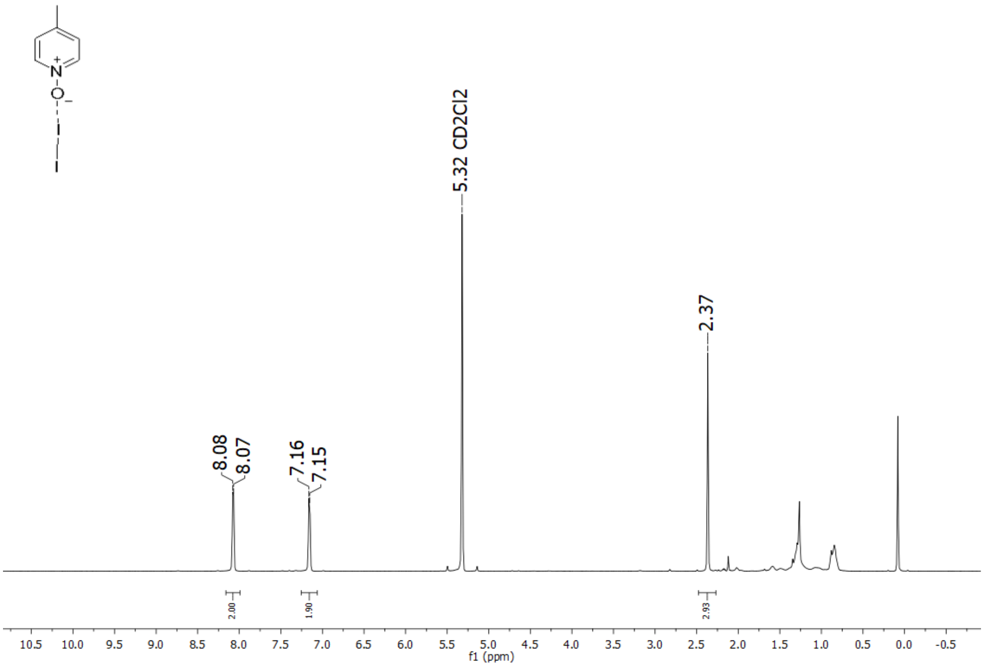

Figure S60. ^{1}H NMR spectrum of the control solution of **(1-*Me*)-I$_2$** (500 MHz, CD_2Cl_2, 25 °C).

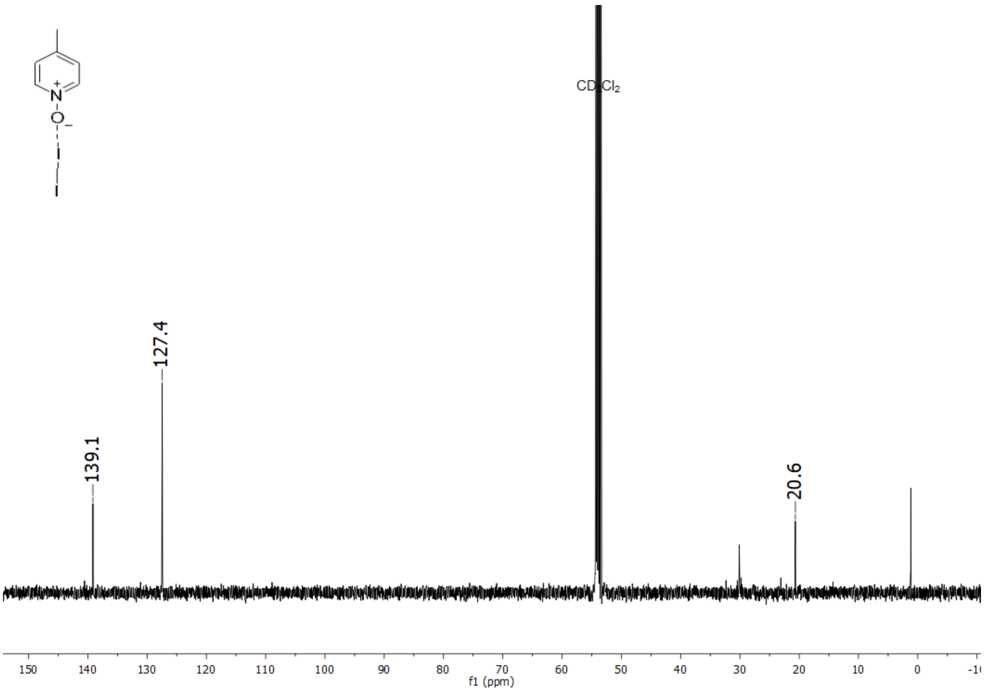

Figure S61. ^{13}C NMR spectrum of the control solution of **(1-*Me*)-I$_2$** (126 MHz, CD_2Cl_2, 25 °C).

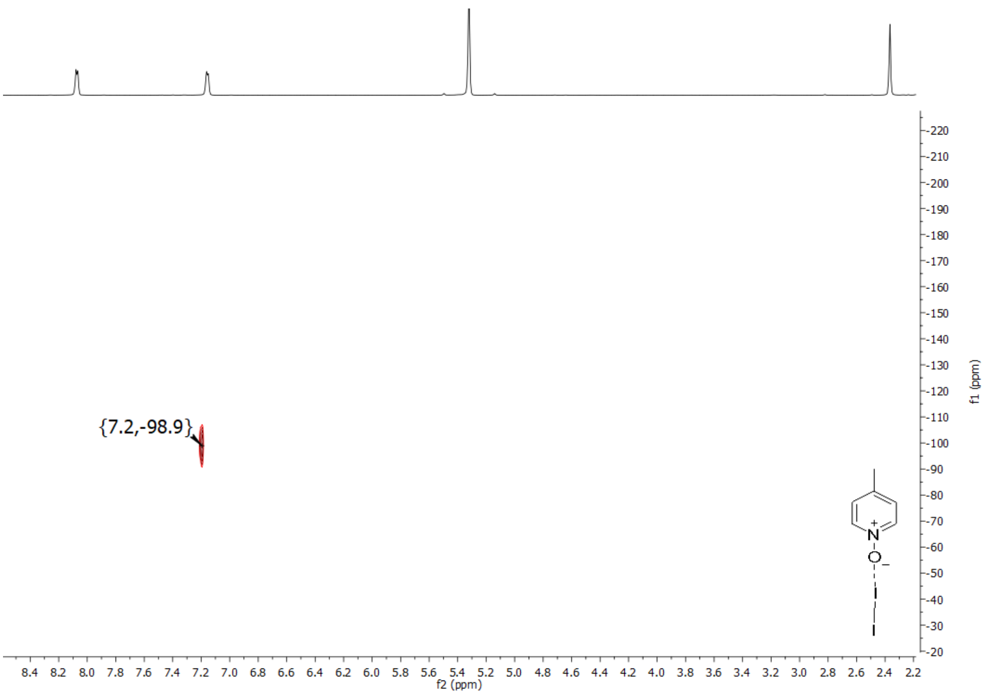

Figure S62. $^{1}H,^{15}N$ HMBC NMR spectrum of the control solution of **(1-*Me*)-I$_2$** (500 and 51 MHz, CD_2Cl_2, 25 °C).

2.3. Dibenzofuran complexes

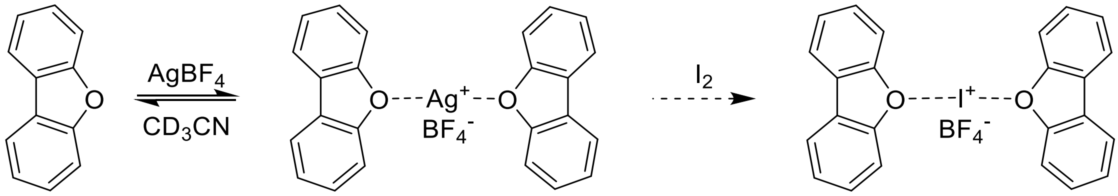

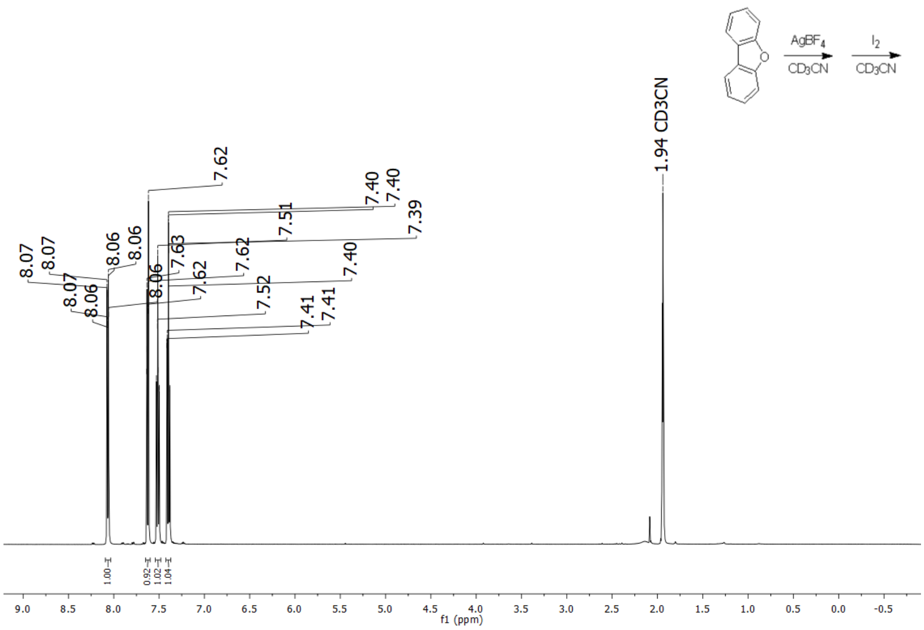

Figure S63. ^{1}H NMR spectrum of the attempt to form [bis(dibenzofuran)iodine(I)]$^+$ tetrafluoroborate (500 MHz, CD_3CN, 25 °C).

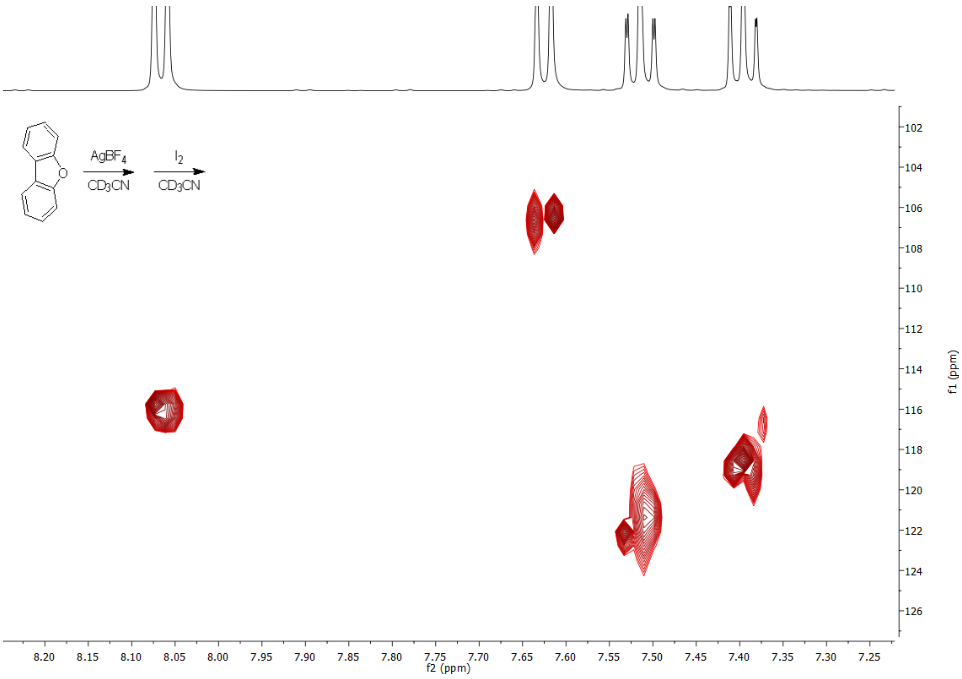

Figure S64. ^{1}H,^{13}C HSQC NMR spectrum of the attempt to form [bis(dibenzofuran)iodine(I)]$^+$ tetrafluoroborate (500 and 126 MHz, CD_3CN, 25 °C).

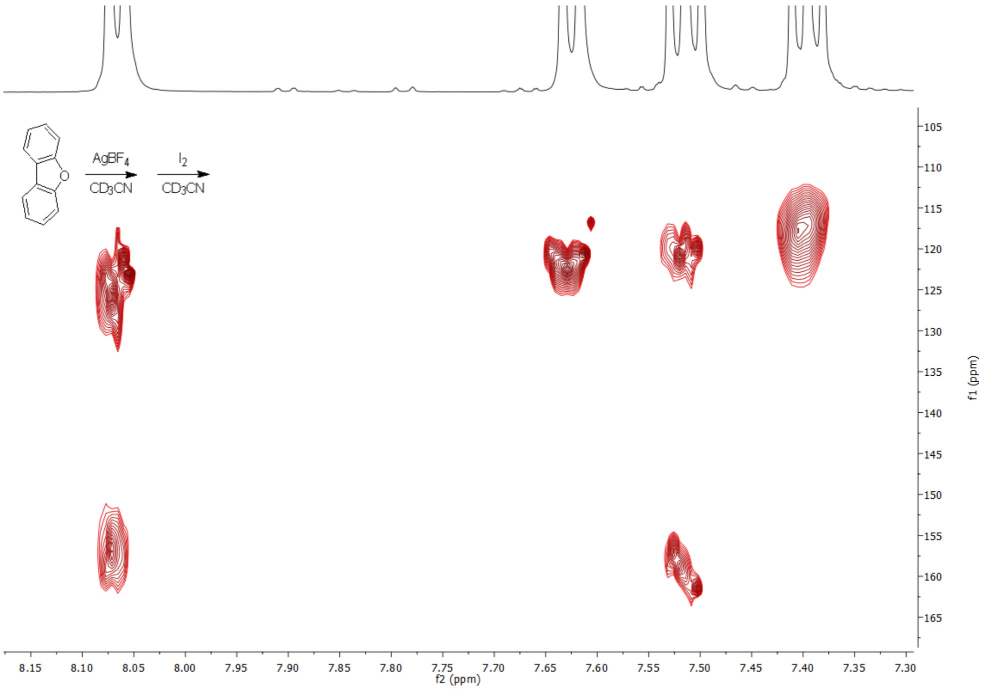

Figure S65. $^{1}H,^{13}C$ HMBC NMR spectrum of the attempt to form [bis(dibenzofuran)iodine(I)]$^{+}$ tetrafluoroborate (500 and 126 MHz, CD_3CN, 25 °C).

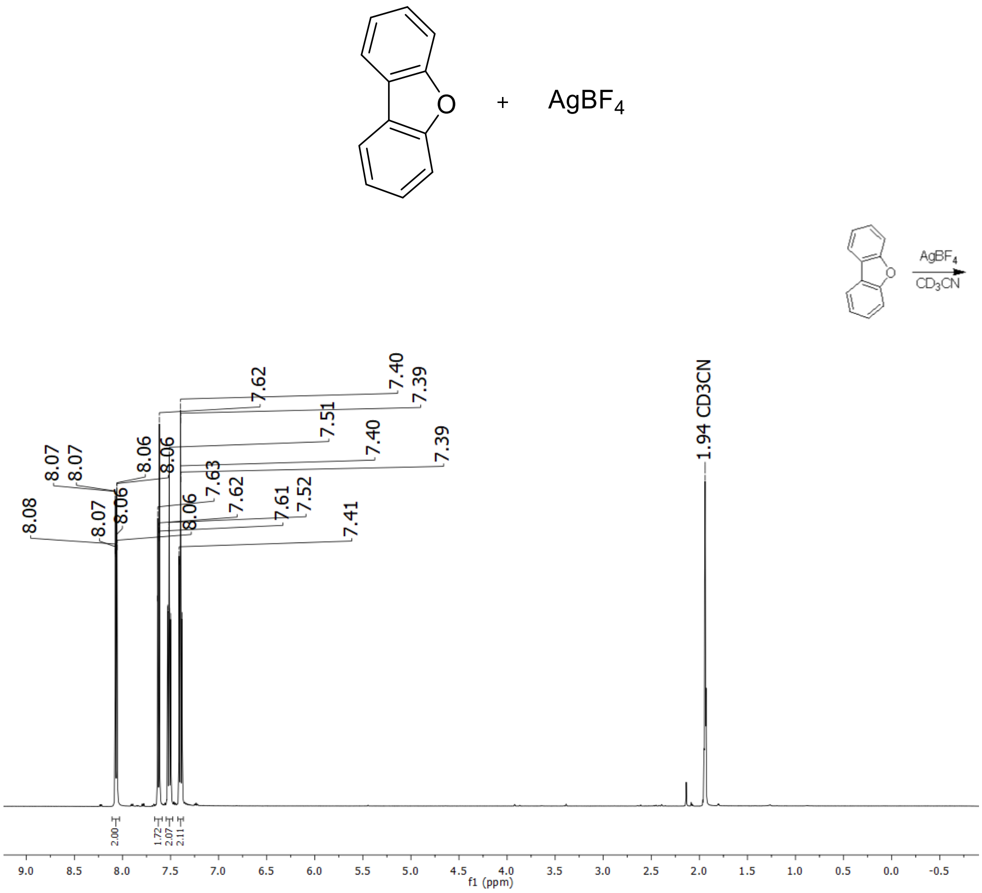

Figure S66. ^{1}H NMR spectrum of the solution of dibenzofuran and silver tetrafluoroborate (500 MHz, CD_3CN, 25 °C).

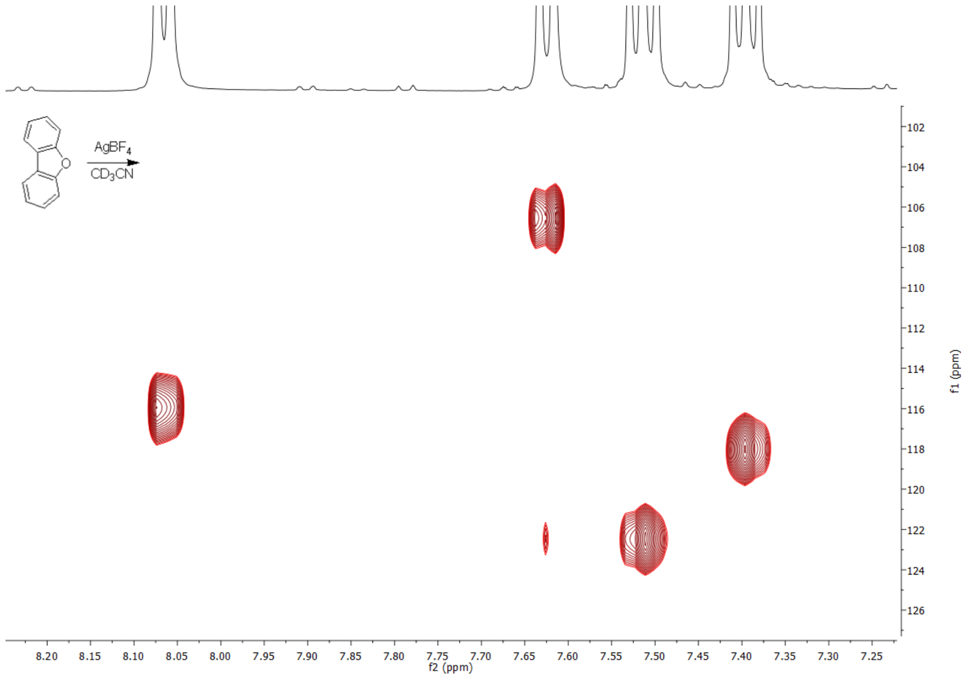

Figure S67. $^{1}H,^{13}C$ HSQC NMR spectrum of the solution of dibenzofuran and silver tetrafluoroborate (500 and 126 MHz, CD_3CN, 25 °C).

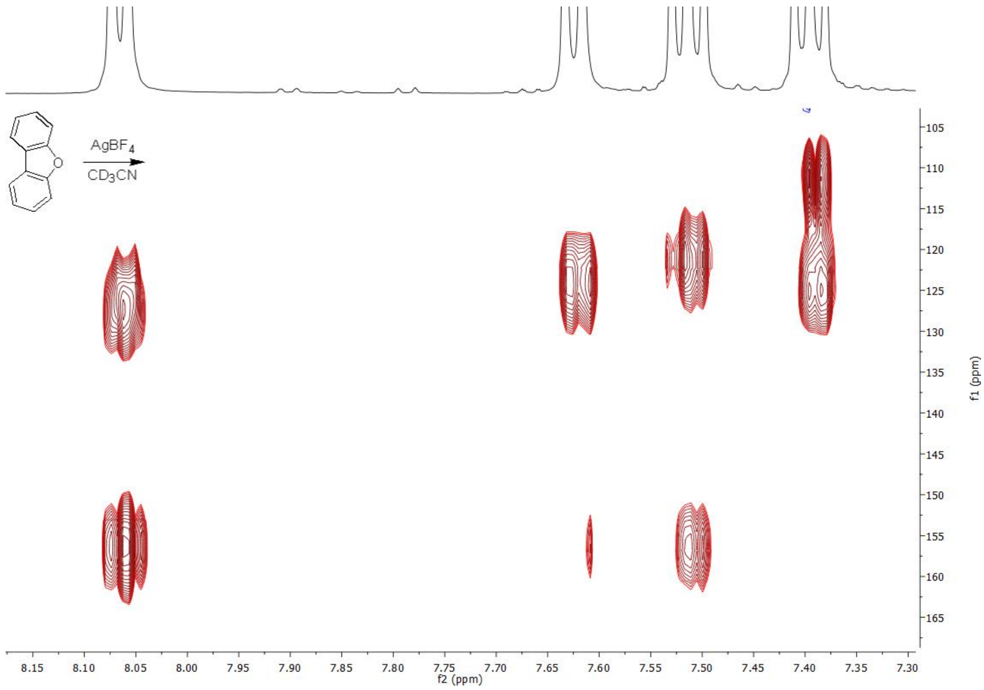

Figure S68. $^{1}H,^{13}C$ HMBC NMR spectrum of the solution of dibenzofuran and silver tetrafluoroborate (500 and 126 MHz, CD_3CN, 25 °C).

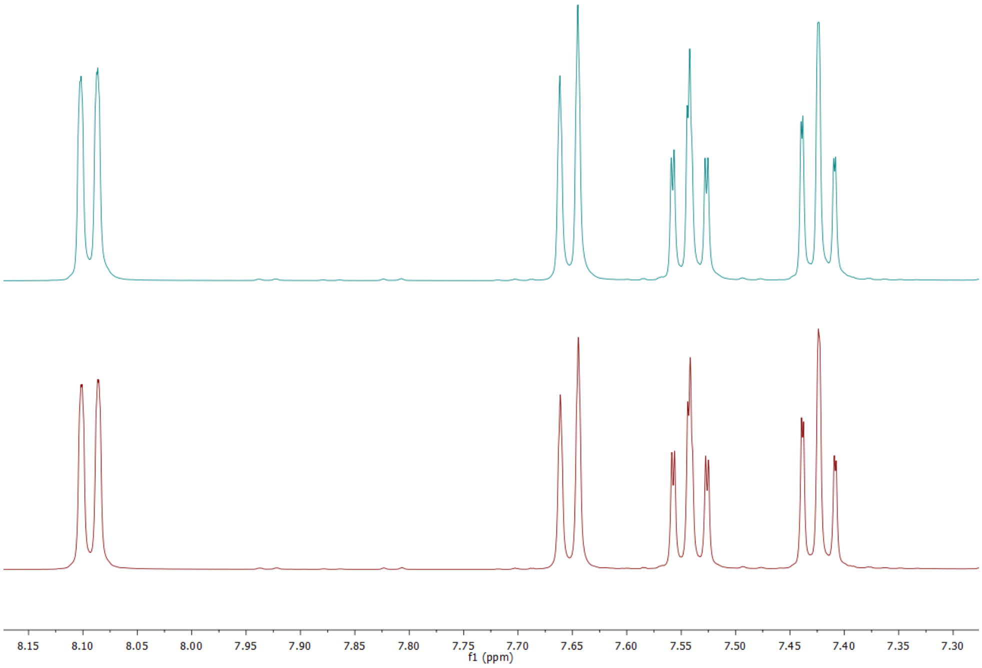

Figure S69. The ^{1}H spectra of the attempt to form [bis(dibenzofuran)iodine(I)]$^{+}$ tetrafluoroborate (top), and the solution of dibenzofuran and silver tetrafluoroborate (bottom) show no difference, confirming no iodine(I) complex was formed.

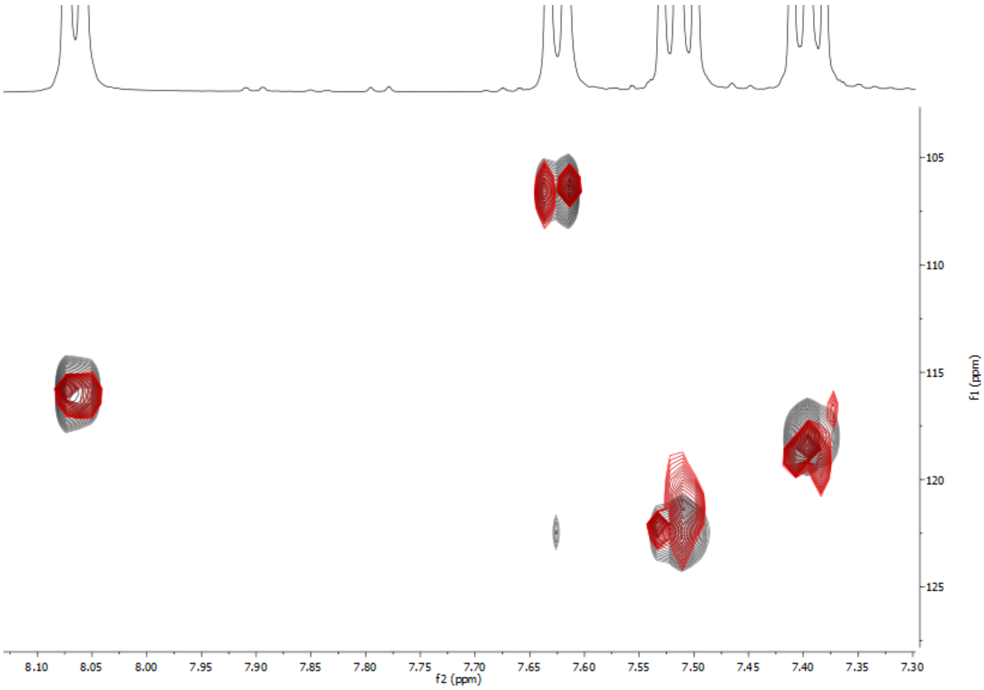

Figure S70. The $^{1}H,^{13}C$ HSQC spectra of the attempts to form [bis(dibenzofuran)iodine(I)]$^{+}$ tetrafluoroborate (red), and [bis(dibenzofuran)silver(I)]$^{+}$ tetrafluoroborate (black), which show no difference and further confirm that the iodine(I) complex was not formed.

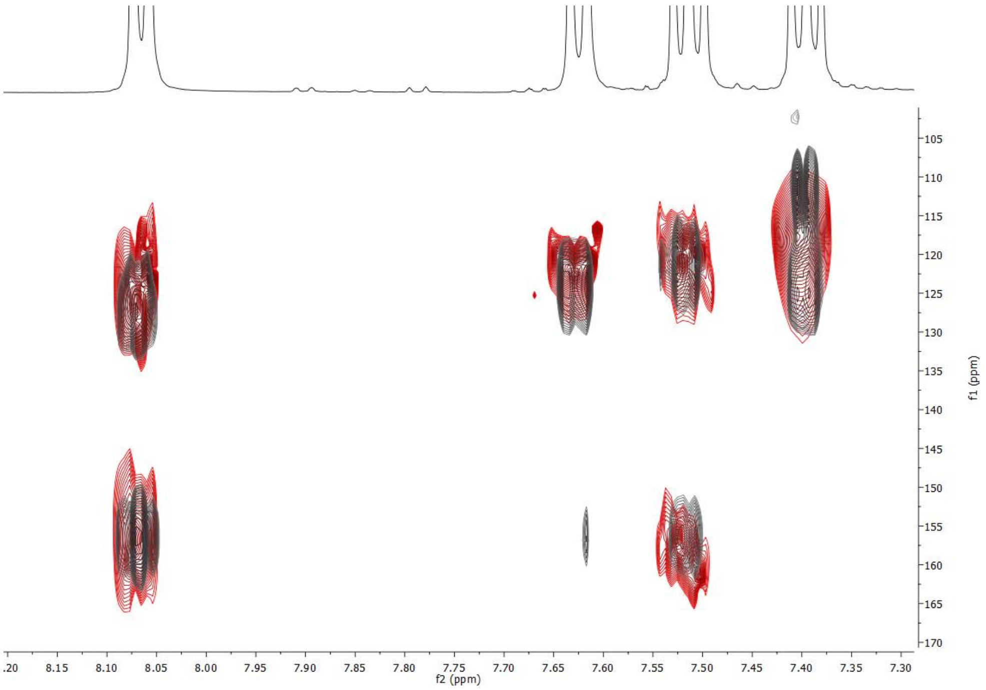

Figure S71. The $^{1}H,^{13}C$ HMBC spectra of the attempts to form [bis(dibenzofuran)iodine(I)]$^{+}$ tetrafluoroborate (red/orange), and [bis(dibenzofuran)silver(+I)]$^{+}$ tetrafluoroborate (black/white). Since the carbon at C4a/5a (the resonance at highest frequency) is the closest measureable nuclei to the oxygen, here one could expect the largest shift difference upon complexation. Since no difference is observed the most plausible conclusion is that the iodine(I) complex was not formed.

3. COMPUTATIONS

3.1. Computational approach

In the computational analysis of the present work, we used density functional theory (DFT) to describe the electronic structure of the investigated complexes. The geometries of all species were optimized in the presence of a solvent (acetonitrile, as one of the solvents used in experiments) at the ωB97X-D[7-9]/Def2SVP[10] level of theory.[7-10] The dispersion-corrected, range-separated hybrid ωB97X-D funcional was shown to provide accurate binding energies and topological properties for halogen-bonded systems.[11] The solvent effects were taken into account using the integral equation formalism variant of the polarizable continuum model (IEFPCM).[12] The atomic radii and non-electrostatic terms in the IEFPCM calculations were those introduced by Truhlar and coworkers (SMD solvation model).[13] For each optimized structure, additional single-point energy calculations were performed with the larger Def2TZVPP basis set[10] also in the presence of the solvent. Vibrational analysis was performed at the ωB97X-D/Def2SVP level, and the results were used to compute the thermal and entropic contributions to the Gibbs free energy. For the estimation of thermodynamic data, the ideal gas – rigid rotor – harmonic oscillator approximation was utilized for 298.15 K and p = 1 atm (ideal gas standard state), but corrections were applied for switching to concentration relevant to solution phase. Namely, concentration of c = 1 mol/dm^3 (ΔG_{conc} = 0.003019 a.u.) was applied for all investigated systems (ligands and complexes), except for acetonitrile, when it was explicitly considered as a coordinating molecule (see section 3.4). The molar concentration of acetonitrile in solvent phase is c = 19.15 mol/dm^3 (r = 786 g/dm^3, M = 41.05 g/mol), so the corresponding correction term is ΔG_{conc} = 0.005805 a.u.. The relative energies reported in the paper refer to solution phase Gibbs free energies computed as $G = E_{0,sol}' + (G_{0,sol} - E_{0,sol}) + \Delta G_{conc}$, where $E_{0,sol}'$ and $E_{0,sol}$ are solution phase electronic energies obtained at the ωB97X-D/Def2TZVPP and ωB97X-D/Def2SVP levels, respectively, and $G_{0,sol}$ is solution phase Gibbs free energy computed at ωB97X-D/Def2SVP level. The ^{15}N NMR chemical shifts (δ^{15}N) were computed from NMR shielding tensors calculated with the Gauge-Independent Atomic Orbital (GIAO) method[14] using the ωB97X-D/Def2SVP level of DFT in solution phase (in acetonitrile). All DFT calculations were carried out with the *Gaussian09* software.[15]

3.2. Structure of [RO-X-OR]$^+$ complexes

The equilibrium structures of [RO-X-OR]$^+$ complexes (with RO = **1-*OMe***, **1-*Me*** and dibenzofuran **2**; $X^+ = I^+$, Ag^+ and H^+) along with those of the free ligands and [RO-X]$^+$ complexes are depicted in Figure S72 to S74.

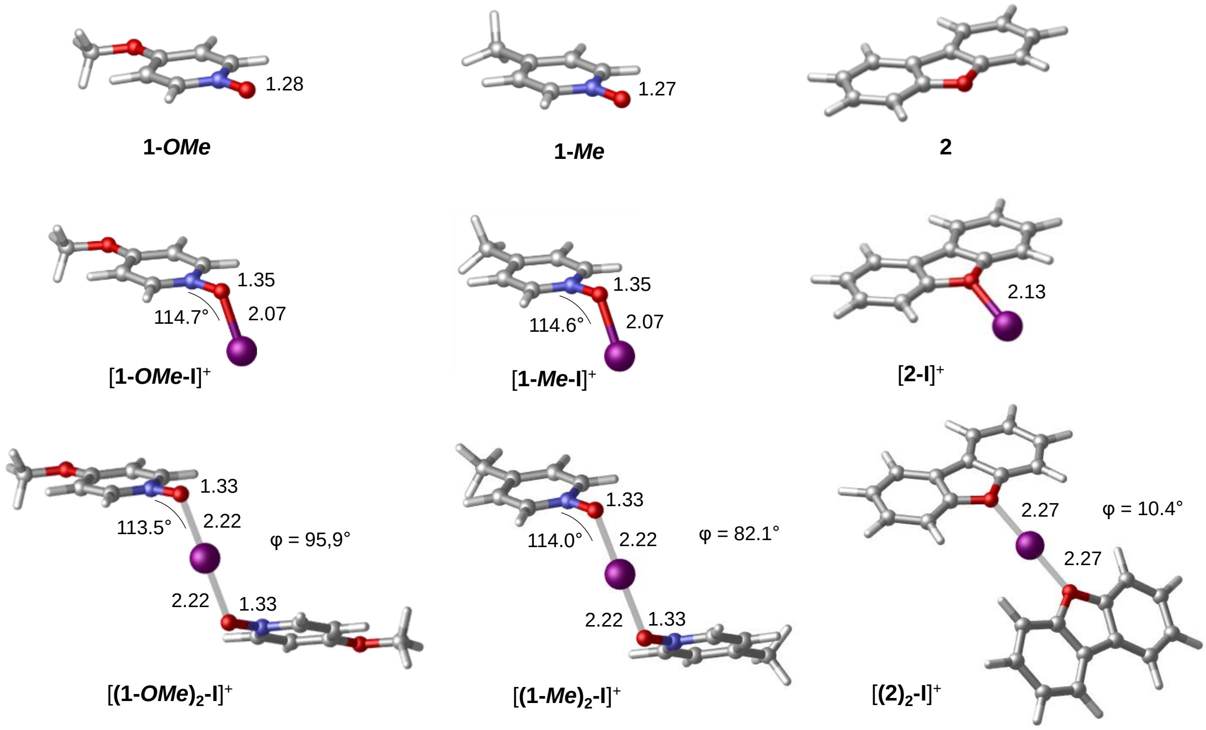

Figure S72. Optimized structures of [RO-I]$^+$ and [RO-I-OR]$^+$ complexes with selected structural parameters. Bond distances are in Å and angles in degrees. φ denotes dihedral angles characterizing the relative position of the two coordinating ligands (N-O···O-N dihedral angles for ligands **1-*OMe*** and **1-*Me***, C-O···O-C dihedral angles for ligand **2**).

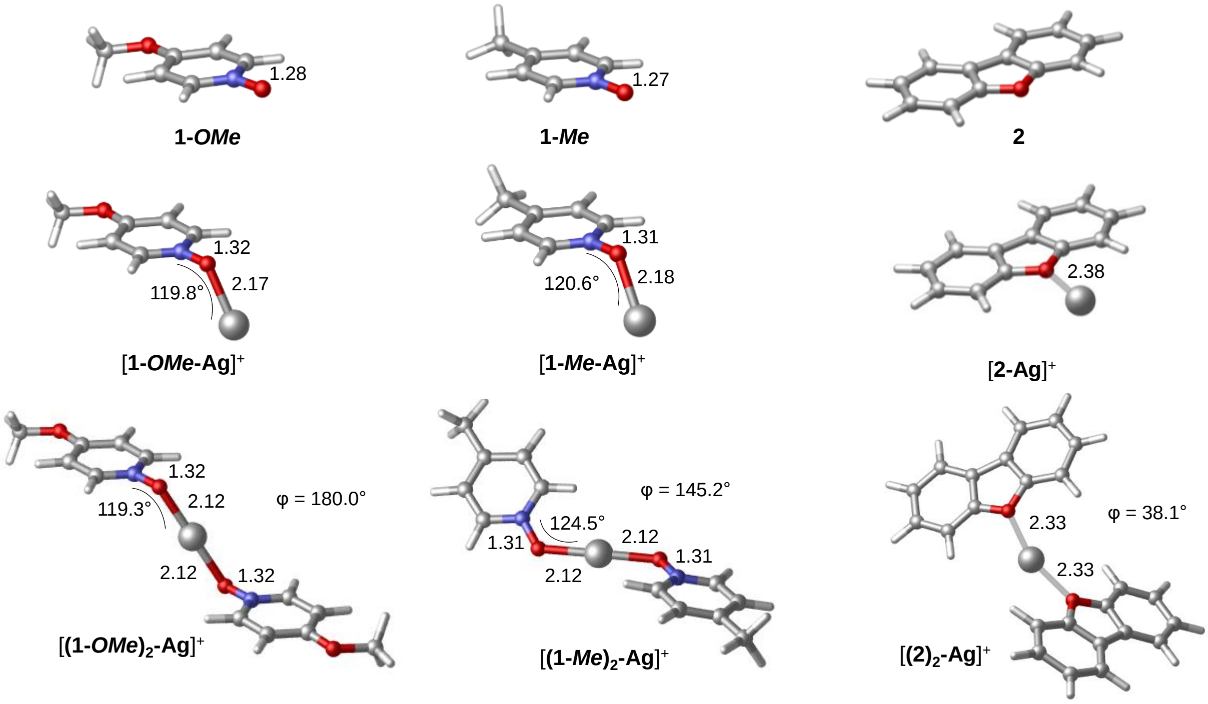

Figure S73. Optimized structures of [RO-Ag]$^+$ and [RO-Ag-OR]$^+$ complexes with selected structural parameters. For notes, see caption of Figure S72.

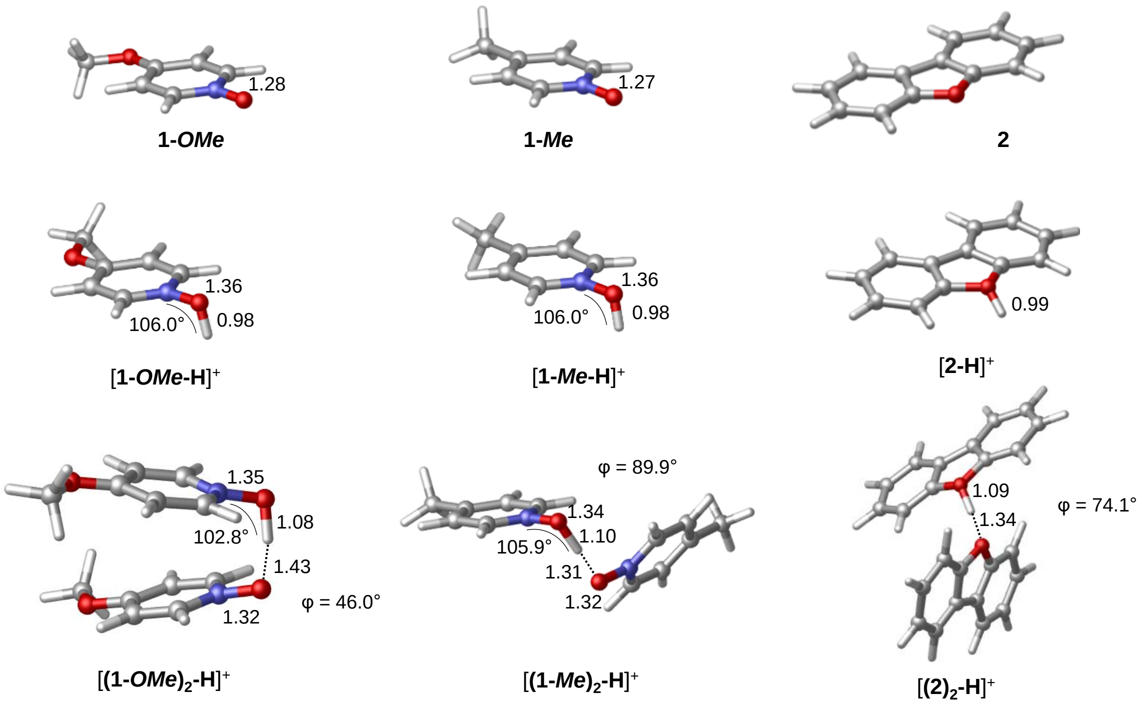

Figure S74. Optimized structures of $[ROH]^+$ and $[RO\text{-}H\text{-}OR]^+$ complexes with selected structural parameters. For notes, see caption of Figure S72.

We note that iodine(I) complexes have a bent structure in that the aromatic rings of the ligands are not aligned with the O-I bonds, which is different from that found for the previously reported bis(pyridine) systems [**Py**-X-**Py**]$^+$ (**Py** = pyridine) that are linear. For $[RO\text{-}I\text{-}OR]^+$ complexes, the two O-I bonds lengths are identical, however, the equilibrium structures are not symmetrical, as the two ligands are displaced from the symmetrical position that would correspond to dihedral angles φ = 0° or 180°. Computations suggest that the rotation around the O-I-O molecular axis is basically free (the rotational barrier is less than 0.3 kcal/mol, as estimated from a constrained potential energy scan along the N-O···O-N dihedral angle). The Ag^+ complexes have similar structural features; however, the Ag-O bonds are predicted to be somewhat shorter as compared to the I-O bonds. The $[RO\text{-}H\text{-}OR]^+$ complexes are hydrogen bonded systems, therefore asymmetric in their O-H bonds. Due to the cationic nature of $R\text{-}OH^+$, the hydrogen bonds are rather strong (fairly short OH···O distances).

Although the influence of the counter-ion on the structure of present complexes was not investigated in detail, we probed this effect by optimizing the structure of [**(1-*OMe*)$_2$-I**]$^+$ and [**(1-*Me*)$_2$-I**]$^+$ complexes in the presence of the BF_4^- anion (see Figure S75).

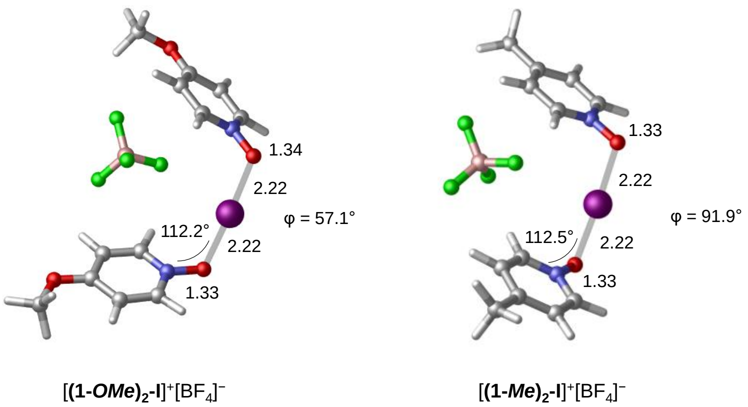

Figure S75. Optimized structures of [**(1-*OMe*)$_2$-I**]$^+BF_4^-$ and [**(1-*Me*)$_2$-I**]$^+BF_4^-$ ion pairs with selected structural parameters.

We find that the BF_4^- anion is not in direct contact with the iodine(I) cation, but rather it interacts with the ligand via F···π and F···H-C type interactions. Due to the flexible nature of the $[RO\text{-}I\text{-}OR]^+$ complexes, the relative position of the ligand varies slightly with respect to their structures without the counter-ion, but the other structural parameters are practically unchanged.

3.3. Relative stability of $[RO\text{-}X\text{-}OR]^+$ complexes

The relative stability of $[RO\text{-}X\text{-}OR]^+$ complexes were quantified in terms of the Gibbs free energies of reactions (1) and (2) in acetonitrile.

$$[RO\text{-}X]^+ + OR \rightarrow [RO\text{-}X\text{-}OR]^+ \quad (1)$$

$$[\mathbf{Py}\text{-}X\text{-}\mathbf{Py}]^+ + 2OR \rightarrow [RO\text{-}X\text{-}OR]^+ + 2\mathbf{Py} \quad (2)$$

The first reaction describes the binding of the second OR ligand to the 1:1 complex, and the associated ΔG measures the thermodynamics of this process. On the other hand, the second reaction quantifies the relative stability of $[RO\text{-}X\text{-}OR]^+$ complexes (only for $X^+ = I^+$ and Ag^+) with respect to the bis-pyridine $[\mathbf{Py}\text{-}X\text{-}\mathbf{Py}]^+$ complex as a reference. The computed free energy data are collected in Table S1 and Table S2.

Table S1. Computed thermodynamics for reaction (1).[a]

	[**(1-*OMe*)$_2$-X**]$^+$	[**(1-*Me*)$_2$-X**]$^+$	[**(2)$_2$-X**]$^+$
$X^+ = I^+$	-15.0	-13.8	-2.0
$X^+ = Ag^+$	-12.0	-10.1	1.6
$X^+ = H^+$	-8.8	-9.1	-3.7

[a] Solution phase Gibbs free energy data are given in kcal/mol.

Table S2. Computed thermodynamics for reaction (2).[a]

	[**(1-*OMe*)$_2$-X**]$^+$	[**(1-*Me*)$_2$-X**]$^+$	[**(2)$_2$-X**]$^+$
$X^+ = I^+$	-2.7	1.9	57.7
$X^+ = Ag^+$	4.5	7.8	29.7

[a] Solution phase Gibbs free energy data are given in kcal/mol.

The results indicate that the coordination of ligands **1-*OMe*** and **1-*Me*** to the corresponding $[RO\text{-}X]^+$ systems is highly exergonic for all $X^+ = I^+$, Ag^+ and H^+ cations (Table S1), so the formation of $[RO\text{-}X\text{-}OR]^+$ complexes is thermodynamically feasible. For ligand **2**, computations predict far less stable $[RO\text{-}X\text{-}OR]^+$ complexes with ΔG values close to zero (for $X^+ = I^+$ and Ag^+), but the hydrogen-bonded complex [**2**-H-**2**]$^+$ is less stable as well than those with ligands **1-*OMe*** and **1-*Me***.

The thermodynamics computed for the ligand exchange reaction (2) point to rather stable halogen-bonded complexes with ligands **1-*OMe*** and **1-*Me***, comparable to that of the reference systems [**Py**-I-**Py**]$^+$, but the analogous complex with **2** is predicted to be highly unstable. A similar trend is obtained for $[RO\text{-}Ag\text{-}OR]^+$ complexes, although these complexes are somewhat destabilized with respect to [**Py**-Ag-**Py**]$^+$.

3.4. Formation of halogen bonded RO···I_2 complexes

Association between ligand **1-*OMe*** and **1-*Me*** and I_2 was examined computationally and complexes **(1-*OMe*)···I_2** and **(1-*Me*)···I_2** were found to be thermodynamically favored relative to their dissociation limits. The optimized structures are depicted in Figure S72.

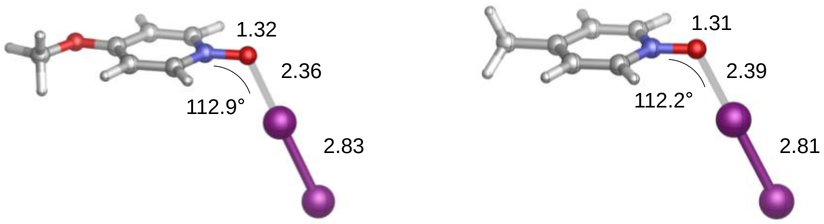

(1-*OMe*)···I_2 (-2.0) **(1-*Me*)···I_2** (-0.4)

Figure S76. Optimized structures of **(1-*OMe*)···I_2** and **(1-*Me*)···I_2** complexes with selected bond distances (in Å) and bond angles (degrees). Relative stabilities with respect to corresponding dissociation limits are shown in parentheses (in kcal/mol).

3.5. Coordination of acetonitrile to $[RO\text{-}X\text{-}OR]^+$ complexes

Since most of the NMR measurements were carried out in acetonitrile, the coordination of the acetonitrile molecule (ACN) to the central cations in thermodynamically stable $[RO\text{-}X\text{-}OR]^+$ complexes ($X^+ = I^+$ and Ag^+ with RO = **1-*OMe*** and **1-*Me***) was examined computationally. We identified several conformers computationally for complexes with one and two coordinating ACN molecules (i.e. $[RO\text{-}X\text{-}OR]^+(ACN)$ and $[RO\text{-}X\text{-}OR]^+(ACN)_2$ complexes, respectively). The optimized structures for complexes with ligand **1-*OMe*** are depicted in Figure S77. We note that very similar structures were found for ligand **1-*Me*** (the optimized structures are provided in xyz format in section 3.8)

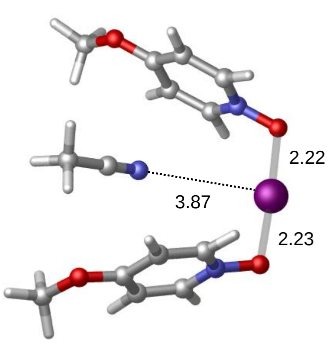

[(**1-*OMe***)$_2$**-I**]$^+$(AcN) (+3.0)

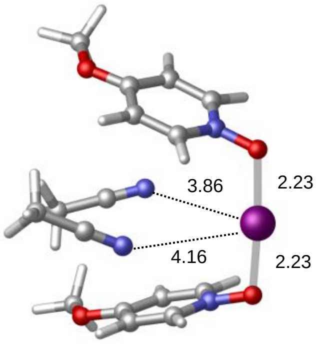

[(**1-*OMe***)$_2$**-I**]$^+$(AcN)$_2$ (+8.2)

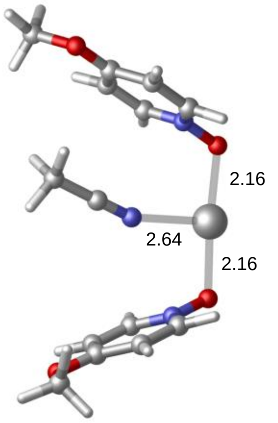

[(**1-*OMe***)$_2$**-Ag**]$^+$(AcN) (+1.4)

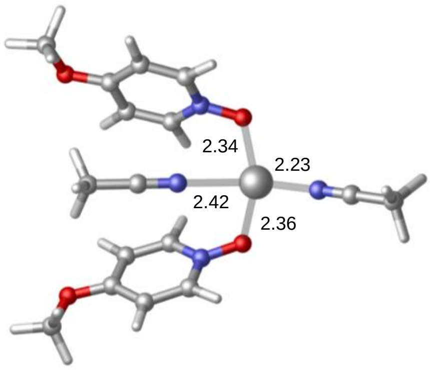

[(**1-*OMe***)$_2$**-Ag**]$^+$(AcN)$_2$ (+2.2)

Figure S77. Optimized structures of [RO-X-OR]$^+$(ACN) and [RO-X-OR]$^+$(ACN)$_2$ complexes with selected bond distances (in Å). Relative stabilities with respect to [RO-X-OR]$^+$ + ACN and [RO-X-OR]$^+$ + 2ACN dissociation limits are shown in parentheses (in kcal/mol).

It is apparent from the obtained structures that ACN does not coordinate to the central iodine of [RO-I-OR]$^+$ complexes, it interacts only weakly with the ligands (ACN-I bond distances are around 4 Å in all structures; the association is clearly unfavored thermodynamically). On the contrary, the short ACN-Ag distances give evidence for coordination to Ag^+ of [RO-Ag-OR]$^+$ complexes. The computed relative stabilities are in line with these observations.

Additionally, we have computed the Gibbs free energy of reaction (3), which measures the relative stabilities with respect to bis(ACN) complexes [ACN-X-ACN]$^+$ (see Table S3). The predicted data suggest that this ligand exchange process is highly unfavored for [RO-I-OR]$^+$ complexes, however, thermodynamic equilibrium between [RO-Ag-OR]$^+$ and [ACN-Ag-ACN]$^+$ complexes may exist in the solution of acetonitrile.

$$[\text{RO-X-OR}]^+ + 2\text{ACN} \rightarrow [\text{ACN-X-ACN}]^+ + 2\text{RO} \quad (3)$$

Table S3. Computed thermodynamics for reaction (3).[a]

	1-*OMe*	**1-*Me***
$X^+ = I^+$	25.2	20.5
$X^+ = Ag^+$	1.5	-1.9

[a] Gibbs free energy data are given in kcal/mol.

3.6. Computed ^{15}N NMR chemical shifts

DFT calculations were also carried out to predict the ^{15}N chemical shifts for the experimentally characterized $[RO\text{-}I\text{-}OR]^+$ complexes (RO = **1**-***OMe*** and **1**-***Me***; $X^+ = I^+$, Ag^+ and H^+). The results are summarized in Table S4.

Table S4. Computed ^{15}N NMR chemical shifts for $[RO\text{-}X\text{-}OR]^+$ complexes.[a]

	1-***OMe***	**1**-***Me***
OR ligand	-98.8 [-103.0]	-86.6 [-91.7]
$[RO\text{-}I\text{-}OR]^+$	-143.5 [-134.2]	-129.0 [-105.0[b]]
$[RO\text{-}Ag\text{-}OR]^+$	-131.4 [-105.1]	-116.6 [-92.0]
$[RO\text{-}H\text{-}OR]^+$	-164.9 / -138.5 [−152.7]	-147.4 / -126.1 [−129.5]

[a] Chemical shifts are given in ppm with respect to nitromethane (-128.6 ppm). Experimental data are shown in brackets.[b] The experimental chemical shift determined in CD_2Cl_2 is in better agreement with calculations (119.4 ppm)

The applied methodology gives quite reasonable $\delta^{15}N$ predictions for the two ligands **1**-***OMe*** and **1**-***Me*** (underestimation by 4-5 ppm). For $[RO\text{-}I\text{-}OR]^+$ complexes, the agreement is still acceptable for **1**-***OMe*** (overestimation by 9 ppm). The calculated chemical shift of the $[RO\text{-}I\text{-}OR]^+$ complex of **1**-***Me*** deviates significantly from the experimental value determined in acetonitrile, however, this could be related to the difficulties forming the complex in acetonitrile. The experimental chemical shift of the $[RO\text{-}I\text{-}OR]^+$ complex of **1**-***Me*** in CD_2Cl_2 is much closer to the calculated value. Our results obtained for the $[(\mathbf{1\text{-}}\boldsymbol{OMe})_2\text{-}\mathbf{I}]^+[BF_4]^-$ and $[(\mathbf{1\text{-}}\boldsymbol{Me})_2\text{-}\mathbf{I}]^+[BF_4]^-$ ion pairs indicate that the deviation does not arise from the omission of the counterions in the model systems (for the ion pairs, computations give -142.9 and -128.6 ppm, respectively). Interestingly, $^{15}\delta N$ data computed for $[RO\text{-}Ag\text{-}OR]^+$ complexes are far off the experimental observations. Computations predict significant variation in the $\delta^{15}N$ chemical shifts upon the coordination of both ligands to Ag^+, however, this contradicts with experiment (only a very small alteration in $^{15}\delta N$ is measured). For hydrogen bonded $[RO\text{-}H\text{-}OR]^+$ complexes, the average values of the two computed $^{15}\delta N$ chemical shifts correlate well with experimental data.

As noted above, the coordination of ACN molecules to $[RO\text{-}Ag\text{-}OR]^+$ complexes to form tri- or tetra-coordinated $[RO\text{-}X\text{-}OR]^+(ACN)$ and $[RO\text{-}X\text{-}OR]^+(ACN)_2$ complexes is thermodynamically feasible (see Figure S77). We have, therefore, computed the $\delta^{15}N$ shifts in these complexes as well (see Table S5). Although the chemical shifts are lowered upon the coordination of ACN molecules as compared to those in $[RO\text{-}Ag\text{-}OR]^+$ (the Ag-OR bonds are weakened), the $\delta^{15}N$ predictions are still far away from those of the **1**-***OMe*** and **1**-***Me*** ligands.

The equilibrium predicted for reaction (3) may imply that the concentration of $[RO\text{-}Ag\text{-}OR]^+$ complexes in acetonitrile is rather low, which could be a plausible explanation for the observed chemical shifts.

Table S5. Computed ^{15}N NMR chemical shifts $[RO\text{-}Ag\text{-}OR]^+(ACN)$ and $[RO\text{-}Ag\text{-}OR]^+(ACN)_2$ complexes.[a]

	1-***OMe***	**1**-***Me***
$[RO\text{-}Ag\text{-}OR]^+(ACN)$	-128.8 / -128.8 (-131.4)	-111.3 / -109.6 (-116.6)
$[RO\text{-}Ag\text{-}OR]^+(ACN)_2$	-116.5 / -117.3 (-131.4)	-103.8 / -106.7 (-116.6)

[a] Chemical shifts are given in ppm with respect to nitromethane. Data obtained for computations of $[RO\text{-}Ag\text{-}OR]^+$ complexes are shown in parenthesis.

3.7. Total energy data

Table S6. Total energy data (in kcal/mol) computed for ωB97X-D/Def2SVP optimized structures.[a]

structure	$E_{0,sol}$	$G_{0,sol}$	$E_{0,sol}'$	G
1-*OMe*	-0.70	-0.70	-0.70	-0.70
1-*Me*	-0.58	-0.58	-0.58	-0.58
2	-0.86	-0.86	-0.86	-0.86
[**1-*OMe*-I**]$^+$	-1.17	-1.17	-1.17	-1.17
[**1-*Me*-I**]$^+$	-1.05	-1.05	-1.05	-1.05
[**2-I**]$^+$	-1.33	-1.33	-1.33	-1.33
[**(1-*OMe*)$_2$-I**]$^+$	-1.87	-1.87	-1.87	-1.87
[**(1-*Me*)$_2$-I**]$^+$	-1.63	-1.63	-1.63	-1.63
[**(2)$_2$-I**]$^+$	-2.18	-2.18	-2.19	-2.19
[**1-*OMe*-Ag**]$^+$	-0.93	-0.93	-0.93	-0.93
[**1-*Me*-Ag**]$^+$	-0.81	-0.81	-0.81	-0.81
[**2-Ag**]$^+$	-1.09	-1.09	-1.09	-1.09
[**(1-*OMe*)$_2$-Ag**]$^+$	-1.63	-1.63	-1.63	-1.63
[**(1-*Me*)$_2$-Ag**]$^+$	-1.39	-1.39	-1.39	-1.39
[**(2)$_2$-Ag**]$^+$	-1.94	-1.94	-1.95	-1.95
[**1-*OMe*-H**]$^+$	-0.70	-0.70	-0.70	-0.70
[**1-*Me*-H**]$^+$	-0.58	-0.58	-0.58	-0.58
[**2-H**]$^+$	-0.86	-0.86	-0.86	-0.86
[**(1-*OMe*)$_2$-H**]$^+$	-1.40	-1.39	-1.40	-1.40
[**(1-*Me*)$_2$-H**]$^+$	-1.16	-1.16	-1.16	-1.16
[**(2)$_2$-H**]$^+$	-1.71	-1.71	-1.71	-1.71
[**(1-*OMe*)$_2$-I**]$^+$[BF$_4$]$^-$	-2.54	-2.54	-2.55	-2.55
[**(1-*Me*)$_2$-I**]$^+$[BF$_4$]$^-$	-2.31	-2.30	-2.31	-2.31
[**Py**-I-**Py**]$^+$	-1.26	-1.26	-1.27	-1.27
[**Py**-Ag-**Py**]$^+$	-1.02	-1.02	-1.03	-1.03
Py	-0.40	-0.40	-0.40	-0.40
(1-*OMe*)···I$_2$	-1.65	-1.65	-1.65	-1.65
(1-*Me*)···I$_2$	-1.53	-1.53	-1.53	-1.53
I$_2$	-0.95	-0.95	-0.95	-0.95
[**(1-*OMe*)$_2$-I**]$^+$(ACN)	-2.08	-2.08	-2.08	-2.08
[**(1-*OMe*)$_2$-I**]$^+$(ACN)$_2$	-2.29	-2.29	-2.29	-2.29
[**(1-*OMe*)$_2$-Ag**]$^+$(ACN)	-1.84	-1.84	-1.84	-1.84
[**(1-*OMe*)$_2$-Ag**]$^+$(ACN)$_2$	-2.05	-2.05	-2.05	-2.05
[**(1-*Me*)$_2$-I**]$^+$(ACN)	-1.84	-1.84	-1.84	-1.84
[**(1-*Me*)$_2$-I**]$^+$(ACN)$_2$	-2.05	-2.05	-2.05	-2.05
[**(1-*Me*)$_2$-Ag**]$^+$(ACN)	-1.60	-1.60	-1.60	-1.60
[**(1-*Me*)$_2$-Ag**]$^+$(ACN)$_2$	-1.81	-1.81	-1.81	-1.81
ACN	-0.21	-0.21	-0.21	-0.21
[ACN-I-ACN]$^+$	-0.90	-0.90	-0.90	-0.90
[ACN-Ag-ACN]$^+$	-0.66	-0.66	-0.66	-0.66

[a] $G = E_{0,sol}' + (G_{0,sol} - E_{0,sol}) + \Delta G_{conc}$, where $E_{0,sol}'$ and $E_{0,sol}$ are solution phase electronic energies obtained at the ωB97X-D/Def2TZVPP and ωB97X-D/Def2SVP levels, respectively, and $G_{0,sol}$ is solution phase Gibbs free energy computed at ωB97X-D/Def2SVP level. ΔG_{conc} = 0.003019 a.u. corresponding to c = 1 mol/dm^3 concentration except for ACN, where ΔG_{conc} = 0.005805 a.u. that corresponds to molar concentration of acetonitrile (c = 19.15 mol/dm^3).

3.8. Cartesian coordinates

Cartesian coordinates of the optimized geometries are given below in standard XYZ format (units are in Å). The first line shows the number of atoms, the second line is the notation used for structures discussed in the main text and the SI (see above in Table S6).

16
1-*OMe*
```
C   0.500544    0.028715    0.535257
C   1.207304   -0.515196   -0.514301
C   1.774090    0.314620   -1.492925
C   1.588402    1.693999   -1.354815
C   0.868200    2.188194   -0.278790
N   0.324113    1.377024    0.665680
H   0.038569   -0.563618    1.324422
H   1.324471   -1.597950   -0.580059
H   1.993146    2.410306   -2.069528
H   0.690724    3.250969   -0.116581
O  -0.334231    1.855647    1.647985
O   2.450243   -0.276444   -2.485886
C   3.034967    0.531963   -3.485350
H   3.531952   -0.149545   -4.186194
H   2.273462    1.114267   -4.030239
H   3.784707    1.219996   -3.060647
```

15
1-*Me*
```
C   0.907921   -0.060839    0.559323
C   1.492535   -0.565824   -0.586443
C   1.529632    0.177809   -1.772351
C   0.941530    1.445262   -1.721205
C   0.363700    1.923349   -0.558236
N   0.342278    1.181053    0.584782
H   0.851876   -0.598555    1.505354
H   1.926041   -1.567533   -0.542036
H   0.924261    2.088535   -2.603828
H  -0.107797    2.901475   -0.467505
O  -0.190704    1.631103    1.645449
C   2.185073   -0.351499   -3.015216
H   1.872247    0.214047   -3.903919
H   3.282119   -0.276130   -2.938117
H   1.941550   -1.412751   -3.171737
```

21
2
```
C   -7.913874   -3.363164    0.012412
C   -6.516017   -3.219940    0.010660
C   -5.913629   -1.962851    0.019121
C   -6.764715   -0.864052    0.029434
C   -8.164705   -0.978919    0.031452
C   -8.749917   -2.249274    0.022746
H   -8.349028   -4.364897    0.005566
H   -5.885584   -4.112135    0.002589
H   -4.829401   -1.840020    0.017890
H   -9.836038   -2.363211    0.024129
C   -7.503090    1.192051    0.047369
C   -7.545680    2.581235    0.058806
C   -8.810358    3.167653    0.066448
C   -9.979864    2.388719    0.062769
```

C	-9.916091	0.997457	0.051145
C	-8.656280	0.389895	0.043410
H	-6.631408	3.176771	0.061586
H	-8.891603	4.257069	0.075537
H	-10.952951	2.884628	0.069076
H	-10.826370	0.394115	0.048330
O	-6.368133	0.439041	0.038881

17
[**1-*OMe*-I**]$^+$

C	0.617378	0.085956	0.712287
C	1.165061	-0.474646	-0.408208
C	1.713278	0.357109	-1.410819
C	1.687760	1.755023	-1.220943
C	1.126388	2.263240	-0.075189
N	0.610516	1.432517	0.852237
H	0.173532	-0.485288	1.528150
H	1.176504	-1.557798	-0.527534
H	2.099049	2.451478	-1.949966
H	1.066742	3.329137	0.148486
O	0.131251	1.960890	1.998402
O	2.215599	-0.240543	-2.463673
C	2.781765	0.526962	-3.523759
H	3.117585	-0.197529	-4.273068
H	2.026758	1.193859	-3.965672
H	3.641166	1.110956	-3.162932
I	-1.898263	2.396922	1.967120

16
[**1-*Me*-I**]$^+$

C	1.008838	-0.037666	0.649391
C	1.433620	-0.584472	-0.541947
C	1.473131	0.196591	-1.706787
C	1.066672	1.537834	-1.609403
C	0.650226	2.053789	-0.403288
N	0.634928	1.255449	0.682992
H	0.952035	-0.580441	1.593405
H	1.735757	-1.632119	-0.557031
H	1.074749	2.191688	-2.482330
H	0.324406	3.083628	-0.250962
O	0.301312	1.794686	1.876278
I	-1.726381	1.743785	2.310035
C	1.955258	-0.363808	-3.003630
H	1.347079	0.006125	-3.840745
H	2.991011	-0.028391	-3.177346
H	1.947345	-1.461050	-2.996503

22
[**2-I**]$^+$

C	-7.912849	-3.349572	0.016470
C	-6.518147	-3.242332	-0.053895
C	-5.883187	-1.997994	-0.081840
C	-6.724154	-0.906332	-0.031815
C	-8.113797	-0.963293	0.038054
C	-8.724787	-2.217462	0.059772
H	-8.371231	-4.340059	0.036155
H	-5.906434	-4.145701	-0.088131
H	-4.797489	-1.905742	-0.136359
H	-9.811590	-2.301845	0.108745
C	-7.504236	1.253022	-0.005909
C	-7.553884	2.630518	-0.025771
C	-8.836890	3.181964	0.022566
C	-9.978212	2.372356	0.082994

C	-9.880118	0.981912	0.096646
C	-8.609186	0.407774	0.054201
H	-6.659160	3.252695	-0.072728
H	-8.943299	4.268226	0.011547
H	-10.963321	2.841216	0.118673
H	-10.770159	0.351967	0.137434
O	-6.324001	0.460062	-0.078490
I	-4.438985	1.133541	0.641840

33

[**(1-*OMe*)$_2$-I**]$^+$

C	9.369537	-0.689835	0.146070
C	9.415488	0.290821	1.152595
C	8.392941	0.355571	2.074992
N	7.361723	-0.507456	2.026330
C	7.289180	-1.463081	1.072078
C	8.275052	-1.576909	0.125135
O	6.404202	-0.437108	2.952926
I	4.680706	0.827987	2.353297
O	2.955612	2.100954	1.774777
N	1.938739	1.413131	1.252223
C	0.962753	0.959516	2.060052
C	-0.118881	0.273757	1.549476
C	-0.193188	0.044680	0.164257
C	0.844311	0.536784	-0.652273
C	1.894701	1.212315	-0.084585
O	-1.172215	-0.603765	-0.437752
C	-2.244314	-1.133707	0.331165
O	10.284681	-0.845709	-0.791883
C	11.412476	0.019119	-0.827361
H	-0.885631	-0.072394	2.240781
H	0.815586	0.379563	-1.730486
H	1.090924	1.176018	3.120830
H	2.731977	1.621236	-0.650143
H	-1.877537	-1.874755	1.057726
H	-2.787326	-0.331346	0.853622
H	-2.916116	-1.623734	-0.382074
H	8.357223	1.086961	2.882793
H	6.414770	-2.111956	1.120624
H	10.231353	1.007670	1.232717
H	8.210237	-2.351071	-0.639577
H	12.007944	-0.073713	0.093661
H	11.101216	1.065358	-0.969927
H	12.014377	-0.301928	-1.684468

31

[**(1-*Me*)$_2$-I**]$^+$

C	-0.044352	0.031481	-0.030958
C	-0.008690	0.019971	1.371643
C	0.982339	0.694359	2.052470
N	1.926720	1.375299	1.371041
C	1.935966	1.412629	0.025345
C	0.959156	0.749603	-0.692394
O	2.850295	2.055526	2.046746
I	4.676278	0.881769	2.512721
O	6.505385	-0.273486	3.012355
N	7.388778	-0.342425	2.019104
C	8.336349	0.611855	1.913095
C	9.283592	0.535508	0.914226
C	9.271603	-0.528931	0.000147
C	8.267173	-1.492584	0.150622
C	7.334388	-1.380414	1.163525
C	10.302701	-0.623889	-1.079910

C	-1.113675	-0.702978	-0.776372
H	10.040265	1.319246	0.851819
H	8.201479	-2.345598	-0.526255
H	8.289597	1.407172	2.657247
H	6.528271	-2.092879	1.338855
H	1.068036	0.730723	3.138469
H	2.741951	1.992016	-0.425196
H	-0.763109	-0.518929	1.946925
H	0.988186	0.800589	-1.781684
H	-1.042750	-0.530690	-1.857819
H	-1.030608	-1.784283	-0.585266
H	-2.108674	-0.387698	-0.428033
H	10.097411	-1.458814	-1.761835
H	10.339781	0.311125	-1.658545
H	11.299485	-0.770350	-0.635190

43

[**(2)$_2$-I**]$^+$

C	-7.810717	-3.333239	0.126824
C	-6.469287	-3.207724	-0.260292
C	-5.885645	-1.957148	-0.472298
C	-6.712696	-0.867013	-0.273556
C	-8.052116	-0.950038	0.111436
C	-8.615499	-2.211481	0.314990
H	-8.230711	-4.328976	0.281977
H	-5.862198	-4.104053	-0.402061
H	-4.842571	-1.853150	-0.775442
H	-9.660537	-2.310056	0.613876
C	-7.481625	1.253015	-0.137452
C	-7.550054	2.633176	-0.178236
C	-8.789069	3.188597	0.147079
C	-9.884530	2.383594	0.489334
C	-9.778642	0.994570	0.518237
C	-8.548143	0.417154	0.198546
H	-6.692996	3.252657	-0.446781
H	-8.901270	4.274474	0.131551
H	-10.837342	2.855816	0.736628
H	-10.632744	0.368643	0.782664
O	-6.354262	0.477658	-0.437390
C	1.393084	0.125581	0.727166
C	0.318329	-0.685633	0.337290
C	-0.900971	-0.136391	-0.064243
C	-0.971969	1.244100	-0.047392
C	0.074510	2.086039	0.333262
C	1.285815	1.514834	0.728364
H	2.330848	-0.341755	1.034043
H	0.431548	-1.771490	0.344301
H	-1.741383	-0.760597	-0.371905
H	2.124240	2.145601	1.029001
C	-1.732086	3.360403	-0.259741
C	-2.546706	4.445924	-0.523366
C	-1.975700	5.700718	-0.302288
C	-0.657604	5.834135	0.155919
C	0.135405	4.716609	0.408539
C	-0.415983	3.451254	0.196724
H	-3.571261	4.334205	-0.881674
H	-2.573608	6.593869	-0.494240
H	-0.246514	6.832846	0.315731
H	1.162460	4.821506	0.762532
O	-2.082012	2.012963	-0.420952
I	-4.219394	1.246416	-0.434250

17

[**1-*OMe*-Ag**]$^+$

C	0.636738	0.103627	0.711550
C	1.175425	-0.466822	-0.416591
C	1.725300	0.349131	-1.421341
C	1.705322	1.738046	-1.224979
C	1.149450	2.250670	-0.068230
N	0.623257	1.447689	0.876456
H	0.191045	-0.469152	1.524435
H	1.172858	-1.551090	-0.530631
H	2.113696	2.437172	-1.953628
H	1.097684	3.317734	0.147519
O	0.132446	1.967547	1.984623
O	2.224776	-0.259302	-2.488545
C	2.783553	0.518430	-3.534952
H	3.117979	-0.191742	-4.299629
H	2.032022	1.195566	-3.970525
H	3.646744	1.101627	-3.177672
Ag	-2.003584	2.403043	2.068030

16

[**1-*Me*-Ag**]$^+$

C	1.043764	-0.030900	0.648122
C	1.460664	-0.578460	-0.551156
C	1.490315	0.192973	-1.717832
C	1.083033	1.528526	-1.601469
C	0.674281	2.038964	-0.385398
N	0.654360	1.259371	0.718611
H	0.994489	-0.582410	1.586586
H	1.761724	-1.627286	-0.564630
H	1.078340	2.190413	-2.469321
H	0.342406	3.066227	-0.234849
O	0.290398	1.766702	1.873271
C	1.954539	-0.368800	-3.026918
H	1.326645	-0.009528	-3.854752
H	2.986680	-0.041237	-3.231680
H	1.943082	-1.466831	-3.018300
Ag	-1.843217	1.839723	2.356115

22

[**2-Ag**]$^+$

C	-7.900175	-3.361487	0.044305
C	-6.503519	-3.216774	0.036497
C	-5.904737	-1.957210	0.030794
C	-6.764240	-0.869885	0.033268
C	-8.160198	-0.978670	0.040972
C	-8.740709	-2.250502	0.046588
H	-8.332677	-4.364147	0.048655
H	-5.870464	-4.106713	0.034899
H	-4.819602	-1.830133	0.024775
H	-9.826131	-2.367405	0.052687
C	-7.523221	1.207197	0.033594
C	-7.568867	2.592414	0.031616
C	-8.839688	3.167336	0.037527
C	-9.999860	2.376409	0.045003
C	-9.924543	0.985348	0.046932
C	-8.660067	0.389205	0.041141
H	-6.658716	3.196042	0.025918
H	-8.931009	4.255632	0.036278
H	-10.977504	2.862825	0.049441
H	-10.828624	0.373376	0.052748
O	-6.375089	0.449502	0.028668
Ag	-4.115476	1.212560	0.027856

33
[**(1-*OMe*)$_2$-Ag**]$^+$

Ag	-2.343030	1.143318	1.539190
O	-0.256190	0.771927	1.586233
O	-4.431636	1.511730	1.484126
N	0.465530	1.410891	2.491680
N	-5.174455	0.832882	0.628255
C	0.597548	0.892767	3.735176
C	1.107840	2.545263	2.156453
C	-6.128467	0.007660	1.097815
C	-5.014094	1.000247	-0.706050
C	1.376955	1.514018	4.680846
H	0.043733	-0.027986	3.918154
C	1.906971	3.216749	3.061920
H	0.946032	2.887008	1.134271
C	-6.961988	-0.692055	0.245681
H	-6.187268	-0.064327	2.183573
C	-5.807482	0.328600	-1.604140
H	-4.218494	1.685568	-0.999784
C	2.054404	2.704278	4.359814
H	1.468069	1.083156	5.678153
H	2.400517	4.130534	2.733772
C	-6.810073	-0.542324	-1.140433
H	-7.714967	-1.346032	0.683548
H	-5.657507	0.473530	-2.674282
O	2.786967	3.257559	5.315733
O	-7.541857	-1.162981	-2.055031
C	3.487203	4.462870	5.050775
C	-8.562230	-2.057270	-1.640621
H	4.221627	4.324722	4.241965
H	2.791805	5.275137	4.787341
H	4.012449	4.721445	5.977109
H	-9.324611	-1.537408	-1.039521
H	-8.142799	-2.896756	-1.064270
H	-9.023386	-2.441685	-2.557365

31
[**(1-*Me*)$_2$-Ag**]$^+$

C	0.754402	0.057693	-0.844115
C	2.085392	-0.182186	-0.549509
C	3.084014	0.695961	-0.977383
C	2.663567	1.815566	-1.708725
C	1.327440	2.020273	-1.983358
N	0.387868	1.145204	-1.553171
H	-0.056459	-0.601347	-0.530014
H	2.331532	-1.077260	0.024089
H	3.384861	2.546471	-2.078647
H	0.941280	2.867919	-2.548340
O	-0.860663	1.402777	-1.847782
C	-5.660984	0.445166	-0.659311
C	-6.940502	0.809383	-0.276237
C	-7.952460	-0.145925	-0.156355
C	-7.599379	-1.472377	-0.441132
C	-6.313427	-1.796930	-0.819247
N	-5.358595	-0.842453	-0.925397
H	-4.843091	1.160179	-0.766940
H	-7.134795	1.863484	-0.071813
H	-8.334922	-2.275745	-0.369748
H	-5.980752	-2.807611	-1.053161
O	-4.161394	-1.221976	-1.292559
C	-9.348297	0.214782	0.252156
H	-10.061905	-0.054980	-0.541591
H	-9.641230	-0.341978	1.155402

H -9.442497 1.289377 0.456234
C 4.532665 0.467204 -0.670305
H 5.134632 0.504314 -1.590618
H 4.910488 1.257091 -0.002285
H 4.691204 -0.503826 -0.183136
Ag -2.494894 0.084349 -1.502273

43
[**(2)₂-Ag**]+

C	-8.522282	-3.082541	-1.107671
C	-7.125598	-3.201495	-1.187970
C	-6.284573	-2.161735	-0.791400
C	-6.907859	-1.017946	-0.319431
C	-8.296323	-0.865431	-0.225910
C	-9.121447	-1.919665	-0.628401
H	-9.148192	-3.918321	-1.427234
H	-6.685439	-4.125785	-1.568222
H	-5.196584	-2.240247	-0.848429
H	-10.207825	-1.830864	-0.567477
C	-7.234544	1.013356	0.500768
C	-6.998964	2.283224	1.002660
C	-8.127759	3.035495	1.327558
C	-9.422828	2.522499	1.151702
C	-9.629370	1.241036	0.645499
C	-8.511192	0.470721	0.313036
H	-5.985261	2.668776	1.135886
H	-7.998035	4.043522	1.727177
H	-10.282472	3.141108	1.417671
H	-10.638026	0.845719	0.510735
O	-6.261596	0.116190	0.119422
C	1.821520	0.765729	1.316670
C	0.821833	-0.211759	1.445225
C	-0.493667	0.040123	1.055752
C	-0.747689	1.300974	0.541006
C	0.223854	2.298761	0.399219
C	1.536481	2.025876	0.795266
H	2.840425	0.531548	1.631921
H	1.076230	-1.190309	1.858026
H	-1.282423	-0.709929	1.149843
H	2.316617	2.783243	0.697032
C	-1.801078	3.043869	-0.328858
C	-2.798221	3.853991	-0.847356
C	-2.412219	5.140347	-1.224126
C	-1.085209	5.576049	-1.080927
C	-0.102878	4.738653	-0.556590
C	-0.469194	3.445413	-0.172427
H	-3.826444	3.500544	-0.953339
H	-3.159806	5.819954	-1.638747
H	-0.820662	6.590348	-1.386891
H	0.927906	5.081152	-0.447008
O	-1.974019	1.747178	0.101480
Ag	-3.976792	0.558239	0.107318

17
[**1-*OMe*-H**]+

C	0.534048	0.597513	0.885962
C	1.432392	0.266970	-0.092165
C	1.968832	1.278395	-0.919894
C	1.554808	2.610821	-0.715881
C	0.650934	2.883656	0.283191
N	0.177027	1.889666	1.054935
H	0.069223	-0.122221	1.560257
H	1.727803	-0.772584	-0.232356

H	1.922423	3.438297	-1.320684
H	0.277461	3.883884	0.504834
O	-0.764565	2.186982	1.991701
O	2.825982	0.898428	-1.837291
C	3.405031	1.857057	-2.719632
H	4.071484	1.293132	-3.380744
H	2.626554	2.354789	-3.316682
H	3.986663	2.602084	-2.156655
H	-0.276718	2.353220	2.820696

16

[**1-*Me*-H**]$^+$

C	0.717215	-0.073537	0.607886
C	1.400675	-0.550248	-0.488388
C	1.506191	0.228282	-1.652834
C	0.891250	1.489026	-1.653529
C	0.216472	1.935981	-0.537106
N	0.159871	1.150364	0.551748
H	0.585336	-0.620553	1.541793
H	1.849502	-1.542719	-0.433622
H	0.930912	2.134064	-2.531912
H	-0.289604	2.898943	-0.463236
O	-0.564143	1.582076	1.619971
H	0.073651	2.010806	2.222390
C	2.264254	-0.269236	-2.839454
H	2.015285	0.299269	-3.744361
H	3.344469	-0.159508	-2.649180
H	2.068654	-1.337385	-3.008036

22

[**2-H**]$^+$

C	-7.858892	-3.334191	0.026183
C	-6.462608	-3.228068	-0.002635
C	-5.827944	-1.982426	-0.034751
C	-6.683613	-0.906406	-0.024107
C	-8.071863	-0.949734	0.007821
C	-8.678889	-2.205296	0.029749
H	-8.315497	-4.325435	0.046016
H	-5.850608	-4.131757	-0.004551
H	-4.743121	-1.874103	-0.064327
H	-9.765790	-2.296098	0.052156
C	-7.470073	1.278112	-0.005123
C	-7.496368	2.652532	0.006856
C	-8.779312	3.206983	0.054152
C	-9.922766	2.398480	0.074902
C	-9.835180	1.006008	0.056199
C	-8.567192	0.426169	0.019633
H	-6.592439	3.261833	-0.016464
H	-8.883627	4.293280	0.070372
H	-10.906288	2.870814	0.106340
H	-10.730371	0.382724	0.072696
O	-6.278637	0.473792	-0.085930
H	-5.504040	0.747708	0.464973

33

[**(1-*OMe*)$_2$-H**]$^+$

C	-2.398294	2.081931	1.531533
C	-1.794939	0.906667	1.895897
C	-0.730132	0.399855	1.122044
C	-0.296660	1.142495	0.008672
C	-0.941244	2.320037	-0.303671
N	-1.972197	2.755233	0.440413
H	-3.238651	2.527747	2.063201

H	-2.145888	0.361643	2.771929
H	0.528319	0.820430	-0.624875
H	-0.673914	2.944403	-1.156109
O	-2.630457	3.871655	0.072192
C	-5.300730	1.776376	-0.316248
C	-5.728244	0.634408	0.334491
C	-5.100842	-0.589258	0.057617
C	-4.065728	-0.602390	-0.895719
C	-3.684311	0.566853	-1.506757
N	-4.290100	1.740822	-1.205785
H	-5.736630	2.760720	-0.145681
H	-6.544178	0.723376	1.050381
H	-3.559735	-1.535493	-1.144282
H	-2.882857	0.634954	-2.242107
O	-3.861691	2.855735	-1.773665
H	-3.205748	3.541010	-0.779840
O	-0.211618	-0.748133	1.506258
O	-5.410592	-1.745009	0.626383
C	-6.437663	-1.787183	1.604748
H	-6.507691	-2.831303	1.929722
H	-6.186463	-1.152711	2.469236
H	-7.403307	-1.472471	1.179328
C	0.857359	-1.327642	0.767485
H	1.740399	-0.671034	0.776393
H	1.097306	-2.270143	1.271378
H	0.549932	-1.532126	-0.269313

31

[**(1-*Me*)$_2$-H**]$^+$

C	-1.782334	0.792067	0.917725
C	-0.747375	-0.095936	1.126684
C	0.577994	0.284665	0.873406
C	0.793160	1.585389	0.398634
C	-0.270981	2.439099	0.186830
N	-1.523851	2.027616	0.449462
H	-2.828731	0.563776	1.122682
H	-0.983989	-1.093421	1.499611
H	1.799923	1.943633	0.179217
H	-0.178932	3.456870	-0.191765
O	-2.534088	2.882842	0.248968
C	-5.574920	1.524777	-0.123112
C	-6.527555	0.683802	0.420640
C	-6.604259	-0.657645	0.029009
C	-5.678817	-1.091230	-0.928988
C	-4.733868	-0.223756	-1.440490
N	-4.693504	1.062790	-1.035243
H	-5.480917	2.579888	0.133017
H	-7.222212	1.094911	1.154959
H	-5.683194	-2.122328	-1.286158
H	-3.981198	-0.500509	-2.177976
O	-3.784333	1.864822	-1.549384
H	-3.123500	2.463080	-0.584265
C	-7.611756	-1.592500	0.624470
H	-7.892106	-2.381628	-0.086441
H	-7.184338	-2.082428	1.514646
H	-8.515117	-1.054311	0.942269
C	1.716516	-0.650073	1.132683
H	2.589354	-0.397829	0.516113
H	2.017922	-0.573893	2.190291
H	1.424680	-1.692427	0.945668

43

[**(2)$_2$-H**]$^+$

C	-6.854461	-2.813572	-1.249151
C	-5.955447	-2.395988	-2.239604
C	-5.417761	-1.106078	-2.235608
C	-5.833946	-0.304548	-1.195026
C	-6.717668	-0.673501	-0.184488
C	-7.246871	-1.964196	-0.214506
H	-7.255244	-3.828210	-1.289018
H	-5.668199	-3.086493	-3.034724
H	-4.718314	-0.758105	-2.996767
H	-7.944952	-2.297383	0.554999
C	-6.041726	1.485666	0.204868
C	-5.858955	2.731034	0.766505
C	-6.566986	2.954194	1.950585
C	-7.399947	1.969667	2.498208
C	-7.553945	0.723124	1.891117
C	-6.849391	0.472382	0.713219
H	-5.213494	3.489806	0.320589
H	-6.468073	3.918856	2.451622
H	-7.940062	2.184638	3.422254
H	-8.202494	-0.039644	2.324814
O	-5.424721	1.038736	-0.992245
C	-1.130351	0.449756	2.553539
C	-1.970101	-0.501809	1.957122
C	-2.655891	-0.225262	0.772740
C	-2.453344	1.036664	0.245043
C	-1.630019	2.012808	0.808957
C	-0.948346	1.711794	1.989926
H	-0.608488	0.194781	3.478079
H	-2.090494	-1.482158	2.422352
H	-3.303361	-0.961863	0.293177
H	-0.293891	2.448892	2.458465
C	-2.603822	2.833962	-1.088847
C	-2.980055	3.673836	-2.120391
C	-2.417306	4.951397	-2.095343
C	-1.527501	5.337586	-1.082267
C	-1.171458	4.462528	-0.057184
C	-1.725942	3.180796	-0.059980
H	-3.671730	3.356504	-2.902066
H	-2.676088	5.660302	-2.884396
H	-1.106778	6.344951	-1.098342
H	-0.480411	4.768502	0.730196
O	-3.049541	1.521778	-0.920752
H	-4.354031	1.251486	-1.055218

38

[**(1-*OMe*)$_2$-I**]$^+$[BF_4]$^-$

C	1.102661	1.968379	2.720671
C	0.304168	0.832433	2.491425
C	1.619559	2.656680	1.609028
C	0.055991	0.422972	1.205873
H	-0.137451	0.279348	3.319350
O	1.308321	2.314261	3.979120
C	1.323815	2.203912	0.340785
H	2.241864	3.544504	1.709022
N	0.566634	1.107212	0.156504
H	-0.562917	-0.439910	0.958838
C	2.091047	3.462264	4.275591
H	1.677795	2.688266	-0.569115
O	0.332645	0.687916	-1.088959
H	3.118431	3.347730	3.897111
H	1.634553	4.370171	3.852057
H	2.112717	3.541558	5.368102
N	-4.700431	0.719021	-1.358095

C	-5.112740	1.368765	-0.254036
C	-5.074594	-0.556799	-1.602671
O	-3.907364	1.345841	-2.232934
C	-5.944185	0.758792	0.658061
H	-4.746073	2.388941	-0.142759
C	-5.897206	-1.219150	-0.728135
H	-4.681075	-0.995170	-2.519518
C	-6.343199	-0.569995	0.439442
H	-6.241471	1.318104	1.543001
H	-6.191185	-2.249253	-0.929196
O	-7.121095	-1.262186	1.248878
C	-7.571676	-0.673381	2.461232
H	-8.205743	0.203947	2.259468
H	-6.717598	-0.390134	3.091817
H	-8.165938	-1.441254	2.969066
I	-1.769412	1.051114	-1.718777
B	-3.137162	-0.624990	2.252124
F	-3.072846	0.768882	2.130364
F	-4.383033	-0.999094	2.783884
F	-2.965029	-1.222656	0.993143
F	-2.116561	-1.067338	3.113935

36

$[(\mathbf{1}\text{-}\boldsymbol{Me})_2\text{-}\mathbf{I}]^+[BF_4]^-$

I	-1.856773	1.741306	-0.697038
N	-4.824379	1.429985	-0.444513
C	-5.574414	0.779163	-1.355832
C	-4.920750	1.158931	0.871708
O	-3.979571	2.368744	-0.869885
C	-6.478165	-0.180868	-0.948865
H	-5.408336	1.069540	-2.393035
C	-5.802979	0.194441	1.315812
H	-4.255766	1.719319	1.530692
C	-6.612697	-0.501075	0.409707
H	-7.073559	-0.690736	-1.707769
H	-5.832813	-0.015960	2.385338
C	-7.597425	-1.527868	0.873826
H	-7.281607	-1.981620	1.822739
H	-8.576631	-1.049483	1.040167
H	-7.736521	-2.315479	0.120741
N	0.747297	1.454749	0.762238
C	0.299794	0.897204	1.904690
C	1.716073	2.391420	0.767398
O	0.241155	1.071309	-0.409159
C	0.833095	1.284103	3.117704
H	-0.500866	0.162888	1.802623
C	2.285628	2.791444	1.959134
H	1.994332	2.782942	-0.210759
C	1.851224	2.244020	3.174417
H	0.426020	0.829609	4.021468
H	3.069892	3.549617	1.933064
C	2.465258	2.651251	4.476737
H	2.840058	3.682891	4.436007
H	3.320670	1.993330	4.701972
H	1.746238	2.556003	5.301615
B	-2.774729	0.306885	3.515343
F	-2.697741	1.657654	3.130059
F	-4.047347	0.043972	4.041664
F	-2.552492	-0.510932	2.392351
F	-1.796809	0.040199	4.484601

23

$[\mathbf{Py}\text{-I-}\mathbf{Py}]^+$

N	2.621068	2.269939	2.068888
I	4.544977	1.169903	2.611700
N	6.474013	0.075558	3.152644
C	1.435468	1.684535	2.286300
C	0.246595	2.327245	1.971388
C	0.299127	3.605578	1.419459
C	1.539949	4.200231	1.199374
C	2.688109	3.498533	1.538298
H	1.452273	0.682524	2.720616
H	-0.703025	1.825076	2.159920
H	-0.620646	4.135059	1.162806
H	1.626369	5.199060	0.770139
H	3.685881	3.916916	1.388300
C	7.062639	0.313878	4.332511
C	8.237927	-0.329237	4.694213
C	8.808257	-1.237588	3.804741
C	8.184358	-1.473614	2.581373
C	7.010485	-0.794897	2.286352
H	6.573974	1.035348	4.991128
H	8.693547	-0.114681	5.661610
H	9.732683	-1.758115	4.062974
H	8.596893	-2.175996	1.856197
H	6.480517	-0.942366	1.342766

23

[**Py**-Ag-**Py**]$^+$

N	2.732404	2.215633	2.109113
Ag	4.548953	1.176074	2.613820
N	6.366939	0.139673	3.118386
C	1.537989	1.637788	2.312903
C	0.343415	2.270482	1.992119
C	0.387639	3.548376	1.439949
C	1.627633	4.146701	1.229159
C	2.776511	3.447368	1.577125
H	1.543591	0.635740	2.746735
H	-0.603608	1.761201	2.175670
H	-0.533813	4.072294	1.176901
H	1.712807	5.145792	0.799772
H	3.766311	3.883401	1.426834
C	6.988469	0.391490	4.281366
C	8.164358	-0.250734	4.648507
C	8.716495	-1.188418	3.779124
C	8.070322	-1.448902	2.573078
C	6.897661	-0.763949	2.279591
H	6.525563	1.132536	4.936348
H	8.634162	-0.013236	5.603910
H	9.639938	-1.710601	4.038615
H	8.464708	-2.174557	1.860547
H	6.362992	-0.941265	1.344124

11

Py

C	2.680691	3.466781	1.505878
N	2.651631	2.260193	2.075547
C	1.457810	1.716088	2.320397
C	0.250944	2.343396	2.011964
C	0.290741	3.603001	1.417251
C	1.533001	4.178659	1.157856
H	1.455968	0.725257	2.788328
H	-0.697503	1.850770	2.234978
H	-0.632261	4.128248	1.160031
H	1.616404	5.163243	0.693604
H	3.670505	3.895757	1.313506

18
(1-*OMe*)···I$_2$

C	9.190127	-0.661253	0.220639
C	9.435087	0.111486	1.367207
C	8.679398	-0.106287	2.501689
N	7.716624	-1.048112	2.531657
C	7.455302	-1.801490	1.437140
C	8.172664	-1.631954	0.278453
O	7.029353	-1.250172	3.642158
I	5.072750	0.058137	3.759437
O	9.849859	-0.547262	-0.921367
C	10.893272	0.408912	-1.033383
H	8.814494	0.451815	3.428034
H	6.656692	-2.533606	1.555449
H	10.203617	0.882695	1.398900
H	7.952760	-2.248570	-0.593290
H	11.696532	0.204126	-0.308397
H	10.510230	1.430828	-0.886987
H	11.288626	0.311656	-2.050642
I	2.717045	1.615978	3.910099

17
(1-*Me*)···I$_2$

C	8.169017	-1.677562	0.315142
C	9.151558	-0.686916	0.201598
C	9.375265	0.117746	1.326973
C	8.651410	-0.075666	2.486349
N	7.716418	-1.048734	2.557481
C	7.465028	-1.840125	1.493118
C	9.949516	-0.507962	-1.053204
O	7.050923	-1.230454	3.675685
I	5.043429	0.060933	3.776091
I	2.680885	1.574118	3.890453
H	8.777733	0.513504	3.394432
H	6.689546	-2.590523	1.645624
H	10.122729	0.912812	1.307502
H	7.937867	-2.336713	-0.523205
H	9.442213	-0.955252	-1.918294
H	10.135730	0.556464	-1.254219
H	10.930399	-0.998807	-0.944400

2
I_2

I	4.834259	0.087184	3.890194
I	2.520822	1.423729	4.222629

39
[**(1-*OMe*)**$_2$**-I**]$^+$(ACN)

C	1.373393	2.152028	0.788832
C	0.540727	3.232009	1.140857
C	1.410340	1.031712	1.636344
C	-0.227681	3.156468	2.274194
H	0.497337	4.120029	0.510244
O	2.065735	2.272090	-0.328764
C	0.613104	1.014658	2.760506
H	2.036422	0.164534	1.432271
N	-0.182794	2.057118	3.060613
H	-0.900228	3.947234	2.606226
C	2.903305	1.206758	-0.756759
H	0.576422	0.177868	3.458217
O	-0.938250	2.009743	4.160921
H	3.696858	1.008865	-0.020207

H	2.315827	0.292343	-0.931377
H	3.355064	1.535391	-1.699167
N	-5.054211	0.276670	1.810000
C	-4.765936	-0.918385	1.262915
C	-5.435739	1.325463	1.046176
O	-4.964478	0.430392	3.132308
C	-4.854984	-1.115075	-0.098952
H	-4.464467	-1.696383	1.964152
C	-5.539367	1.193107	-0.315365
H	-5.646556	2.249607	1.584317
C	-5.240708	-0.042658	-0.919829
H	-4.610853	-2.098558	-0.497284
H	-5.846009	2.044042	-0.923598
O	-5.333929	-0.100531	-2.238016
C	-4.986960	-1.301736	-2.915128
H	-5.648987	-2.127511	-2.613645
H	-3.937303	-1.571802	-2.721506
H	-5.121519	-1.097770	-3.982980
I	-2.963993	1.220105	3.707907
C	-2.178901	1.367938	-2.359759
H	-1.641425	0.705255	-3.051955
H	-1.848791	2.403558	-2.519909
H	-3.257386	1.297451	-2.557414
C	-1.900700	0.972254	-0.988647
N	-1.679358	0.653104	0.100761

45

[**(1-*OMe*)$_2$-I**]$^+$(ACN)$_2$

C	0.928327	1.127902	1.372500
C	0.230557	1.283272	2.585152
C	1.138216	-0.172721	0.883765
C	-0.257768	0.178728	3.235458
H	0.063032	2.277500	2.999674
O	1.332973	2.232496	0.771136
C	0.618047	-1.242547	1.579720
H	1.677669	-0.371146	-0.041020
N	-0.064361	-1.057986	2.724653
H	-0.821909	0.222936	4.166605
C	2.005166	2.147106	-0.478110
H	0.716828	-2.277826	1.253230
O	-0.563956	-2.116827	3.367031
H	2.949553	1.590319	-0.380220
H	1.364266	1.669548	-1.235217
H	2.219666	3.178429	-0.779039
N	-5.133473	-1.625300	1.320278
C	-5.055666	-1.850427	-0.004426
C	-5.515111	-0.423549	1.807652
O	-4.820834	-2.606601	2.170030
C	-5.356756	-0.856782	-0.910879
H	-4.737898	-2.852443	-0.292822
C	-5.823161	0.606315	0.955378
H	-5.543118	-0.339726	2.893350
C	-5.729734	0.412081	-0.435472
H	-5.272944	-1.082127	-1.972853
H	-6.120144	1.574579	1.358043
O	-5.988839	1.456148	-1.203325
C	-5.844368	1.345721	-2.612596
H	-6.554676	0.613015	-3.025001
H	-4.815192	1.062225	-2.881397
H	-6.068076	2.337893	-3.019699
I	-2.695474	-2.428738	2.807432
C	-2.511018	4.071274	3.110851
H	-2.484544	4.553254	4.097863

H	-3.181725	4.637019	2.449852
H	-1.498607	4.066604	2.684006
C	-2.990181	2.705600	3.245212
N	-3.361932	1.615031	3.346103
C	-2.825570	2.595667	-0.228883
H	-3.757651	2.752458	0.331103
H	-2.989025	2.856153	-1.283908
H	-2.037967	3.241233	0.184087
C	-2.418121	1.204109	-0.126490
N	-2.096315	0.095551	-0.055856

39

[**(1-*OMe*)$_2$-Ag**]$^+$(ACN)

Ag	0.541723	0.794254	-2.611973
O	-1.568206	1.247674	-2.514886
O	2.641537	0.376892	-2.926272
N	-2.093656	1.026672	-1.325447
N	3.260918	-0.000388	-1.825534
C	-2.106720	2.016714	-0.402641
C	-2.619271	-0.177616	-1.032741
C	3.792351	0.920101	-0.999792
C	3.355280	-1.316469	-1.525746
C	-2.638737	1.813817	0.848281
H	-1.658097	2.956332	-0.723785
C	-3.169955	-0.444435	0.206674
H	-2.562518	-0.916411	-1.832134
C	4.439702	0.558791	0.166396
H	3.662716	1.955930	-1.312863
C	3.986671	-1.740390	-0.380550
H	2.890957	-1.990984	-2.244661
C	-3.179519	0.560702	1.184440
H	-2.630792	2.622999	1.578998
H	-3.572502	-1.440146	0.387122
C	4.544075	-0.798705	0.501855
H	4.845870	1.349510	0.795345
H	4.047946	-2.805721	-0.156832
O	-3.650505	0.416230	2.416997
O	5.131391	-1.266575	1.596322
C	-4.197311	-0.831995	2.809516
C	5.711193	-0.356236	2.516270
H	-5.074612	-1.090818	2.195903
H	-3.446236	-1.634424	2.738768
H	-4.506913	-0.716338	3.854318
H	4.954284	0.331368	2.925635
H	6.521492	0.222181	2.044970
H	6.125691	-0.963672	3.328797
C	-0.108142	-0.617680	2.292242
H	-0.600489	0.232778	2.783758
H	0.743862	-0.948617	2.902093
H	-0.825517	-1.443680	2.188092
C	0.358925	-0.215394	0.977839
N	0.721892	0.105827	-0.071233

45

[**(1-*OMe*)$_2$-Ag**]$^+$(ACN)$_2$

Ag	0.546059	-0.566378	2.443686
O	-1.263249	-1.721473	1.461002
O	2.490989	-1.647647	1.735303
N	-1.615863	-1.169793	0.335241
N	2.925801	-1.152142	0.610522
C	-1.131187	-1.650701	-0.837549
C	-2.445188	-0.105423	0.322071
C	3.774389	-0.103715	0.607445

C 2.507636 -1.675613 -0.569028
C -1.436865 -1.054069 -2.038395
H -0.483231 -2.520819 -0.743387
C -2.794478 0.534468 -0.854307
H -2.793596 0.219556 1.302135
C 4.213274 0.476617 -0.569646
H 4.063630 0.257735 1.593912
C 2.902045 -1.138112 -1.771894
H 1.835469 -2.527729 -0.479494
C -2.275133 0.071840 -2.069208
H -1.019005 -1.453404 -2.963080
H -3.458335 1.395725 -0.792123
C 3.764862 -0.030444 -1.795317
H 4.889202 1.328063 -0.501274
H 2.535929 -1.569164 -2.704209
O -2.500644 0.629142 -3.259089
O 4.080577 0.468847 -2.989826
C -3.329845 1.775022 -3.335711
C 4.941472 1.591737 -3.061531
H -4.350547 1.551841 -2.986329
H -2.912585 2.609059 -2.748940
H -3.364912 2.059916 -4.393502
H 5.930439 1.363251 -2.633262
H 4.506636 2.461438 -2.543445
H 5.054308 1.825649 -4.126406
C 0.765985 2.093559 -1.764949
H -0.058000 1.721655 -2.388652
H 1.721647 1.851161 -2.248726
H 0.677427 3.182980 -1.655188
C 0.707633 1.468438 -0.456113
N 0.660855 0.973420 0.586238
C -0.209944 0.658672 7.055930
H -1.280632 0.557755 7.280667
H 0.101363 1.700664 7.211734
H 0.367825 -0.000542 7.718139
C 0.029674 0.285606 5.675600
N 0.219292 -0.011127 4.577441

37
[**(1-*Me*)$_2$-I**]$^+$(ACN)
I -0.927347 1.129984 -1.940089
N -3.876716 0.848228 -1.607255
C -4.125570 -0.306261 -0.958099
C -4.485065 1.998813 -1.258720
O -3.022176 0.851457 -2.629122
C -5.016131 -0.328508 0.095427
H -3.584163 -1.179135 -1.323089
C -5.384786 2.015958 -0.212029
H -4.214149 2.872542 -1.851347
C -5.665490 0.844275 0.503240
H -5.197004 -1.276078 0.604826
H -5.865125 2.960623 0.046927
C -6.587856 0.852304 1.680433
H -6.002801 1.042537 2.595553
H -7.341284 1.646619 1.593729
H -7.089450 -0.117152 1.802232
N 1.140057 1.595363 0.157021
C 1.186667 0.526751 0.977525
C 1.111999 2.853482 0.637497
O 1.136157 1.405156 -1.161450
C 1.201206 0.706388 2.344973
H 1.208367 -0.445229 0.484920
C 1.126826 3.073695 2.000517

H	1.077964	3.643249	-0.113182
C	1.161871	1.995434	2.894067
H	1.235871	-0.175401	2.986298
H	1.104764	4.102653	2.361963
C	1.118786	2.203792	4.374629
H	1.466233	3.208146	4.650328
H	1.722647	1.450592	4.899163
H	0.078759	2.096271	4.724626
C	-2.393381	3.573807	1.235796
H	-1.765743	4.166073	1.915869
H	-3.433744	3.920401	1.305988
H	-2.035429	3.704613	0.204905
C	-2.320716	2.167749	1.599203
N	-2.263187	1.047360	1.882123

43

[**(1-*Me*)$_2$-I**]$^+$(ACN)$_2$

I	-0.986936	0.642748	-1.705389
N	-3.959601	0.379829	-1.661842
C	-4.286340	-0.916850	-1.493681
C	-4.550361	1.353507	-0.942388
O	-3.040616	0.705968	-2.571125
C	-5.240344	-1.274741	-0.563462
H	-3.752793	-1.623799	-2.129033
C	-5.510946	1.035397	-0.003542
H	-4.221995	2.369024	-1.159406
C	-5.873658	-0.299307	0.218200
H	-5.483088	-2.331916	-0.446944
H	-5.974069	1.845203	0.561747
C	-6.862756	-0.672285	1.276011
H	-6.323229	-0.894891	2.211662
H	-7.562158	0.149574	1.479169
H	-7.426150	-1.572823	0.996351
N	0.875820	0.625558	0.607164
C	0.975275	-0.540570	1.276602
C	0.661276	1.791102	1.246246
O	1.001009	0.620342	-0.719710
C	0.854741	-0.559273	2.649936
H	1.146738	-1.423070	0.660476
C	0.527384	1.811641	2.620508
H	0.594869	2.675269	0.612182
C	0.612930	0.625837	3.359664
H	0.935511	-1.515994	3.167915
H	0.344891	2.768996	3.110383
C	0.425070	0.607628	4.843539
H	0.363415	1.623028	5.255217
H	1.250652	0.069930	5.332756
H	-0.504359	0.071268	5.092828
C	-2.213154	4.341265	-2.262698
H	-2.611022	3.383670	-2.628708
H	-1.278487	4.570865	-2.792783
H	-2.944535	5.139008	-2.451665
C	-1.955081	4.238155	-0.835822
N	-1.755883	4.138860	0.299182
C	-2.974693	1.676647	2.539593
H	-2.482148	1.791370	3.515373
H	-4.056984	1.824066	2.661486
H	-2.579642	2.432055	1.844294
C	-2.720134	0.343915	2.018527
N	-2.516855	-0.716763	1.603289

37

[**(1-*Me*)$_2$-Ag**]$^+$(ACN)

C	0.898250	0.431378	-0.837609
C	2.022536	0.385258	-0.031147
C	3.298974	0.572788	-0.566725
C	3.369237	0.808582	-1.946541
C	2.226129	0.847557	-2.718129
N	1.003198	0.659665	-2.164494
H	-0.116394	0.289696	-0.462202
H	1.882175	0.198155	1.034846
H	4.330279	0.966401	-2.439675
H	2.219381	1.026804	-3.792682
O	-0.038375	0.714114	-2.945293
C	-5.287471	0.922018	-0.640533
C	-6.644398	1.034774	-0.884128
C	-7.401276	-0.080956	-1.254759
C	-6.717173	-1.299325	-1.351545
C	-5.360729	-1.371680	-1.101488
N	-4.657669	-0.267916	-0.757082
H	-4.645536	1.759213	-0.367212
H	-7.106213	2.019147	-0.789835
H	-7.240494	-2.213653	-1.637591
H	-4.772911	-2.285895	-1.177370
O	-3.373986	-0.353760	-0.553793
C	-8.870580	0.012826	-1.535863
H	-9.130826	-0.540312	-2.450169
H	-9.446844	-0.433469	-0.709511
H	-9.190895	1.057080	-1.649124
C	4.536294	0.515132	0.277440
H	5.144177	-0.362051	0.004969
H	5.160505	1.406515	0.114806
H	4.290547	0.445983	1.345329
Ag	-2.099852	0.264071	-2.332543
C	-6.423752	0.358337	-4.627709
H	-6.850442	-0.643805	-4.483358
H	-6.422372	0.607045	-5.697822
H	-7.025832	1.095619	-4.078695
C	-5.064892	0.377301	-4.122002
N	-3.987667	0.388850	-3.707481

43

[**(1-*Me*)$_2$-Ag**]$^+$(ACN)$_2$

C	-1.184905	1.465292	-0.529333
C	-0.123630	0.632001	-0.233606
C	0.888674	0.392967	-1.171276
C	0.768419	1.053724	-2.397203
C	-0.311637	1.877535	-2.659371
N	-1.287808	2.067771	-1.740081
H	-1.993360	1.686655	0.165851
H	-0.095737	0.163666	0.752265
H	1.521544	0.928264	-3.177315
H	-0.461329	2.397288	-3.606032
O	-2.316212	2.806099	-2.010018
C	-4.632794	0.821564	-0.931366
C	-4.449324	-0.139521	0.047110
C	-4.984981	-1.422494	-0.095621
C	-5.713815	-1.669873	-1.266010
C	-5.875830	-0.685761	-2.221508
N	-5.334921	0.544189	-2.053097
H	-4.194111	1.820160	-0.901003
H	-3.864413	0.127334	0.929273
H	-6.160785	-2.648725	-1.450337
H	-6.419492	-0.823830	-3.155505
O	-5.483047	1.444749	-2.977924
C	-4.776232	-2.493617	0.932463

H -5.741234 -2.848657 1.325904
H -4.268900 -3.362801 0.485901
H -4.170008 -2.130551 1.773025
C 2.028121 -0.534592 -0.870204
H 2.801710 -0.484602 -1.648075
H 2.486870 -0.291198 0.099727
H 1.669793 -1.574594 -0.808867
Ag -3.522670 2.049727 -4.007357
C -2.029904 -2.133454 -1.906260
H -1.022488 -2.500588 -2.146066
H -2.754976 -2.950764 -2.022716
H -2.052444 -1.770197 -0.869494
C -2.378112 -1.046898 -2.802630
N -2.657232 -0.176722 -3.509566
C -2.080163 4.717908 -7.732965
H -2.895461 4.846688 -8.457999
H -1.231426 4.217773 -8.219053
H -1.762591 5.700618 -7.358358
C -2.546025 3.908378 -6.624797
N -2.917677 3.264335 -5.743532

6
ACN
C 2.578598 -8.378771 3.080091
H 2.942487 -9.415445 3.076139
H 2.942511 -7.863898 2.180243
H 1.479824 -8.381143 3.076007
C 3.063241 -7.693172 4.267558
N 3.448795 -7.148163 5.211682

13
$[ACN\text{-}I\text{-}ACN]^{+}$
N -6.275357 -0.529865 1.062920
C -7.426323 -0.509681 1.053836
C -8.869614 -0.479340 1.041130
H -9.223104 0.092337 1.910542
H -9.208953 0.002329 0.113523
H -9.251185 -1.508528 1.090158
I -4.052194 -0.533721 1.066880
N -1.828887 -0.526539 1.065702
C -0.677917 -0.506945 1.056362
C 0.765391 -0.478942 1.042009
H 1.141545 -0.845405 2.007118
H 1.128241 -1.124025 0.229748
H 1.101523 0.554238 0.877673

13
$[ACN\text{-}Ag\text{-}ACN]^{+}$
N -6.166275 -0.539366 1.063319
C -7.317538 -0.513212 1.054108
C -8.763997 -0.475326 1.041302
H -9.119941 0.048595 1.939072
H -9.103308 0.057577 0.142357
H -9.153858 -1.502333 1.032527
Ag -4.052118 -0.548746 1.068217
N -1.937983 -0.537631 1.065554
C -0.786724 -0.511713 1.055895
C 0.659744 -0.475086 1.041541
H 1.039775 -0.764584 2.030843
H 1.032443 -1.176018 0.282087
H 0.992945 0.543757 0.800777

4. REFERENCES

1. J. Barluenga, J. M. González, P. J. Campos and G. Asensio, *Angew. Chem.Int.Ed. Engl.*, 1985, **24**, 319.
2. L. Koskinen, P. Hirva, E. Kalenius, S. Jääskeläinen, K. Rissanen and M. Haukka, *CrystEngComm*, 2015, **17**, 1231.
3. A. Karim, M. Reitti, A.-C. C. Carlsson, J. Gräfenstein and M. Erdelyi, *Chem. Sci.*, 2014, **5**, 3226.
4. A.-C. C. Carlsson, J. Gräfenstein, J. L. Laurila, J. Bergquist and M. Erdélyi, *Chem. Commun.*, 2012, **48**, 1458.
5. A.-C. C. Carlsson, J. Gräfenstein, A. Budnjo, J. L. Laurila, J. Bergquist, A. Karim, R. Kleinmaier, U. Brath and M. Erdélyi, *Journal of the American Chemical Society*, 2012, **134**, 5706.
6. R. Puttreddy, O. Jurček, S. Bhowmik, T. Mäkelä and K. Rissanen, *Chem. Commun.*, 2016, **52**, 2338.
7. R. Puttreddy, O. Jurcek, S. Bhowmik, T. Makela and K. Rissanen, *Chem Commun*, 2016, **52**, 2338.
8. K. Zhao, Y. Zhi, X. Li, R. Puttreddy, K. Rissanen and D. Enders, *Chem Commun*, 2016, **52**, 2249.
9. U. Kaya, P. Chauhan, D. Hack, K. Deckers, R. Puttreddy, K. Rissanen and D. Enders, *Chem. Commun.*, 2016, **52**, 1669.
10. M. Dommaschk, V. Thoms, C. Schutt, C. Nather, R. Puttreddy, K. Rissanen and R. Herges, *Inorg Chem*, 2015, **54**, 9390.
11. (a) S. Kozuch, J. M. L. Martin, *J. Chem. Theory Comput.* 2013, **9**, 1918–1931; (b) A. Forni, S. Pieraccini, D. Franchini, M. Sironi, *J. Phys. Chem. A* 2016, **120**, 9071−9080
12. J. Tomasi, B. Mennucci and E. Cancès, *J. Mol. Struct.*, 1999, **464**, 211.
13. H. Valkenier, C. M. Dias, K. L. Porter Goff, O. Jurcek, R. Puttreddy, K. Rissanen and A. P. Davis, *Chem Commun*, 2015, **51**, 14235.
14. J. R. Cheeseman, G. W. Trucks, T. A. Keith and M. J. Frisch, *The J. Chem. Phys.*, 1996, **104**, 5497.
15. M. J. T. Frisch, G. W.; Schlegel, H. B.; Scuseria, G. E.; Robb, M. A.; Cheeseman, J. R.; Scalmani, G.; Barone, V.; Mennucci, B.; Petersson, G. A.; Nakatsuji, H.; Caricato, M.; Li, X.; Hratchian, H. P.; Izmaylov, A. F.; Bloino, J.; Zheng, G.; Sonnenberg, J. L.; Hada, M.; Ehara, M.; Toyota, K.; Fukuda, R.; Hasegawa, J.; Ishida, M.; Nakajima, T.; Honda, Y.; Kitao, O.; Nakai, H.; Vreven, T.; Montgomery, J. A., Jr.; Peralta, J. E.; Ogliaro, F.; Bearpark, M.; Heyd, J. J.; Brothers, E.; Kudin, K. N.; Staroverov, V. N.; Kobayashi, R.; Normand, J.; Raghavachari, K.; Rendell, A.; Burant, J. C.; Iyengar, S. S.; Tomasi, J.; Cossi, M.; Rega, N.; Millam, J. M.; Klene, M.; Knox, J. E.; Cross, J. B.; Bakken, V.; Adamo, C.; Jaramillo, J.; Gomperts, R.; Stratmann, R. E.; Yazyev, O.; Austin, A. J.; Cammi, R.; Pomelli, C.; Ochterski, J. W.; Martin, R. L.; Morokuma, K.; Zakrzewski, V. G.; Voth, G. A.; Salvador, P.; Dannenberg, J. J.; Dapprich, S.; Daniels, A. D.; Farkas, Ö.; Foresman, J. B.; Ortiz, J. V.; Cioslowski, J.; Fox, D. J., Gaussian, Inc., Wallingford CT, 2009.